UNIONE EUROPEA
Fondo Sociale Europeo

Ministero dell'Università e della Ricerca

PON RICERCA E INNOVAZIONE 2014 - 2020

UNIVERSITÀ DEGLI STUDI FIRENZE
Da un secolo, oltre.

DOTTORATO DI RICERCA IN
Scienze Biomediche

CICLO XXXVII - PON ex DM1061

Exploring Cardiac Remodeling in Different Cellular Models

A Molecular and Genetic Approach to Identifying Key Players

Settore Scientifico Disciplinare
BIOS-06/A - Fisiologia

Dottoranda

Dottoressa Viola Marian

Supervisori

Prof.ssa Tesi Chiara

Prof.ssa Ferrantini Cecilia

Prof. van Nieuwenhoven Frans

Coordinatore

Prof. Chiti Fabrizio

Table of Contents

Abstract

Cardiac remodeling is a complex process that occurs under both physiological and pathological conditions, involving significant morphological, functional and structural changes in cardiac cells, particularly cardiomyocytes and cardiac fibroblasts. Understanding the key factors regulating these processes remains one of the main challenges in cardiovascular research. One of the primary difficulties is obtaining human cardiac tissue samples, especially in the early stages of disease when cellular changes are crucial for understanding the underlying mechanisms. Traditionally, to overcome this challenge, cardiovascular research has relied on animal models to study disease mechanisms and test new therapies. However, the use of animal models raises ethical concerns related to animal experimentation and welfare. These challenges have driven the scientific community to seek more effective and less invasive alternatives, such as the use of *in vitro* cellular models.

A key advancement has been the use of embryonic stem cells, which have enabled the generation of cellular models capable of replicating certain characteristics of the human heart and providing insights into differentiation processes and cardiac remodeling. However, the use of embryonic stem cells also raises ethical concerns related to their derivation, prompting research into alternative solutions. A valuable alternative is the use of cardiomyocytes derived from human induced pluripotent stem cells (hiPSC-CMs). These cells have become a fundamental tool in cardiac regeneration, as induced pluripotent stem cells (iPSCs) retain the full genetic profile of the patient and offer the possibility of testing personalized pharmacological treatments aimed at correcting specific alterations. However, a major challenge in using iPSCs is the difficulty of precisely replicating the development of cardiac muscle cells, making it challenging to obtain fully reliable models for studying cardiac diseases and testing new therapies.
A promising approach is the application of tissue engineering techniques to develop 3D cardiac tissue models derived from hiPSC-CMs. In this process, immature cardiomyocytes are seeded into a three-dimensional (3D) matrix and subjected to mechanical stress, stimulating their maturation and creating more physiologically relevant models for studying development, regeneration, and cardiovascular diseases.

In our project, we developed and characterized 2D cellular models, including cardiac fibroblasts derived from embryonic stem cells (hESC-CFs) and hiPSC-CMs and subsequently created a 3D co-culture model of fibroblasts and cardiomyocytes. These models allowed us to investigate the profibrotic, pro-inflammatory and hypertrophic effects of two coagulation factors, Thrombin and FIIa, which influence the cardiac cellular environment. In particular, our study confirmed the profibrotic and pro-inflammatory effects of these coagulation factors on hESC-CFs, previously observed in primary cardiac fibroblast cultures, as well as their hypertrophic effect on hiPSC-CMs. These findings demonstrate that these coagulation factors actively contribute to cardiac remodeling by promoting a fibrotic state, inducing the transformation of fibroblasts into myofibroblasts, stimulating inflammatory processes and favoring hypertrophy in cardiomyocytes. Specifically, for hiPSC-CMs, we observed that the hypertrophic response is mediated by the activation of the *PAR1* receptor, a member of the protease-activated receptor (*PAR*) family.
In the last part of the study, we provided a preliminary characterization of the co-culture model, which should enable a more accurate simulation of cardiac cell behavior and maturation, with the future aim of evaluating the effects of coagulation factors on this model.

Our results underscore the importance of developing advanced *in vitro* models to enhance our understanding of the mechanisms underlying cardiac remodeling and to identify potential therapeutic targets, paving the way for future research in regenerative medicine and personalized treatments.

Chapter 1

Introduction

1.1 Heart Function

The heart is the main organ of the circulatory system. This organ is structured to form four cardiac chambers. The two upper chambers are known as atria, while the two lower chambers are called ventricles. The heart provides sufficient oxygenated blood containing nutrients, metabolites and hormones to all organs, ensuring their proper function. In the pulmonary circulation, the "oxygen-poor" blood from all parts of the body is collected in the right atrium and is pumped through the tricuspid valve into the right ventricle. This blood is then pumped from the right ventricle through the pulmonary valve into the pulmonary artery, which divides into two branches (left and right) that carry the blood to the right and left lungs, respectively, to be oxygenated. After oxygenation, the left atrium receives the oxygenated blood from the pulmonary circulation via the pulmonary veins and sends it to the left ventricle through the mitral valve. The left ventricle is the chamber of the heart that receives the oxygenated blood from the left atrium and is responsible for pumping the blood into the aorta through the aortic valve. The aorta is responsible for carrying the blood throughout the body to supply the systemic circulation, delivering oxygen to all the tissues of our body (Voorhees and Han, 2015). The pumping action is achieved through a complex interplay of electrical and mechanical processes that drive the cardiac cycle (Klabunde, 2021). In particular, the cardiac electrical activation begins with depolarization of specialized pacemaker cells, primarily located in the sinoatrial (SA) node in the upper right atrium (Hall and Michael, 2021). The electrical pacemaker signal from the right atrium spreads to the left atrium allowing coordinated contraction of the upper two chambers (atrial systole). Next, the electrical impulse reaches the middle of the heart, near the junction of all four chambers, a structure called the atrioventricular (AV) node, providing direct conduction of the impulse from the atria to the ventricles. The AV node itself has a slower pacemaker activity; this region of slow conductance delays activation of the bundle of His, allowing completion of ventricular filling. From the bundle of His, the electrical impulse bifurcates to the branches serving the lower right and left ventricles. Specialized conduction fibers, termed Purkinje fibers, act to speedily conduct the impulse to the rest of ventricular muscle (Figure 1) (Wilcken, 2006; Leemans and Amàlio, 2016).

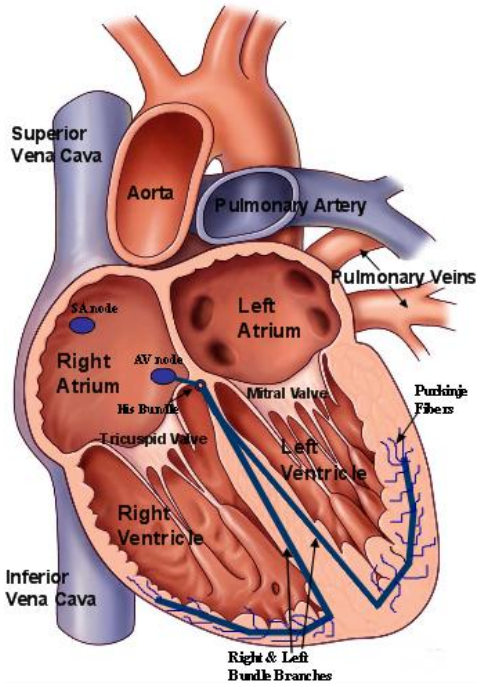

Figure 1. Human Heart and its conduction system (Leemans and Amàlio, 2016).

Anomalies in cardiac function can lead to a wide range of pathologies, primarily due to disruptions in the electrical and mechanical processes that regulate heart contraction and blood flow. For example, increased stresses in the myocardium due to hypertension can lead to cardiac structural remodeling, such as hypertrophy and fibrosis. Structural remodeling contributes to an increased risk of developing heart failure and may result in cardiac arrhythmias (Camm et al., 2012). However, the molecular mechanisms responsible for structural changes such as hypertrophy and fibrosis are not yet fully understood.

1.2 Cardiac Excitation-Contraction Coupling in Cardiac Muscle

Excitation-contraction (E-C) coupling in the heart represents the essential biological process whereby an electrical signal is translated into mechanical contraction. While it shares fundamental mechanisms with skeletal muscle, cardiac E-C coupling exhibits distinct temporal and molecular features. The

electrical impulse originates from pacemaker cells in the sinoatrial (SA) node, which possess intrinsic automaticity. The signal then propagates sequentially through the atrioventricular (AV) node, the His-Purkinje conduction system, and eventually depolarizes ventricular myocytes (Bers, 2002).
The rapid spread of depolarization across the myocardium is enabled by gap junctions, ensuring synchronous contraction. A critical distinction from skeletal muscle is the reliance on extracellular calcium for contraction in cardiomyocytes (Bers, 2000). Depolarization activates voltage-gated L-type Ca^{2+} channels, allowing a small influx of calcium into the cytosol (ICa). This calcium entry then triggers a much larger release of Ca^{2+} from the sarcoplasmic reticulum (SR) through ryanodine receptor type 2 (RyR2) channels, in a process termed calcium-induced calcium release (CICR) (Fabiato, 1983).
Unlike skeletal muscle, where RyRs are mechanically coupled to dihydropyridine receptors, cardiac RyR2 channels are activated solely by the incoming Ca^{2+} ions (Brette and Orchard, 2003). The resultant rise in intracellular calcium concentration ($[Ca^{2+}]_i$) allows calcium to bind to troponin C, inducing a conformational change that removes tropomyosin from actin's binding sites, thereby facilitating actin–myosin interaction and initiating contraction.
For the myocardium to relax, $[Ca^{2+}]_i$ must return to resting levels. This is achieved through: (1) Reuptake into the SR via the SERCA (SR Ca^{2+}-ATPase) pump, whose function is regulated by phospholamban (PLB). When PLB is unphosphorylated, it inhibits SERCA by decreasing its affinity for Ca^{2+} (MacLennan & Kranias, 2003); (2) extrusion from the cytosol, primarily via the sodium–calcium exchanger (NCX) and, to a lesser extent, the plasma membrane Ca^{2+}-ATPase (PMCA).
Once calcium dissociates from troponin, tropomyosin re-blocks the actin sites, and the muscle cell returns to its relaxed state.

1.2.1 Sympathetic Modulation of Intracellular Calcium Dynamics

Sympathetic stimulation exerts a significant regulatory role on cardiac performance by modulating both the strength and kinetics of contraction. Activation of β-adrenergic receptors, primarily the β_1 subtype, increases intracellular cAMP levels via Gs protein-mediated stimulation of adenylyl cyclase. This, in turn, activates protein kinase A (PKA), which phosphorylates multiple key proteins involved in excitation–contraction coupling (Zaccolo and Pozzan, 2002).
In terms of lusitropy (enhanced relaxation), PKA acts by: (a) phosphorylating phospholamban, thereby relieving its inhibition of SERCA and accelerating SR Ca^{2+} reuptake (MacLennan and Kranias, 2003); (b) phosphorylating troponin I, which decreases the affinity of troponin C for Ca^{2+}, promoting faster dissociation and relaxation. The inotropic effects (increased contractile force) are mediated by: (a) enhanced L-type Ca^{2+} current (ICa) due to channel phosphorylation, leading to greater Ca^{2+} influx during depolarization; (b) increased SR Ca^{2+} load, driven by augmented SERCA activity and increased RyR2 sensitivity or open probability. Additionally, PKA phosphorylation can influence RyR2 function, promoting a more robust and timely release of calcium from the SR.
In ventricular myocytes:

- β_1-adrenergic receptors, distributed broadly across the sarcolemma, are the main mediators of positive inotropic and lusitropic responses.
- β_2-adrenergic receptors are primarily localized within caveolae, specialized membrane microdomains. Their effects are more spatially restricted and tend to focus on potentiating ICa, with less influence on global Ca^{2+} handling (Nikolaev et al., 2006).

This compartmentalized signaling allows for fine-tuned regulation of cardiac performance under sympathetic control.

1.3 Cardiac Remodeling

The term "remodeling" was first introduced in 1982 by Hockman and Buckey in a myocardial infarction (MI) model. At the beginning it was used to describe the replacement of infarcted tissue by scar tissue

(Hochman and Bulkley, 1982). Later, Janice Pfeffer used this term referring to the progressive enlargement of the left ventricular cavity in an experimental MI in rat models (Pfeffer et al., 1985). In subsequent years, "remodeling" began to be used more broadly, describing various clinical situations and pathophysiological changes. In 2000, a consensus from an International Forum defined cardiac remodeling as a group of molecular, cellular, and interstitial alterations that manifest clinically as changes in the size, shape, and function of the heart following cardiac injury. Cardiac remodeling can be described as a physiological and pathological condition that can arise after various cardiovascular events. Despite the differing causes of these conditions, they share common molecular, biochemical, and mechanical pathways. The myocyte is the major cardiac cell involved in the remodeling process. Additionally, the interstitial space, fibroblasts, collagen, and coronary blood vessels play significant roles, with other key processes including ischemia, cell death (necrosis) and apoptosis. After an injury in the heart, the number of myocytes decreases, and the remaining cells either become elongated or hypertrophied as part of an early compensatory response (Cohn et al., 2000). To detect these changes, methods like echocardiography, ventriculography and nuclear magnetic resonance are commonly used. Another, less commonly used method in routine clinical practice involves detecting cell markers based on the re-expression of fetal genes. These include an increase in α myosin heavy chain (gene name: *MYH6*) and a decrease in β myosin heavy chain (gene name: *MYH7*), along with increased expression of Glucose Transporter Type 1 (GLUT-1), α-actin, natriuretic peptide, and neuronal nitric oxide synthase. Additionally, there is decreased expression of Glucose Transporter Type 4 (GLUT-4), Sarcoplasmic/Endoplasmic Reticulum Calcium ATPase 2a (SERCA2a), and a metabolic shift from fatty acid oxidation to glucose metabolism (Zornoff et al., 2009; Swynghedauw, 2006).

One of pathophysiological mechanisms of cardiac dysfunction is the cell death. Myocyte death is due to different mechanisms such as apoptosis, necrosis or autophagy. Each of these mechanisms affects the heart in distinct ways, contributing to the structural and functional deterioration associated with cardiac remodeling. The exact involvement of apoptosis and necrosis in cardiac dysfunction has been a subject of intense debate. However, recent evidence suggests that they can represent different aspects of the same process called necroptosis (Burchfield et al., 2013). Autophagy is essential for maintaining protein homeostasis or proteostasis and the disruptions in this balance can lead to the accumulation of defective proteins, a phenomenon known as proteotoxicity. Alterations in the autophagic process are involved in ventricular dysfunction (Tarone and Brancaccio, 2014). Furthermore, it is well defined that inflammatory mediators have been identified in patients with heart failure (Anker and von Haehling; 2004). Moreover, experimental studies have shown repeatedly that activation of inflammation in the heart provokes left ventricular remodeling and left ventricular dysfunction (Mann, 2015). The inflammatory mediators can trigger the re-expression of fetal genes, promote cellular growth, activation of collagenolytic matrix metalloproteinase and myocardial fibrosis (Mann, 2002).

One of the most frequent cardiac remodeling mechanisms in cardiac pathologies is atrial and/or ventricular hypertrophy, which is characterized by an increase of cardiomyocytes size and the consequent thickening of the cardiac wall.

1.4 Cardiac Hypertrophy

Cardiac hypertrophy is a process often involved in heart dysfunction, which at the cellular level corresponds to an increase in cardiomyocyte size and other typical features. This phenomenon can be physiological or pathological: physiological hypertrophy of the heart can ensue as a result of exercise or pregnancy and is deemed mild and/or reversible (Chung and Leinwand, 2014; Ellison et al., 2012). Both kind of hypertrophy initially arise as an adaptive response to cardiac stress, however, in the presence of chronic stressful conditions such as hypertension and valvular disease, a form of pathological hypertrophy develops, which is characterized by excessive increase in ventricular dimensions, accompanied by myocardial dysfunction and fibrosis (Heineke and Molkentin, 2006; Kannel and

Dannenberg, 1987). Both physiological and pathological hypertrophy involve an enlargement of individual cardiomyocytes, but their characteristics are notably different. Physiological hypertrophy is characterized by a modest (10-20%) increase in cardiac mass and a balanced growth of cardiomyocytes in both length and width. In this case, the heart maintains or even improves its contractile ability, without obvious signs of interstitial or replacement fibrosis, nor cell death (Maillet et al., 2013). In contrast, pathological hypertrophy, initially compensatory with concentric ventricular growth, later progresses to ventricular chamber dilation and wall thinning due to the elongation of individual cardiomyocytes, resulting in reduced contractility (Schiattarella and Hill, 2015). Furthermore, pathological cardiac hypertrophy is marked by more significant changes, including a switch to the fetal gene expression profile (Dirkx et al., 2013). This switch involves an increase in the expression of skeletal α-actin (gene name: ACTA1), atrial natriuretic peptide (gene name: *NPPA*), brain natriuretic peptide (gene name: *NPPB*) (Sergeeva and Christoffels, 2013), and myosin heavy chain β isoform (gene name: *MYH7*) (Gupta, 2007). In physiological hypertrophy, however, these markers remain unchanged or decrease.
At the cellular level, in addition to the enlargement of cardiomyocytes, pathological hypertrophy also involves an increase in protein production and a decrease in the organization of the sarcomere structure (Carreño et al., 2006; Frey et al., 2000). Additionally, cardiomyocytes switch to carbohydrate-dependent energetic machinery instead of fatty acid oxidation, which in turn necessitates alterations in expression levels of metabolic genes (Taegtmeyer et al., 2010). Table 1 describes the main differences between physiological hypertrophy and pathological hypertrophy.

Table 1. Main characteristics of physiological and pathological cardiac hypertrophy.

Triggers and Characteristics	Physiological hypertrophy	Pathological hypertrophy
Triggers	Normal postnatal growth/ Pregnancy/ Exercise	Pressure overload owing to hypertension or aortic stenosis Volume overload induced by mitral and aortic regurgitation and chronic kidney disease Myocardial hypoxia as a result of myocardial infarction, obesity, diabetes mellitus, ageing, chronic obstructive pulmonary disease, or anaemia Storage diseases (lipid, glycogen, or misfolded protein diseases) Inherited diseases such as hypertrophic cardiomyopathy
Reversibility	Yes	Might be possible with treatment
Cardiomyocyte size	Increased	Increased
Fibrosis	No	Yes (advanced)
Type I collagen levels	Unchanged	Increased
Myofibroblast activation	Unchanged	Yes (such as increased smooth muscle α-actin)
Cardiomyocyte death	No	Yes (advanced)
Fetal genes	Unchanged or Decreased	Increased (for example *ACTA1*, *MYH7*, *NPPA* and *NPPB*)

1.4.1 Hypertrophy and Mechanotransduction

The increased size of the cardiomyocyte is not the only characteristic of cardiac hypertrophy, but it is the result of a complex molecular process that involves changing in protein synthesis (membrane receptors, second messengers and transcription factors) and re-organization of the sarcomere structure (Carreño et al., 2006). Mechanical stress can induce a hypertrophic response downstream of mechanosensitive molecules. The sarcomere Z-disc and its associated proteins are thought to play a key role in mechanical stress-induced signal transduction, a process known as "mechanotransduction" (Heineke and Molkentin, 2006). Its downstream effects function initially as adaptive responses that serve as compensatory mechanisms during adaptation to the initial load. However, under prolonged or abnormal loading conditions, these remodeling processes result in impaired physiological function and the onset of pathological cardiac hypertrophy. External forces acting on the cardiomyocytes are transmitted through structural proteins to the sarcomere, where several molecules could be involved in sensing and transducing signals. An example is the interaction of Titin and muscle LIM protein (MLP, also known as cysteine-rich protein 3) with a network of proteins to form complex signalosomes, which play roles in mechanotransduction pathways (Lyon et al., 2015).

The intercalated discs, complex structures that connect adjacent cardiomyocytes, are also involved in mechanotransduction. The three types of cell junction recognised as making up an intercalated disc are desmosomes, fascia adherens junctions, and gap junctions (Zhao et al., 2019). Fascia adherens and desmosomal junctions are able to transmit mechanical stress to the cells through actin and intermediate filaments, respectively (Hoshijima, 2006). However, genetic evidence, based on a distinct cardiomyocyte remodeling response associated with desmosomal deficiencies and mutations (separate from the fascia adherens junction), indicates that desmosomal proteins seem to have a more robust role in intermediate filament–based mechanotransduction (Sheikh et al., 2009).

1.4.2 Hypertrophy and Switch to the Fetal Gene Program

The switch to the fetal gene program is an important key topic to understanding cardiac disease and pathological cardiac remodeling. It has been observed that in failing and diseased hearts, there is often a reversion to fetal gene expression, driven by the reactivation of developmental transcription factors such as NFAT and MEF2 (Dirkx et al., 2013; Rajabi et al., 2007). These fetal genes are abundantly expressed in the prenatal heart but become downregulated after birth. For example, during the fetal development, lactate and glucose oxidation (carbohydrate substrates) constitute the major sources of adenosine triphosphate (ATP) synthesis (Fisher et al., 1980). In contrast, the fetal heart has a limited capacity to oxidize long-chain fatty acids (Bartelds et al., 2000). After birth, there is a metabolic switch, accompanied by changes in the expression of enzymes (Lehman and Kelly, 2002), from lactate and glucose oxidation to fatty acid oxidation (Bartelds et al., 1998). During an acute increase in workload, adult heart responds by shifting from fatty acid oxidation to glycogen, lactate, and glucose metabolism (Goodwin et al., 1998). If the stress is chronic and sustained, these metabolic pathways are transcriptionally regulated (Sack et al., 1997). Another molecular response to various triggers results in new sarcomere organization by remodeling the adult cardiac gene program to the fetal gene profile. The major isoform switch of many sarcomere proteins occurs at birth: during development and under pathophysiological conditions, the expression of the two cardiac α and β Myosin Heavy Chain (MHC) isoforms is regulated in a chamber-specific manner and influenced by hormonal control, particularly by thyroid hormones. These changes are closely linked to the heart's mechanical performance and efficiency as it transitions from fetal to postnatal circulation. Across species, differences in contraction speeds are correlated with variations in the ratio of α and β MHC isoforms (Swynghedauw, 1986). The α MHC is associated with higher actomyosin ATPase activity compared with β MHC. In the mouse and rat, for example, the β MHC isoform is fetal-specific whose expression in ventricular myocytes is down-regulated to low levels soon after birth and replaced by α MHC isoform, also predominant in the

ventricles (Sassoon et al., 1988). Conversely, in other mammalian species (including humans), α MHC isoform is expressed in the atria throughout life and β MHC remains the predominant ventricular isoform throughout adulthood.

While numerous studies have been conducted on α/β MHC (*MYH6*/*MYH7*) switch in rodents in context of cardiac hypertrophy; to date, few studies have been conducted on this genetic switch in the human heart. A study of 1990 from Kurabayashi et al., analyzed the isozymic transitions from α to β MHC of cardiac myosins in response to pressure overload in atria. The authors observed that increased expression of β MHC induced in the atria subjected to severe pressure overload together with the isogene switch from α MHC (*MYH6* gene) to β MHC (*MYH7* gene) may participate in the adaptation of myocardium to new functional requirement (Figure 2) (Kurabayashi et al., 1990).

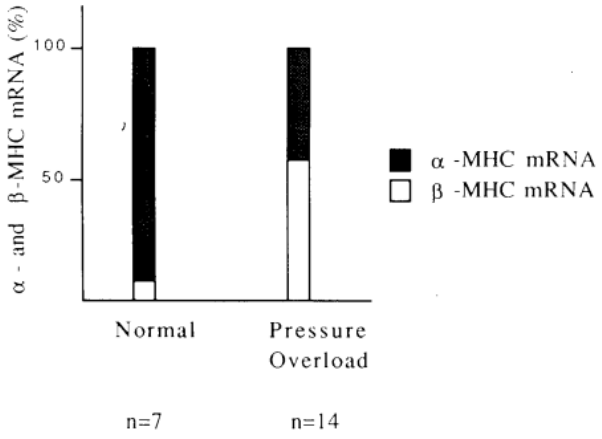

Figure 2. Relative levels of α MHC and β MHC mRNAs in normal and pressure-overloaded atria (Kurabayashi et al., 1990).

Pressure overload leads to specific changes in the composition of MHC also in the human ventricles. It has been observed a decrease in α MHC expression (mRNA) and content (protein) in the failing human left ventricle (Reiser et al., 2001) and a relative increase in β MHC expression in the left ventricles of patients with cardiomyopathy. The authors of this study concluded that adult human ventricular myosin isoform expression changes during the development of cardiomyopathy (Nakao et al., 1997). Furthermore, this study indicates that there is a much greater relative amount of the β MHC isoform in the left atrium during heart failure compared to non-failure cases.

Another example of reactivation of the Fetal Gene Program is the re-expression of the atrial natriuretic peptide (ANP) or atrial natriuretic factor (ANF) and brain natriuretic peptide (BNP). The genes that encode these factors are named *NPPA* and *NPPB*, respectively. During embryonic and fetal development of the heart *NPPA* and *NPPB* are highly expressed in the differentiating atrial and trabecular ventricular chamber; after birth *NPPB* remains expressed in both atria and ventricles while the expression of *NPPA* becomes restricted to the atria (Houweling et al, 2005; Sergeeva and Christoffels, 2013). After cardiac stress, there is an increase of these pro-peptides in the heart and an up-regulation of *NPPA* and *NPPB* expression in ventricular cardiomyocytes (Sergeeva et al., 2014). In clinic, the plasma levels of these peptides are used as early and specific markers to evaluate the severity of hypertrophy and as a marker for development of heart failure (Battistoni et al., 2012). During hypertrophic response to different *stimuli*, there is a reactivation of early response genes such as c-fos, c-jun, and c-myc followed by a re-expression of fetal gene program. In this case, a c-fos/c-jun hetrodimer was found to directly bind the AP-1 site of the *NPPA* promoter, suggesting a direct interaction between these two pathways (Rosenzweig et al, 1991). However, the regulation *NPPA* seems to be more complex and extensive. To date, we know that *NPPA* and *NPPB* are two paralogous gene positioned close to each other and organized in conserved cluster (Inoue et al., 2005). Deciphering transcriptional regulation of *NPPA* and *NPPB* during heart development and disease has proven to be complex and challenging. *NPPA* and *NPPB* are regulated by different regulatory elements during cardiac stress. The *NPPA* promoter interacts with *NPPB* promoter and several distal and proximal regulatory elements to regulate its dynamic expression in the embryonic/fetal and adult heart. *NPPB* expression relies on the interaction of its promoter and a conserved large distal regulatory region, classified as a “super enhancer”. Moreover, the *NPPA-NPPB* cluster shares (developmental) enhancers found in the super enhancer region (Man et al., 2018). The switch to the fetal gene program represents a complex regulatory

mechanism observed in cardiac remodeling in which numerous genetic and epigenetic factors are involved (Dirkx et al., 2013) so understanding the molecular mechanisms behind this process is crucial for identifying new therapeutic targets to prevent maladaptive remodeling and improve cardiac function in diseases such as hypertrophic cardiomyopathy and heart failure.

1.5 Cardiac Fibrosis

Cardiac fibrosis is characterized by multifactorial processes that involve cellular (Xie et al., 2014) and molecular mediators (Li et al., 2013) leading to accumulation of myocardial connective tissue. Among them, the Transforming Growth Factor β1 (TGFβ1) signalling (for collagen synthesis), matrix metalloproteinases (MMPs), and tissue inhibitors of matrix metalloproteinases (TIMPs) play a pivotal role in fibrosis initiation. During this process, the extracellular matrix (ECM) undergoes important modifications due to modified ratios of collagen subtypes and ratio MMPs/TIMPs (Xu et al., 2004). In a goat model, prolonged Atrial Fibrillation (AF) induced by electrical stimulation led to a significant increase in ECM surface area per myocyte and it was reversed after cardioversion (Allessie et., al 2002). The deposition of ECM in myocardial interstitial space is due to excessive proliferation of fibroblasts that differentiate into myofibroblasts, highly specialized synthetic and contractile cells that increase fibrillar collagen, matricellular protein production/secretion, as well as the expression of α-smooth muscle actin (α-SMA, gene name: *ACTA2*) (Frangogiannis, 2018). ECM protein deposition is initially protective and is critical for wound healing and tissue regeneration, but when ECM deposition becomes significant, persistent fibrosis, a common response to chronic inflammation, may ultimately lead to heart failure (Antar et al., 2023). Cardiac fibroblasts (CFs) play an essential role in the cardiac homeostasis and they play an important role in the inflammatory processes that occur within the heart upon acute and chronic injury (van Nieuwenhoven and Turner, 2013). After an injury or inflammation, fibroblasts become activated exhibiting a pronounced collagen production (Figure 3).

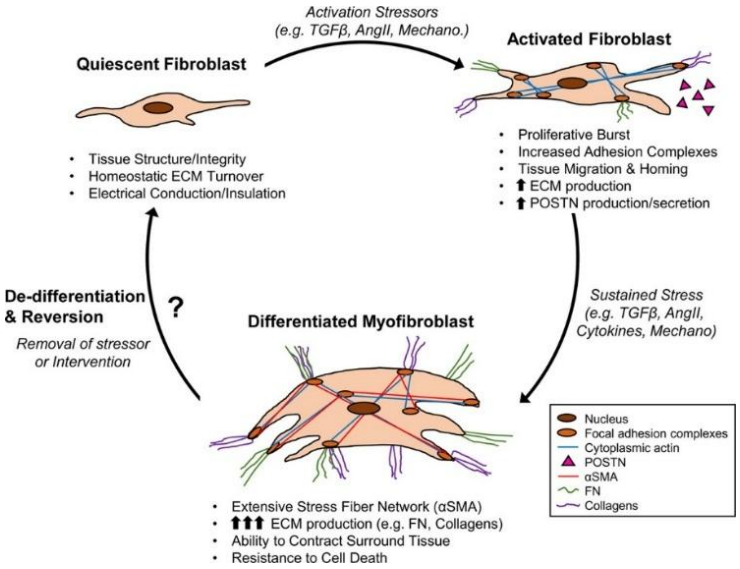

Figure 3. Resident fibroblasts maintain cardiac homeostasis under normal conditions. In response to mechanical stress and profibrotic signals (e.g., TGFβ, AngII), they activate, proliferate, and remodel the ECM. Prolonged activation drives differentiation into myofibroblasts, marked by α-SMA expression and excessive ECM production (FN, collagens). Their resistance to cell death leads to persistent maladaptive remodeling. Emerging evidence suggests myofibroblasts can de-differentiate once stress is removed, but the underlying mechanisms and therapeutic potential remain unclear. *POSTN* indicates periostin (Gibb et al., 2020).

In addition to CFs, various inflammatory cells have been shown to play a role in the profibrotic process, for example it has been observed that during cardiac injury, numerous blood-borne monocytes infiltrate the myocardium and differentiate into macrophages (Kim et al., 2018) that can lead to the production of multiple profibrotic growth factors (IL-10, TGFβ , IGF-1 and PDGF) and pro-inflammatory cytokines (IL-6, TNF-α, ROS). It has been demonstrated that increased serum levels of IL-6 were associated with an increased left atrial size as the result from IL-6 stimulation on matrix-metalloproteinase-2 (MMP2) (Marcus et al.,2008). Other cells of the innate immunity, the mast cells, are involved in cardiac fibrosis: under pressure overload, mast cells multiply and release pre-formed inflammatory and fibrotic (e.g.,

TGFβ 1, TNF, IL-1) mediators. Furthermore, animal studies demonstrated that histamine produced by mast cells play a role in cardiac fibrosis (Zeng et al., 2014). It is well-known that development and progression of atrial fibrosis is the hallmark of structural remodeling in atrial fibrillation and is considered the substrate for AF perpetuation (Dzeshka et al., 2015).

1.5.1 Atrial Fibrillation

Atrial fibrillation (AF) is the most common form of cardiac arrhythmia in Western countries (Hindricks et al., 2021). The prevalence of AF varies from 2% in the general population to 10-12% in older individuals (>70 years of age) (Staerk et al., 2017) and those with lifestyle-related conditions hypertension, diabetes mellitus and obesity. AF occurs when abnormal electrical impulses suddenly start firing in the atria disrupting the heart's natural pacemaker, which can no longer regulate the heart's rhythm. This leads to irregular and often excessively rapid contractions of the ventricles, causing a range of symptoms such as dyspnea, palpitations, irregular heartbeat, shortness of breath, and fatigue (Brundel et al., 2022). AF can be also congenital, in this case the onset occurs at a younger age and often progresses rapidly from persistent to permanent AF (Teuwen et al., 2018). The pathophysiology of AF is complex, involving both increased spontaneous ectopic firing of atrial cells and impulse re-entry through atrial tissue. Its development consists of three key stages: initiation, maintenance and progression to more persistent forms of AF (Wakili et al., 2011). Unlike most arrhythmic conditions, AF is characterized by highly irregular electrical impulses that vary in frequency, direction and duration from beat to beat. This results in significant temporal fluctuations in the timing and morphology of intracardiac atrial electrograms (Atienza et al., 2012).

Atrial Fibrillation and Electrical Remodeling

The electrical impulse of the heart is generated by the controlled influx and efflux of ions through ion channels in the sinoatrial node. During normal sinus rhythm, atrial action potentials (APs) are generated by the voltage-dependent activation of cardiac Na^+ channels, leading to a depolarizing current (INa) that are responsible for the AP upstroke. The activation of L-type Ca^{2+} current (ICa,L) facilitates Ca^{2+} entry, which triggers a significant release of Ca^{2+} from the sarcoplasmic reticulum (SR) through ryanodine receptor channel type 2 (RyR2), resulting in a systolic intracellular Ca^{2+} transient. AP repolarization and duration (APD) are regulated by time-dependent delayed-rectifier K^+ currents, including slow (IKs), rapid (IKr), and ultrarapid (IKur) currents, as well as the transient outward K^+ current (Ito). During diastole, Ca^{2+} is removed from the cell through the electrogenic Na^+/Ca^{2+} exchanger (NCX) type 1, which brings in 3 Na^+ ions for each Ca^{2+} ion expelled, creating a depolarizing inward current. Additionally, Ca^{2+} is reabsorbed into the sarcoplasmic reticulum (SR) via the SR Ca^{2+}-ATPase type 2a (SERCA2a). These processes work together to lower cytosolic Ca^{2+} concentrations and facilitate atrial relaxation during diastole (Heijman et al., 2014). The impulse generated from ions currents in the sinoatrial node travels through Bachmann's bundle from the left to the right atria through gap junctional that directly connect adjacent cells by providing chemical and electrical communication between adjacent myocytes. Then via the atrioventricular node through the bundle of His and two bundle branches in the interventricular septum to the apex of the heart muscle, causing a coordinated contraction in the ventricles circulating the blood through the human body (Denham et al., 2018).

AF may be generated and maintained by a variety of electrophysiological mechanisms (Workman et al. 2008) that are often attributed to either abnormal automaticity (AA) or triggered activity. These ectopic activities represent spontaneous depolarizations of atrial tissue outside the sinoatrial node at rates faster than the sinus rhythm. AA refers to premature firing of action potentials, favored by an increase in diastolic inward, depolarising, ion current (the funny current (If), and potentially L-type Ca^{2+} (ICaL) and Na^+/Ca^{2+} exchanger (NCX) currents) and a decrease in outward, hyperpolarising, currents (K^+ currents). Triggered activity, on the other hand are caused by oscillations in membrane potential following the

upstroke of an action potential, known as afterdepolarizations. These may be delayed afterdepolarizations (DADs), which occur after full repolarization. DADs are favored by high heart rates and excessive intracellular Ca^{2+} (ICa^{2+}) loading (Figure 4) (Workman, 2010). The abnormal atrial conduction during AF is also linked to changes in Na^{+} channels and gap junctions (Yan et al., 2018; et al., 2013). The process of electrical remodeling develops within the first days, but it is reversible upon sinus rhythm (SR) restoration (Schotten et al., 2003).

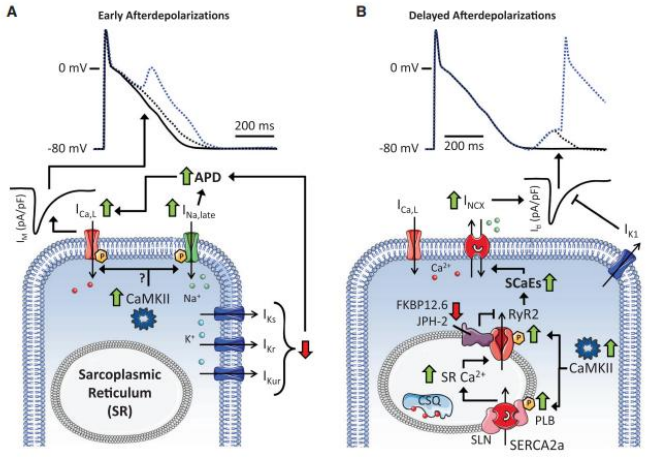

Figure 4. Mechanisms of Early and Delayed Afterdepolarizations. **(A)** Early afterdepolarizations result from prolonged action potential duration (APD) due to reduced repolarizing K^{+} currents (IKs, IKr, IKur) or increased depolarizing currents (INa,late, ICa,L). This allows ICa,L recovery, enhancing inward currents and triggering membrane depolarization during AP phase 2 or 3. **(B)** Delayed afterdepolarizations arise from RyR2 dysfunction due to CaMKII hyperphosphorylation or loss of stabilizing subunits (FKBP12.6, JPH-2), combined with increased SR Ca^{2+} uptake from PLB hyperphosphorylation. This promotes spontaneous SR Ca^{2+} releases (SCaEs), activating NCX and generating a transient-inward current (Iti) that triggers delayed depolarization, counteracted by inward-rectifier K^{+} currents. Abbreviations: CSQ (calsequestrin), IM (membrane current), SERCA2a (SR Ca^{2+}-ATPase type 2a), SLN (sarcolipin). (Heijman et al., 2014).

Atrial Fibrillation and Thrombogenesis

The association between atrial fibrillation and prothrombotic represents well-known evidence (Khan and Lip, 2019). To date the molecular mechanisms underlying the thrombotic events are not yet entirely clear and remain only partially understood. The development of thrombus formation in AF could be influenced by multiple factors like abnormal changes in blood flow/stasis, endothelium alterations and hypercoagulability (Virchow's triad) (Watson et al., 2009). Blood stasis in the atria cavity often occurs after failure of atrial systole or progressive atrial dilatation. Furthermore, the loss of synchronous contractility altered atrial flow velocity and vorticity which is likely to decrease endocardial shear stress. This phenomenon has been demonstrated to reduce the endothelial production of nitric oxide, a substance that facilitates vasodilation and possesses anti-thrombotic properties (Uematsu et al., 1995). The deterioration of endothelial function in atrial cardiomyopathy is also associated to inflammatory processes (Nso et al., 2020) where areas of endothelial denudation may predispose to thrombotic events (Yau et al., 2015). The third element of Virchow's triad is hypercoagulability state, the alterations in fibrin turnover. Abnormal concentration in prothrombotic indices is common in patients with AF (Ohara et al., 2008): plasma von Willebrand factor (vWf) and D-dimer, for example, have been utilized to enhance clinical risk assessment for stroke. Anticoagulant treatment has been shown to reduce concentrations of some prothrombotic markers (Lip et al., 1995; Zeuthen et al., 2003).

1.6 Role of Coagulation Factors in Cardiac structural Remodeling

Cardiac remodeling is also associated with hypercoagulability state that can contribute to profibrotic and pro-inflammatory events (Spronk et al., 2017). This heightened coagulation activity underscores the intricate relationship between cardiovascular alterations and the coagulation cascade. Coagulation cascade can be divided in three different pathways: intrinsic pathway (activated by damage to blood vessels), extrinsic pathway (triggered by external trauma), and the common pathway which together are responsible for the activation and arresting the production of the product fibrin, the main component of

a thrombus (Chaudhry et al., 2023). In particular, two coagulation factors: Thrombin or FIIa and activated Factor X (FXa), are central factors in the common coagulation pathway leading to the formation of Fibrin.

Thrombin is a serine protease that is involved in hemostatic and non hemostatic effects. For hemostatic effects, it can be involved in primary hemostasis activating platelets and the subsequent the release of platelet activators such as adenosine diphosphate, serotonin, and thromboxane A2. While in secondary hemostasis, Thrombin converts fibrinogen into fibrin monomers, which ultimately form a stable clot to stop bleeding at sites of vascular injury. Moreover, Thrombin regulates its own production by forming a complex with the endothelial cell surface receptor thrombomodulin (TM). This complex activates protein C, which becomes activated protein C (APC), the main inhibitor of activated factor V and factor VIII (Bae et al., 2010). FX is activated into FXa by either the extrinsic pathway, involving the tissue factor (TF)-factor VIIa (FVIIa) complex, or the intrinsic pathway, driven by FVIIIa-FIXa (Hertzberg, 1994). Once activated, FXa binds with its cofactor, Factor Va (FVa) and forms proThrombinase, a complex enzyme responsible for converting proThrombin into Thrombin (Mann et al., 1990).

Recently, the discovery that coagulation factors can be also implicated in non hemostatic effects has attracted the attention of many researchers, especially for their role in the activation of CFs and promotion of cardiac remodelling (Spronk et al., 2017; D'Alessandro et al., 2018). Activating FIIa and FXa seems to influence the structure and function of heart cells, particularly cardiac fibroblasts and cardiomyocytes (CMs). This suggests that FIIa and FXa may play a role in initiating and contributing to structural remodeling, inflammation, and fibrosis (D'Alessandro et al., 2022). The non-haemostatic effects are mediated by activation of a family of G protein-coupled receptors, the protease activated receptors (PARs) expressed in many different cell types throughout the body (Posma et al., 2016). PARs are part of the G-protein-coupled receptor (GPCR) family, which are characterized by a single polypeptide chain with seven transmembrane alpha-helices and three intracellular and extracellular loops. The extracellular loops contain the site where ligands bind, while the N-terminal extracellular domain houses a "tethered ligand" that's involved in receptor activation. On the intracellular side, the loops provide binding sites for the G-protein trimer (composed of Gα, Gβ and Gγ subunits), which is key signal transduction (Rosenbaum et al, 2009). During the activation, PARs are proteolytically cleaved at their N-terminal extracellular domain generating a new tethered ligand, which self activates the receptor (Gieseler et al., 2013). The intracellular domains of PARs bind tightly to the Gα and Gβγ subunits of G-proteins stimulating the exchange of GTP for GDP. This process leads to the phosphorylation of the intracellular Gα subunit, causing it to detach from the Gβγ subunit (Gieseler et al., 2013).

The PAR family comprises four different isoforms (*PAR1, PAR2, PAR3* and *PAR4*). Depending on the conditions of PAR activation, Thrombin can have opposing effects on a cell; for instance, it contributes to both anti-inflammatory and pro-inflammatory processes, regulates both endothelial integrity and permeability, and can trigger both vasodilation and vasoconstriction (Ossovskaya and Bunnett, 2004; Alberelli and De Candia, 2014). *PAR1* and *PAR3* have a high affinity for Thrombin, meaning they can be activated by lower Thrombin concentrations (less than 5 nM). In contrast, *PAR4* has a lower affinity for Thrombin and requires higher concentrations for activation (Ossovskaya et al, 2004). *PAR1* and *PAR2* are the most important isoforms in the heart. In a study by D'Alessandro et al., it was shown that *PAR1* activation by Thrombin promotes the expression of profibrotic markers, such as α smooth muscle actin (α-SMA, gene name: *ACTA2*) and *TGFβ*, but also of pro-inflammatory markers, such as *IL-6* and C-C motif chemokine ligand 2 (*CCL2*) in adult rat CFs. Similarly, FXa has been reported to be a strong *in vitro* inducer of pro-inflammatory responses (D'Alessandro, et al., 2018). The complex effects of Thrombin and FXa and their involvement in cardiac remodeling can be further explored using other different systems that comprise new cellular model in 2D and 3D arrangement offering a more physiologically relevant platform to study coagulation factors pro-inflammatory and profibrotic responses in cardiac remodeling.

1.7 Cell Models

1.7.1 Human Embryonic Stem Cells

Human embryonic stem cells (hESCs) are pluripotent cells capable of self-renewal and multiplying indefinitely with an unlimited self-renewal potential. They fulfil all requirements of stem cells: clonality, self renewal and multipotentiality (Garry and Olson, 2006) for *in vitro* applications to generate an unlimited number of distinct cell types opening new avenues for regenerative medicine. During the first 7 days of development, the embryo develops from a fertilized zygote to a blastocyst, a structure that comprises of the epiblast (precursor to the embryo proper), the hypoblast (precursor to the yolk sac), and the trophectoderm (precursor to the embryonic portion of the placenta) (Petropoulos et al., 2016; Molè et al., 2020). The hESCs are obtained from the inner cell mass (ICM) of a human blastocyst and subsequently forms the embryo while the outer layer of trophoblast gives rise to the chorion and amnion, the two fetal membranes that surround the embryo.

For *in vitro* applications, hESCs were first derived from the blastocyst-stage epiblast in 1998 (Thomson et al., 1998). To date, more advances in culturing techniques were developed to culture hESC lines *in vitro* establishing the differentiation of hESCs into various lineages of biologically active cells, including cardiomyocytes, oligodendrocytes and pancreatic β cells (Cohen and Melton, 2011; Fu and Xu, 2011). The ICM has typically been separated from the trophectoderm at the blastocyst stage using immunosurgery or mechanical dissection (Bosma et al., 1983; Cowan et al., 2004; Ellerström et al., 2006). The destruction of the embryo has led to significant ethical and political issues: derivation and even culture of hESC are forbidden by law in some European countries (Hovatta et al., 2010). In the USA, there are limitations for making hESCs when human *in vitro* fertilization (IVF) embryos are destroyed. To overcome these ethical issues, one proposed alternative was to isolate cells from earlier stages of embryonic development without damaging the embryo, but early attempts to remove a single cell at the 8-cell or morula stage produced inconsistent results and necessitated the co-culture of isolated blastomeres with already established hESC lines (Klimanskaya et al., 2007; Strelchenko et al., 2004). Another obstacle is the immune mediated rejection of hESC-derived cells by the recipient because these cells are allogeneic to the recipient patients (Boyd et al., 2012). In addition, therapies with immunosuppression greatly increases the risk for cancer and infection (Gallagher et al., 2010).

Despite the various obstacles and numerous critical issues, hESCs represented a progenitor model useful to understand the basic mechanisms of pluripotency and cell renewal. Over the years new cellular models have been discovered and developed, among these the hiPSCs (human induced pluripotent stem cells) model represents to date one of the most promising and revolutionary advance for multiple scientific and therapeutic applications.

1.7.2 Human Induced Pluripotent Stem Cells and hiPSC-Derived Cardiomyocytes

In 2006, Takahashi and Yamanaka succeeded in transforming the adult mouse fibroblasts into induced pluripotent stem cells (iPSC) using four select transcription factors: Oct4, Sox2, c-Myc and Klf4. One year later the same group demonstrated the generation of iPSCs from adult human dermal fibroblasts with the use of the same four factors (Yamanaka, 2007). Since this discovery, the reprogramming of somatic cells into the embryonic-state-like of iPSC has become a widely used method. One of the major applications of iPSCs is the differentiation into specific cell types. This aspect avoids ethical controversies that hinder the applications of hESCs. The human iPSCs (hiPSCs) are like hESCs in many aspects, including morphology, proliferation, surface markers, gene expression, and *in vitro* differentiation. One of the most exciting applications of stem cells is regenerative medicine: stem cells can differentiate into any kind of cell type and have the potential to completely regenerate the organs. The advent iPSCs technology has enabled the reliable generation of individual-derived cardiomyocytes (CMs) (Yoshida and Yamanaka, 2017). The human iPSC-Derived Cardiomyocytes (hiPSC-CMs) can offer

significant potential in modeling cardiopathological diseases and for use in autologous tissue transplantation. However, despite their promising potential, the hiPSC-CMs more closely resemble cardiomyocytes in their embryonic or fetal stages and exhibit immaturity in terms of marker expression, electrophysiological behavior, ultrastructural characteristics, and metabolic profiles. For example, immature cardiomyocytes use glycolysis for energy metabolism rather than β-oxidation of fatty acids (Nose et al., 2018). "Immaturity" comprises a wide spectrum of fetal-type features, such as automaticity, gene expression patterns (van den Berg et al., 2015) including ion channels (Beqqali et al., 2006), electrophysiological signals, contractile properties at whole cell (Ribeiro et al., 2015) and myofibril level (Pioner et al., 2016). For cardiac differentiation and development of cardiovascular system different signalling pathways like activin/nodal/transforming growth factor β, Wint signaling and bone morphogenetic protein are involved (Evans et al. 2010; Noseda et al., 2011). Recently, different combinations of growth factors and small molecules have been found to enhance the consistency and efficiency of hiPSC-CM differentiation protocols (Kattman et al., 2011). An interesting aspect is related to the heterogeneous pool of atrial, ventricular, and nodal-like cell population obtained post-differentiation. In this respect, recent reports suggest that pluripotent stem cells could be directed either to atrial-like or to ventricular-like cardiomyocytes by modulating the retinoic acid (Devalla et al., 2015) and Wnt signaling pathways (Karakikes et al., 2013).

Cardiac muscle cells take 6 to 10 years *in vivo* to reach their adult phenotype. A logical strategy to obtain more mature cardiomyocytes is long-term culture. At later stages (80-100 days post-differentiation), healthy hiPSC-CMs exhibit a significant increase in cell aspect *ratio* and myofibril alignment, along with the emergence of caveolae, transverse (T) tubules, and sarcomere protein isoforms typically absent at earlier stages (Pioner et al., 2020). Another key approach is the use of chemical compounds that inhibit Wnt signaling, enhancing differentiation (Ren et al., 2011). Burridge et al. (2014) further refined this process by developing a three-stage system with chemically defined factors, eliminating the need for serum. Combining these strategies has significantly improved hiPSC-derived cardiomyocyte maturation and functionality. A particularly promising direction is the development of engineered heart tissues (EHTs), which provide a physiologically relevant environment by integrating biomechanical and biochemical cues, further enhancing structural and functional properties.

1.7.3 Engineered Heart Tissue (EHTs)

2D cell cultures represent a fundamental model for understanding the molecular mechanisms underlying numerous cellular processes in physiological and pathological conditions. However, this cannot reliably reproduce the molecular and cellular interactions that occur *in vivo* in a three-dimensional system. For this reason, scientific research in recent years has been developing increasingly accurate three-dimensional cellular models that allow a better understanding of the interactions between cells and the extracellular matrix and between different cell populations residing within the same organ. Furthermore, this approach can help hiPSC-CMs maturation. During their maturation *in vivo*, cardiomyocytes are continuously exposed to cyclic mechanical strain induced by the rhythmic beating of the heart so seeding immature cardiomyocytes into a suitable 3D matrix subjected to mechanical stress can promote their development (Ronaldson-Bouchard et al., 2019).

In general, designing an engineered tissue requires creating a scaffold, incorporating the cell type, and culturing the "tissue'' *in vitro*. The scaffold can derive from different matrix such as biodegradable synthetic polymers (Lesman et al., 2010; Madden et al., 2010), natural matrix proteins (Shachar et al., 2011) or no exogenous scaffold.

Over the years, several Engineered Heart Tissue (EHTs) models have been developed; one of these involved the generation of fibrin- EHT in strip format. This approach follows a general hydrogel-based tissue engineering strategy, which requires cardiomyocytes, a liquid matrix capable of gel formation, a casting mold, and a structural support system to stabilize the developing tissue. In this specific

protocol, fibrin is used as the extracellular matrix. A prepared mixture of freshly isolated cells, culture medium, fibrinogen and Thrombin are pipetted into the mold, where it undergoes polymerization over approximately 2 hours, forming a fibrin-based cell construct around the silicone posts. During tissue formation, fibrinogen is converted to fibrin by Thrombin, and the resulting gel must be soaked in aprotinin-supplemented medium to prevent proteolytic degradation (Schaaf et al., 2014). Other 3D arrangements include EHTs that form rings of tissue, in this case cardiomyocytes are embedded in a collagen-hydrogel into circular casting molds to create chamber-specific, ring-shaped (Ploeg et al., 2022; Goldfracht et al., 2020). In general, the 3D system more closely mimics intact myocardium compared to 2D hiPSC-CMs, often exhibiting densely interconnected elongated cells and higher proportion of multinucleated cardiomyocytes. This includes densely packed, aligned sarcomeres, numerous organized mitochondria and, in some cases, the development of T-tubule systems (de Lange et al., 2021).

Another interesting model is the EHT co-cultures consisting in the incorporation of non-myocyte cell types, such as cardiac fibroblasts or endothelial cells into EHTs and cardiomyocytes. It was noticed that the interaction of different kind of cells seeded in the same 3D matrix can help better recapitulate the cell-to-cell and cell-to-matrix interactions present in the human myocardium. As demonstrated in Cumberland et al.'s study, the subsequent integration of the cells into co-culture EHTs resulted in improved contractile function (Cumberland et al., 2024). EHTs that included cardiac fibroblasts from hiPCs (hiPSC-CFs) and hiPSC-CMs showed increased tissue compaction, crucial for determining the contractile ability, after just 72 hours in culture and a decrease in beat rate after two weeks in culture (Rivera-Arbeláez et al., 2022). The decrease in beat rate is likely attributed to increased maturity of the cardiomyocytes and a reduction in the expression of the funny current (Ronaldson-Bouchard et al., 2018). In a study conducted by Windt et al., EHT co-cultures containing hiPSC-CMs (70%), hiPSC-CFs (15%), and endothelial cells (ECs) from hiPSC (hiPSC-ECs) (15%) were developed. In this model it emerged that all cell types in the co-culture were able to contribute to the maturation of cardiomyocytes. For example, the ECs synthesize endothelin -1 which binds the receptor on the CMs allows the activation of adelinate cyclase and the increase in intracellular cyclic adenosine monophosphate (cAMP) levels, furthermore the ECs produce nitric oxide (NO) that activates the cyclic guanosine monophosphate (cGMP) in cardiac fibroblasts which is transferred through cell junctions in CMs and contribute to increasing intracellular cAMP. These pathways are involved in the processes of cardiac maturation and differentiation (Windt et al., 2023).

These advancements in engineered heart tissue models not only provide valuable insights into cardiac maturation and function but also pave the way for more physiologically relevant platforms for disease modeling, drug testing and potential therapeutic applications.

1.8 Aim

The PhD Project originates from a Collaboration between the Department of Physiology at the University of Florence and the Department of Physiology at Maastricht University. Throughout this Project, numerous experiments are conducted to characterize *in vitro* cellular models, such as human Embryonic Stem Cell-derived Cardiac Fibroblasts (hESC-CFs), human induced Pluripotent Stem Cell-derived Cardiomyocytes (hiPSC-CMs) and three-dimensional Engineered Heart Tissues (EHTs), at both the molecular and morphological/structural levels.

In **Chapter 3** a characterization of hESC-CFs model is provided: basal levels of specific fibroblast markers are evaluated, along with the expression levels of stem cell markers at different timepoints of the differentiation protocol. Additionally, the characterization of this model includes the study of the effects of *TGFβ*, a well-known factor that plays a crucial role in fibrosis and extracellular matrix remodeling. In the same Chapter we investigate the effects of two coagulation factors, FXa and Thrombin, on the activation of hESC-CFs. One of the goals of this study is to verify the effect of coagulation factors on this cellular model which could determine whether cardiac fibroblasts derived from embryonic stem cells represent a reliable model for studying the effects of coagulation factors in the context of cardiac fibrosis and inflammation.

In **Chapter 4** a basic characterization of hiPSC-CMs model is performed: the baseline expression levels of key marker genes associated with mature cardiomyocytes are measured at different timepoints post-differentiation. Furthermore, imaging studies are carried out on cardiomyocytes derived from beating monolayers to assess the development of sarcomere structure. In the second part of this Chapter, we investigate the possible pro-hypertrophic effect of FXa and Thrombin on hiPSC-CMs. Furthermore, we characterize the role of PAR, a G-protein-coupled receptor whose activation appears to play a central role in non-hemostatic processes mediated by FXa and Thrombin. To assess the impact of these factors, post-incubation responses are evaluated by analyzing changes in the gene expression of key pro-hypertrophic markers. Additionally, the levels of B-type natriuretic peptide (BNP), a well-established biomarker of cardiac hypertrophy, secreted into the culture medium are measured.

In **Chapter 5** we provide a preliminary characterization of EHT model from both molecular and structural perspective, aiming to improve its physiological relevance and functionality. Initially, we characterize hESC-CFs EHTs using different culture media to determine the optimal conditions for long-term culture. Subsequently, we provide a hESC-CFs and human Embryonic Stem Cells-derived Cardiomyocytes (hESC-CMs) co-culture, assessing cell density at different timepoints and examining the spatial distribution of the cells along the ring structure.

Overall, the aim of this thesis is to evaluate the reliability of these *in vitro* models and use them as a valid tool for understanding the molecular mechanisms underlying several cardiac diseases, such as fibrosis, inflammation and cardiac hypertrophy. This research is driven by the need to develop increasingly reliable and effective models that can accurately replicate the structure and environment of *in vivo* conditions. Furthermore, this thesis provides a better understanding of the non-hemostatic effects exerted by coagulation factors like Thrombin and activated Factor X through PAR receptor activation, with the goal of identifying new therapeutic targets to prevent or treat cardiac diseases.

Chapter 2

Materials and Methods

2.1 HESC-CFs culture

2.1.1 HESC-CFs Differentiation Protocol

Cardiac fibroblasts were obtained from HUES9 line, human embryonic stem cells generated by Harvard Stem Cell Institute (Cowan et al., 2004). The protocol of differentiation has been described previously (Zhang et al., 2019) and was performed by the Genetics Department of Maastricht University. This method provides sequential Wnt activation and basic fibroblast growth factor (bFGF) support that at specific stages of differentiation can effectively drive human embrionic stem cells (hESCs) into cardiac fibroblasts (CFs) through second heart field progenitors (SHFPs) (Figure 5). The derived hESC-CFs share key characteristics with native human CFs, including gene expression profiles, cell morphology, proliferation rates, extracellular matrix (ECM) production and the ability to transform into myofibroblasts (Zhang et al., 2019).

Protocol in short: HUES9 stem cells were dissociated using 1ml/well Versene solution (Gibco) at 37 °C for 5 minutes and seeded on Matrigel (GFR, BD Biosciences) coated 6-well plates at the density of 1.5–2.0 × 10^6 cells/well in mTeSR1 medium supplemented with 10 µM ROCK inhibitor (Y-27632) (Tocris). Cells were cultured in mTeSR1 medium for 5-6 days with daily medium changes until reaching full confluence (100%). *Day 0*. The cells underwent a medium change to RPMI 1640 (ThermoFisher® #21875158) + B27 (ThermoFisher® #A18956-01) without insulin (Gibco) supplemented with 12 µM CHIR99021(Tocris), for Wnt pathway activation. Cells were incubated in this medium for 24 hours (until day 1). *Day 1*. The medium was changed to 2.5 ml RPMI + B27 without insulin (Gibco) and cells were cultured in this medium for 24 h (day 2). *Day 2*. The medium was changed to 2,5 ml of cardiac fibroblast growth medium (CFGM-bFGF) containing DMEM (22320, Gibco, Invitrogen, Breda, the Netherlands) to which we added 10% (v/v) fetal bovine serum (FBS, Gibco), gentamicin (50 µg/ml, Gibco), 1% (v/v) insulin-transferrin-selenium-sodium Pyruvate (ITS-A , Gibco) and high concentration of bFGF (75 ng/ml, Gibco). *Days 4-20*. The cells were supplemented with CFGM and bFGF every other day. *Day 20*. The cells were detached and plated on non-coated cell culture plates and cultured in CFGM (same as above but bFGF 1 ng/ml). An overall timeline of the differentiation process of hESC-CFs is descripted below in Figure 5.

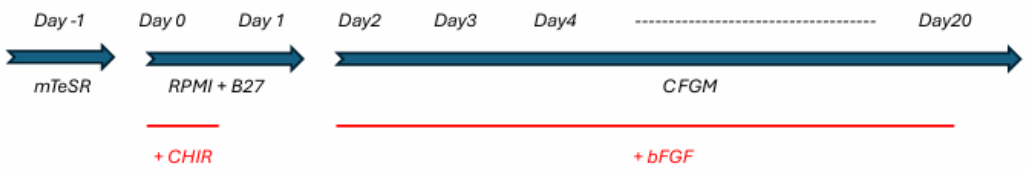

Figure 5. Differentiation Protocol of hESCs to hESC-CFs. Abbreviations: CHIR: CHIR99021; CFGM: cardiac fibroblast growth medium; bFGF: basic fibroblast growth factor.

2.1.2 HESC-CFs Culturing Protocol

The hESC-CFs were cultured in CFs growth medium (CFGM) with a cell density of 30.000 cells/cm^2. A detailed description of the medium components is provided in Table 2. The medium was changed every 2 days. hESC-CFs were cultured in a T175 2D culture flask (Cellstar, Greiner Bio-One, Frickenhausen, Germany) to scale up cell quantity until a confluency around 80% was reached. At that point, cells were dissociated with Accutase (ThermoFisher® #11599686) and counted with a hemacytometer and Erythrosine B dye, then collected by centrifugation before being sub-cultured or plated for an experiment. In the current research Project, we used 4 separate differentiations: PSC018, PSC019, PSC020, PSC021.

Table 2. Composition of the CFGM medium and catalog numbers.

Medium	Composition
CFs Growth Medium (CFGM)	DMEM (ThermoFisher® #22320)
	Fetal bovine serum (FBS) 10% (ThermoFisher® #10500064)
	Insulin-transferrin-selenium-sodium Pyruvate 1% (ThermoFisher® #51300044)
	Basic fibroblast growth factor 1 ng/ mL (ThermoFisher® #100-18B 1MG)
	Vitamin C (Vit C) 500 µM (Sigma® #A4403-100MG)
	Gentamicin 50 µg/ mL (ThermoFisher® #15750-037)

The Figure 6 shows the different confluency levels of hESC-CFs cells in culture. The first image (Figure 6, A) depicts the cells right after seeding (30% confluency), where they appear poorly attached, with many floating and non-adherent cells (mostly round). After a couple of days, confluency increases to approximately 70-80%, with cells now adhering to the surface and displaying various cellular extensions. There are fewer floating cells, and their distribution is more homogeneous (Figure 6, B). In the last image, the cells have almost completely covered the surface of the flask, with confluency estimated to be around 90%. At this stage, it is necessary to collect the cells and transfer them to a larger flask (Figure 6, C).

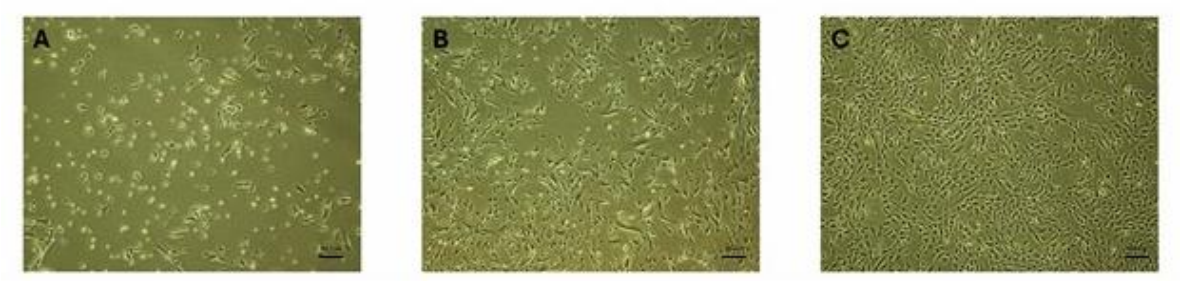

Figure 6. Progression of hESC-CFs confluency in culture. **(A)** Cells after seeding (~30% confluency) with many floating, non-adherent cells. **(B)** Adherent cells with extensions and a more homogeneous distribution (~80% confluency). **(C)** Near-complete surface coverage, requiring passaging (~90% confluency).

2.1.3 Incubation with *TGFβ* and Coagulation Factors

HESC-CFs were differentiated as previous described and then cultured in CFGM with a cell density of 30.000 cells/cm^2 until they reached a confluency of 80%. When the confluency was around 80% the cells were plated in 12 multiwell plate. A day after, hESC-CFs were incubated in serum-free medium containing vitamin C (Sigma® #A4403-100MG) and gentamycin (ThermoFisher® #15750-037) for 24 hours to avoid the proliferative activity of the cells. Then, the cells were incubated either 4 or 24 hours with different *stimuli*: *TGFβ* (1 ng/mL, R&D Systems), a canonic fibrotic marker for fibroblasts; human purified Thrombin or FIIa (0.008 nM, Hyphen, Biomed); human purified FXa (50 nM, Hyphen, Biomed) at two different concentrations (50 nM and 10 nM). In the experiments conducted by D'Alessandro et al. on primary cultures it was seen that the exposure to hFXa up-regulated pro-inflammatory and profibrotic genes at 4 hours (D'Alessandro et al., 2021). In that experiment, 4 hours of incubation with FIIa increased the gene expression of *CCL2* and this induction was still significantly increased at 24 hours, although it was not as strong as the earlier timepoint while *IL-6* expression was also up-regulated by FXa at both timepoints. Table 3 shows the incubation reagents used for these experiments.

Table 3. Incubation Factors of hESC-CFs experiments.

Stimuli hESC-CFs	Function	Work solution
FXa	Coagulation Factor	10 nM or 50 nM
FIIa	Coagulation Factor	0.008 nM
Transforming Growth Factor β (*TGFβ*)	Inducing fibroblasts differentiation in myofibroblast	1 ng/mL

2.2 HiPSC-CMs culture

The hiPSC cells (WTC11 from Corriel Institute) used for these experiments were sent from the University of Florence (Department of Physiology) where they were differentiated into cardiomyocytes. In a subsequent phase of the Project, the differentiation protocol was carried out directly in Maastricht University (Department of Physiology).

2.2.1 Florence hiPSC-CMs Differentiation Protocol

Undifferentiated hiPSC cells were expanded under serum-free conditions in mTeSR medium (StemCell Technologies) on a Corning® Matrigel hESC-Qualified Matrix (StemCell Technologies), at 37°C, 5% CO_2. For cardiac differentiation, a monolayer directed differentiation protocol was applied using the cardiac PSC Cardiomyocyte Differentiation Kit (Life Technologies). Reaching a confluence of 70-80%, hiPSC colonies were chemically dissociated using Tryple 1X (Life Technologies) and incubated at 37° C for approximately 3-5 minutes, until cells rounded up and detached. The cell suspension was centrifuged at 200 x g for 4 minutes at room temperature and the pellet was resuspended in the appropriate volume of mTeSR with 5μM of Y-27632 ROCK inhibitor (StemCell Technologies). The single cells were seeded in each well of a 24-well plate at cell density of 60,000-80,000 cell/well; after 24 hours, the cells reached 5-15% confluence and the mTeSR medium was changed, without the addition of ROCK inhibitor.
Protocol in short: Day 0. At 70% of confluency (~2 days after dissociation) the medium was changed to Cardiomyocyte Differentiation Medium A (Mesoderm Induction) (referred to as day 0 of the differentiation protocol). This medium contains specific growth factors (e.g., BMP4, Activin A). The cells were incubated for 2 days to induce mesoderm formation. *Day 2*. Two days later, Medium A was replaced with Cardiomyocyte Differentiation Medium B. This medium can promote cardiac lineage commitment. *Day 4*. After a further 2 days the medium was replaced with Cardiomyocyte Differentiation Medium C, which was subsequently changed every 2 days, until spontaneously beating appear (day 8 of differentiation). *Day 12*. Medium C was replaced with cardiomyocyte medium (CM RPMI: RPMI medium 1640(1x) + GlutaMAX™ #61870 Gibco Thermofisher + B27™ supplement (50x) (#17504044, 17504001 Gibco Thermofisher) + Penicillin/Streptomycin (Gibco)). Differentiated cells can be cultured until day 12-15 for dissociation and/or cryopreservation, as beyond this time cells are difficult to harvest and recover. Alternatively, the cardiomyocytes can be maintained for a month or more for long-term studies.
Beating monolayers were pre-incubated with CM RPMI with Y-27632 ROCK inhibitor (1:1000) 1h before dissociation of single cells. Monolayers were chemically digested at day 15 using Tryple 1X for 10-15 minutes at 37 °C. Single cells are harvested and pelleted in CM RPMI plus 50% fetal bovine serum (FBS). Single hiPSC-CMs are replaced in CM RPMI plus 10% FBS and Y-27632 ROCK inhibitor. For the experiments in this thesis, beating monolayer was kept in culture for an average of 30-40 days and then frozen at -80 °C at the University of Florence and subsequently shipped to Maastricht University. Here the cells were first stored in liquid nitrogen and subsequently thawed and plated in 24 multiwell-plate. Before plating the cells, the multiwells were treated for 24 hours with Matrigel coating. Then, the cells

were plated with CM RPMI. A schematic representation of the differentiation protocol is shown in Figure 7, which also includes images of the cells transitioning from stem cells to cardiomyocytes.

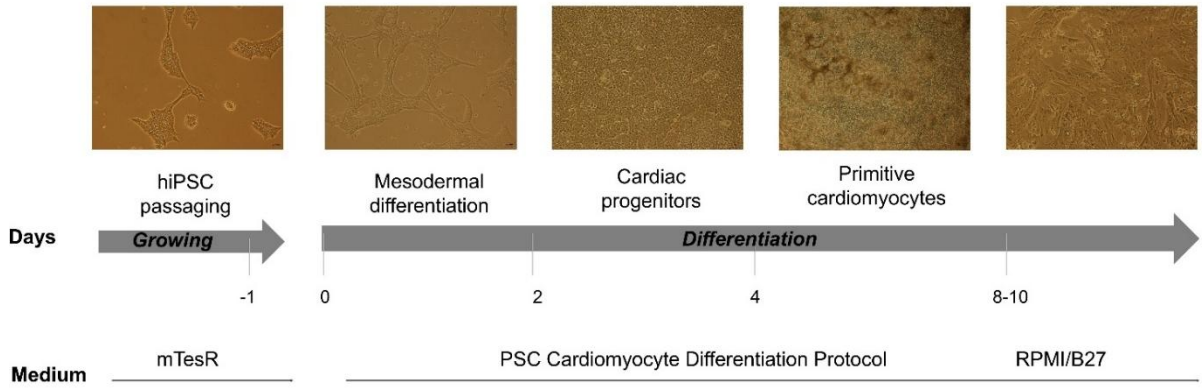

Figure 7. Cardiomyocyte differentiation Protocol from human induced pluripotent stem cells (hiPSCs).

2.2.2 Maastricht hiPSC-CMs Differentiation Protocol

Human iPSC line (WTC11, Coriell Institute for Medical Research, UCSFi001-A) were cultured in mTesR1 (StemCell Technologies) supplemented with Penicillin/Streptomycin (Gibco). Cells were seeded on Matrigel (Corning; 1:100 diluted in DMEM/F12 GlutaMAX ™, Gibco) and passaged twice a week using Fasudil (5μM, LC Laboratories). For passage, cells were washed with DPBS (Life Technologies) and detached with Accutase (Sigma-Aldrich) thereafter. The protocols for differentiating atrial cardiomyocytes (aCMs) and ventricular cardiomyocytes (vCMs) were adapted from Ncardia's proprietary vCMs differentiation method as previously described (Hutschalik et al., 2024).

Protocol in short: *Day -1*. WTC11 cells were seeded in monolayers at 74,000 cells/cm^2 on Matrigel (Corning) in mTesR1 at 1:100 dilution. *Day 0.* cardiac mesoderm was induced by switching to a cardiac differentiation medium (Ncardia) containing small molecules that modulate Wnt pathway activity. To induce the atrial subtype, Retinoic Acid (RA) was added to the medium. Every 2-3 days. Medium was changed. *Day 14.* Cells were dissociated with TrypLE Select (1x) (Life Technologies) and cryopreserved in cardiac cryopreservation medium (Ncardia) containing 10% DMSO (Sigma-Aldrich).

2.2.3 HiPSC-CMs Culturing Protocol

The hiPSC-CMs were cultured in 500 μL of CM RPMI using 100,000 cells/cm^2 in 24-well plate. Culturing hiPSC-CMs requires providing wells with a Matrigel® coating (Matrigel® hESC Qualified Matrix, Corning®) to enhance cell attachment. The Matrigel® coating solution was made with DMEM-F12 + GlutaMAX™ (ThermoFisher® #31331028) and incubated in the wells for 24 hours. HiPSC-CMs were thawed and collected in a stop solution (50% CM RPMI and 50% FBS) to dilute DMSO in the freezing medium. The stop solution was replaced by a plating solution composed of CM RPMI medium containing 10% FBS and 5μM of Rock Inhibitor (RI). RI enhances hiPSC-CMs to attach to the Matrigel® coating. Hereafter, the amount RI was gradually lowered by changing medium for 50% after one day and 100% after 2 days with CM RPMI. The medium was refreshed every other day.

2.2.4 Incubation with Coagulation Factors

The hiPSC-CMs were cultured in CM RPMI medium (100,000 cells/cm^2 in a 24-well plate). After thawing hiPSC-CMs started to beat within 7 days. Between 7-10 days after thawing, beating hiPSC-CMs were incubated for 24 hours using following *stimuli*: human purified Thrombin (0.008 nM, Hyphen, Biomed); human purified FXa (50 nM, Hyphen, Biomed); *PAR1* agonist (100 μM, TRAP14, Bachem); *PAR1* antagonist (1 μM, SCH79797, Tocris, Bioscience). FXa and Thrombin were incubated with their

respective inhibitors, Rivaroxaban (400 ng/mL, Bayer) and Dabigatran (350 ng/mL, Boehringer Ingelheim) for 10 minutes before addition to the cells. Hereafter, the cells were harvested in PBS and then collected in TRK lysis buffer (BioTek®) and β-mercaptoethanol. Prior to proceeding with cell lysis, the culture medium, following 24 hours of treatment with those factors, was preserved for subsequent ELISA assay analysis. Table 4 shows the incubation reagents used for these experiments.

Table 4. Incubation Factors of hiPSC-CMs experiments.

Stimuli hiPSC-CMs	Function	Work solution
FXa	Coagulation Factor	10 nM or 50 nM
FIIa	Coagulation Factor	0.008 nM
TRAP14	*PAR1* Agonist	100 µM
Rivaroxaban (Riva)	hFXa Inhibitor	400 ng/mL
Dabigatran (Dabi)	FIIa Inhibitor	350 ng/mL

2.3 Human BNP assay

Human B-type Natriuretic Peptide (BNP) levels were quantified using the Invitrogen Human BNP ELISA kit, following the manufacturer's protocol. Briefly, 50 µL of standard curve, controls, and samples were added to a 96-well plate pre-coated with anti-BNP antibody, followed by the addition of 50 µL of the detection antibody. The plate was incubated for 2 hours at room temperature (RT) with gentle shaking. After incubation, wells were washed four times with wash buffer to remove unbound substances. Subsequently, 100 µL of the TMB (3,3',5,5'-tetramethylbenzidine) substrate solution was added to each well, and the plate was incubated for 15 minutes in the dark at RT. The reaction was stopped by adding 100 µL of stop solution to each well, and absorbance was measured at 450 nm using a microplate reader. BNP concentrations in samples were calculated based on the standard curve generated in each assay.

2.4 The 3D Engineered Heart Tissue (EHT)

2.4.1 Assembly of the Ring Formation Molds

3D ring cultures were created in silicone polydimethylsiloxane (PDMS) molds (Figure 8). Sylgard-184 silicone elastomer base and curing agent (Dow Chemical, Midland, MI, USA) were mixed and poured into a well of a 12-well culture plate. Custom made 3D-printed casts (Maastricht, The Netherlands) were used to provide the shape with an outer diameter of 22 mm. An area with a 12 mm diameter was created to load 250 µL of gel. A 2 mm central pole created the ring shape. The mold was allowed to be cured at room temperature for 3 days after which the 3D-printed casts were removed. The custom-made molds were cleaned and sterilized by autoclavation.

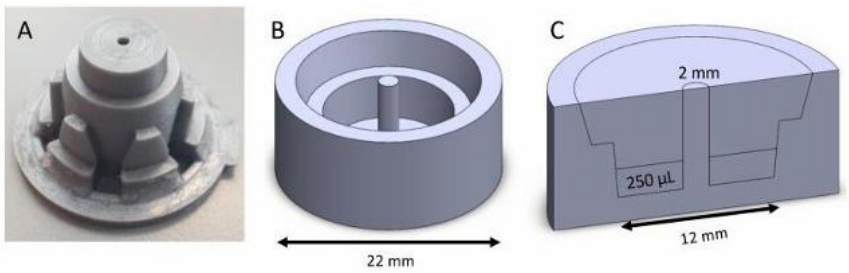

Figure 8. Silicone mold design. Custom-made 3D-printed casts provide the shape for the silicone mold (left); the silicone mold has a diameter of 22 mm (middle) and a centrally placed post of 2 mm (right).

2.4.2 HESC-CFs 3D rings

In the initial phase, we developed hESC-CFs 3D Engineered Heart Tissues (EHTs) in a ring-shaped according to the Protocol based on Ploeg et al. publication (Ploeg et al., 2022). In this part specific culture medium for hESC-CFs was tested to optimize cell viability: hESC-CFs were cultured as previously described in cardiac fibroblast growth medium (CFGM) containing DMEM (22320, Gibco, Invitrogen, Breda, the Netherlands) supplemented with 10% (v/v) fetal bovine serum (FBS, Gibco), gentamicin (50 µg/ml, Gibco), 1% (v/v) Insulin-Transferrin-Selenium-Sodium Pyruvate (ITS-A , Gibco), bFGF (1 ng/ml, Gibco) and vitamin C (500 uM, Sigma Aldrich, Saint Louis, MO, USA) on standard cell culture flasks (Cellstar, Greiner Bio-One, Frickenhausen, Germany). When hESC-CFs reached 80-90% confluency, they were detached using Accutase (ThermoFisher® #11599686) and taken up in CFGM medium. Cells were centrifuged for 5 minutes at 200 x g and then resuspended in hydrogel (composition and concentrations are detailed in Table 5) and transferred in an Eppendorf on ice. The hydrogel-cell mixture (250 µL) was reverse pipetted into the molds and put into a 5% CO_2 incubator at 37 °C. After approximately 1 hour, to polymerize the collagen, 500 µL of hESC-CFs CFGM with 1% FBS was added on top of the gels. Each 3D ring was prepared with a 250 µL matrix suspension containing 1,000,000 hESC-CFs, resulting in a total cell density of 4,000,000 cells/mL.

To assess and compare the stability and the viability of the hESC-CFs in 3D cultures, hESC-CF 3D rings were kept in culture using specific cardiac fibroblast medium (CFGM supplemented with serum 1% and CFGM supplemented with serum 10% respectively) and specific cardiomyocyte medium (CM RPMI: RPMI medium 1640(1x) + GlutaMAX™ #61870 Gibco Thermofisher + B27™ supplement (50x) (#17504044, 17504001 Gibco Thermofisher) + Penicillin/Streptomycin (Gibco)). In CM RPMI medium 500 µM of vitamin C was added. The medium was changed every other day because of a higher metabolic rate. Multiple culture timepoints were selected: 1 day, 7 days and 14 days during these experiments. After the timepoint was reached the 3D rings were harvested by first washing in PBS and then collected in TRK lysis buffer (BioTek®) and β-mercaptoethanol. Subsequently, the 3D rings were homogenized using the ultra-thurax (Dijkstra Vereenigde b.v.) and stored at -20 °C.

Table 5. Composition of the 3D hESC-CFs rings.

Compound	Volume per Ring in µL	Final concentration
Collagen stock (4.24 mg/mL)	88	1.5 mg/mL
Corning® Matrigel® stock (10 mg/mL)	25	1 mg/mL
DMEM (10x)	25	1x
Sodium bicarbonate ($NaHCO_3$) (20x)	12.5	1x
Sterile water	97	
hESC-CFs	1,000,000	4,000,000/mL
FBS	2.5	1%
Total volume (µl)	**250**	

2.4.3 Co-culture hESC-CFs hiPSC-CMs Engineering 3D Rings

Subsequently we combined hESC-CFs and hESC-CMs and co-cultured them in Engineering 3D rings to mimic the human myocardium environment. 3D co-culture rings were cultured in CM RPMI with the addition of vitamin C (500μM). The culture medium was changed every day because of a higher metabolic rate. The 3D EHT co-culture rings were cultured for one week. After the timepoint was reached the 3D rings were harvested by first washing in PBS and then collected in TRK lysis buffer (BioTek®) and β-mercaptoethanol. Subsequently, the 3D rings were homogenized using the ultra-thurax and stored at -20 °C.

2.5 Gene expression analysis

Total RNA was collected using the Micro-Elute Total RNA kit (Omega-Bio-Tek, Norcross, GA, USA). The RNA samples were reverse transcribed into cDNA with the use of iscript cDNA synthesis kit (Biorad, Hercules, CA, USA) according to the manufacturer's protocol. Gene expression levels were measured with a CFX96 Touch Real-Time quantitative PCR (RT-qPCR) detection system (BioRad) and SYBR Green Supermix technology (BioRad). RT-qPCR reactions were performed according to the manufacturer's instructions, the samples containing 7.5 mL SYBR Green, 1μL primer, 1.5 μL nuclease free water and 5 μl diluted cDNA. The Biorad protocols mixtures of RT-qPCR were at temperatures of 60 ºC or 62 ºC depending on the gene used. The mixtures were first incubated at 95 ºC for 2 minutes, followed by 95 ºC for 15 seconds and then 60 or 62 ºC for 30 seconds. The two last steps were repeated 40 times. For the analysis, expression levels were normalized for Cyclophilin-A and calculated using the comparative threshold cycle method (ΔCt).

To evaluate the PCR reactions the real time graphs and Ct values were analyzed using Microsoft Excel (Redmond, USA). The fold change was calculated by the ΔCt method: *2^Ct (reference gene) - Ct (target)*. The RT-qPCR protocol includes a no template control and performs a melt curve program that indicates specificity within the reaction. The cDNA samples were stored at - 80 °C. Results are expressed as fold-change relative to control. The sequences of the specific primers used are provided in Table 6.

Table 6. Description of the main genes investigated and the sequences of primers used for PCR amplification.

Gene	Description	Forward primer	Reverse primer
Reference gene			
CYPA (Cyclophilin A)	A ubiquitously distributed protein belonging to the immunophilin family used as housekeeping gene (Nigro et al., 2013).	CCCACCGTGTTCTTCGACAT	CCAGTGCTCAGAGCAGAA
Pro-inflammatory markers			
CCL2 (Monocyte Chemotactic Protein-1: MCP1)	Chemokine involved in immunoregulatory and inflammatory processes (Catalán et al., 2018).	CAGCCAGATGCAATCAATGCC	TGGAATCCTGAACCCACTTCT
IL-6 (Interleukin-6)	Cytokine involved in inflammation and maturation of B cells. The protein is primarily produced at sites of acute and chronic inflammation, where it is secreted into the serum and induces a transcriptional inflammatory response through interleukin 6 receptor, alpha (Tanaka et al., 2014).	AGTCCTGATCCAGTTCCTGC	CTGGCATTTGTGGTTGGGTC

Profibrotic markers			
ACTA2 (Actin α 2, Smooth Muscle)	Highly expressed in mature myofibroblasts (Shinde et al., 2017).	TGTGCTGGACTCTGGAGATG	GAAGGAATAGCCACGCTCAG
CTGF (Cellular Communication Network Factor 2: CCN2)	Protein expression is induced upon TGF-β. CTGF triggers several cellular processes that is associated with cardiac fibrosis (Chen et al., 2000)	CACAGAGTGGAGCGCCTGTTC	GATGCACTTTTTGCCCTTCTTAATG
TGFβ-1 (Transforming Growth Factor, β-1)	Crucial for fibroblast-to-myofibroblast conversion in fibrotic tissues (Frangogiannis, 2018).	CGACTCGCCAGAGTGGTTAT	GTGAACCCGTTGATGTCCA
COL1A1 (Collagen, Type i, Alpha-1)	Abundantly secreted in CFs. An increased COL1A1 secretion is a well- known characteristic of myofibroblasts (D'Alessandro et al., 2021).	AACAGCCGCTTCACCTACAG	GGAGGTCTTGGTGGTTTTGT
POSTN (Periostin)	Extracellular matrix protein. Marker for fibroblasts activation. Upregulated during cardiac injury and supports differentiation into myofibroblasts (Ivey and Tallquist, 2016).	TGCGGGAAGAAAACCACTGT	TAGTGTTGAGTGGTCGTGGC
VIM (Vimentin)	Intermediate filament protein. Well-established marker for mature CFs (Ivey and Tallquist, 2016).	ATTCCACTTTGCGTTCAAGG	CTTCAGAGAGAGGAAGCCG
Cardiac markers			
MYH7 (β Myosin Heavy Chain)	Beta (or slow) heavy chain subunit of cardiac myosin expressed predominantly in the cardiac ventricles and slow skeletal (type 1) myofibers (Beecroft et al., 2019).	AGACACACTTGAGTAGCCCA	TCTTGAGGTCAAAAGGCCTGG
MYH6 (α Myosin Heavy Chain)	Alpha heavy chain subunit of cardiac myosin, a fast ATPase primarily expressed in atrial tissue. The level of expression of fetal and adult MYH genes varies throughout the life span of the animal (OMIM * 160710).	CCGTGAAGGGATAACCAGGG	GCTCCTTCTCTGACTTGCGG
TNNT2 (Troponin 2)	Cardiac isoform of troponin T, the tropomyosin-binding subunit of the troponin complex, which is located on the thin filament of striated muscles and regulates muscle contraction in response to alterations in intracellular calcium ion concentration (OMIM * 191045).	AGCGGAAAAGTGGGAAGAGG	CACAGCTCCTTGGCCTTCTC
TNNI3 (Troponin I)	One of 3 subunits that form the troponin complex of the thin filaments of striated muscle (OMIM * 191044).	AGACTGGCGGAAGAACATCG	CAGTAGGCAGGAAGGCTCAG
Hypertrophic markers			

NPPA (Natriuretic Peptide Precursor A)	Important biomarkers in clinical cardiology. Both genes are predominantly expressed by the heart muscle during the embryonic and fetal stages, and in particular *NPPA* expression is strongly reduced in the ventricles after birth (Man et al., 2018).	CACCGTGAGCTTCCTCCTTT	CCAAATGGTCCAGCAAATTCTTG
NPPB (Natriuretic Peptide Precursor B)		CTTTCCTGGGAGGTCGTTCC	GTTGCGCTGCTCCTGTAAC

2.6 Immunocytochemistry hiPSC-CMs culture

A monolayer of beating hiPSC-CMs was cultured on a 4-Well Culture Slide (Figure 9) for immunocytochemistry (ICC). The cells were then washed with 1 mL of phosphate-buffered saline (PBS) for each chamber to remove any residual medium. Subsequently, the cells were fixed using 1 mL of 4% formaldehyde (Sigma; 1.00496) for 30 minutes. After fixation, the cells were washed three times with 1 mL of PBS to eliminate excess formaldehyde. To enhance cellular permeability, the cells were incubated with 1 mL PBS containing 0.1% Triton X-100 (Sigma; T8787) for 3 minutes. Following this incubation, the cells were washed three times with 1 mL of PBS per chamber to remove any excess detergent and prepare for subsequent analysis. A blocking step was performed using 1 mL of 2% Bovine Serum Albumin (BSA) (Sigma; A7906) in PBS for 15 to 30 minutes. Following this, the samples were washed four times with 1 mL of PBS. The samples were then incubated overnight at room temperature (RT) with the primary antibody (Table 7). After the incubation period, the samples were incubated in the dark for 1 hour with a secondary antibody and Hoechst stain. Finally, a few droplets of Vectashield (VECTASHIELD® HardSet™ Antifade Mounting Medium; Vectorlabs; H-1400-10) were applied to cover glass slides, and the samples were stored at 4 °C. The pictures were taken at Leica® DMI3000B Inverted microscope (Department of Physiology, Maastricht University) and Leica® confocal microscope (Department of Genetics, Maastricht University).

Figure 9. 4-Well Culture Slide, a type of specialized microscopy slide used for cell culture and imaging. These slides have multiple chambers, allowing for the separate cultivation of different cell samples on the same slide.

Table 7. Reagents used for immunocytochemistry.

Name	Raised in	Dilution	Reactivity	Product-code
Anti-α-Actinin	Mouse	1:200 in PBS-1% BSA	Mouse, bovine, human, chicken	Sigma (# A5044)
Troponin I cardiac (cTnI) antibody	Mouse	1:200	Human	Hytest (# 4T21/4T21)
Troponin T cardiac (cTnT) antibody	Mouse	1:500	Human	Hytest (# 8RTT5)
Trihydrochloride, Trihydrate 33342 (Hoechst)	-	1:1000	All species	Thermo Fisher (#62249)
Phalloidine iFluor 488	-	1:1000 in PBS-1% BSA	All species	Abcam (# 176753)

2.7 Immunohistochemistry EHT rings

EHT rings were fixed for histological and immunohistochemical analyses to visualize the cell distribution and protein expression. The rings were transferred in 4% paraformaldehyde for 20 minutes to fixate the tissue. To make the tissue more visible the rings were stained with Eosin after fixation. The rings were embedded in paraffin wax after being dehydrated using different ethanol concentrations and cleared in xylene for 24 hours. 4 µm thick tissue sections were made using the Slee™ Aquatec microtome. The sections were incubated overnight in the oven at 48 °C to dry. Hematoxylin and Eosin (H&E) staining was conducted to visualize the cytoplasm and extracellular matrix proteins (Eosin) and the cell nuclei (Hematoxylin). The sections were re-hydrated before adding H&E and then dehydrated. Hematoxylin turns nuclei purple, and Eosin turns the cytoplasm and extracellular matrix pink. Stained sections were analyzed and pictures were obtained by a light microscope. Furthermore, other 3D rings were analyzed by immunohistochemistry staining (Table 8). This procedure was initiated by deparaffinate the sections by xylene and then rehydrating multiple concentrations of ethanol. Antigen retrieval was achieved by heating the sections in citrate buffer (1x) which enhanced antibody binding. Subsequently, the sections were incubated by applying 3% bovine serum albumin (BSA) in PBS to reduce the background staining. After washing in PBS, monoclonal antibodies were added to the sections and incubated overnight. Fluorescent-labeled secondary antibodies were added to emit the fluorescent signal of monoclonal antibodies bound to vimentin and α-actinin. Images were made at multiple magnifications using the Leica® DFC350 FX fluorescent microscope.

Table 8. Reagents used for Immunohistochemistry .

Staining	Marker	Product-code
Vimentin	CFs cytoskeletal protein	Abcam (# 92547)
Anti-α-Actinin	Sarcomere structure	Sigma (# A5044)
Wheat Germ Agglutinin (WGA)	Fluorescent WGA conjugates bind to carbohydrates enabling researchers to label the plasma membrane	ThermoFisher (# W11262)
Trihydrochloride, Trihydrate 33342 (Hoechst)	Hoechst binds to DNA in the nuclei	ThermoFisher (# 62249)

2.8 Statistical analysis

Protocols, cell culture pictures, measurements and gene expression data are analyzed and stored in Microsoft Excel (Redmond, United States). Graphs are created using GraphPad Prism 8® accompanied by statistical analysis if possible. The data were statistically analyzed using the non-parametric Kruskall-Wallis test and Dunn's *post-hoc* test for multiple comparisons. All statistical analysis were performed using GraphPad Prism 8®, P values lower than 0.05 were considered statistically significant. Via ImageJ® (National Institutes of Health) it was possible to calculate the surface area of the 3D rings by pictures. The circumference of the 3D rings in the picture was drawn and ImageJ® calculated and converted these values in square millimeters (mm^2). Finally, the area of the center post ($r^2 * \pi$; in this case the diameter of the center post is 2 mm, see Figure 8, the radius is 1 mm^2 resulting in an area of approximately 3.1415 mm^2) was subtracted from the total measured surface are giving the surface area in mm^2 of only the 3D ring.

Chapter 3

Results and Discussion

Activated Coagulation Factors FXa and Thrombin induce profibrotic and pro-inflammatory gene expression in hESC-CFs

3.1 Characterization of the hESC-CFs Cellular Model: Molecular and Functional Analyses

3.1.1 Marker gene expression Levels during hESC-CFs Differentiation Protocol

Stem cells markers

To evaluate whether the differentiation protocol was efficient we measured the gene expression of some stem cell markers at Day 1 (d1), Day 20 (d20) and Day 25 (d25) during the differentiation protocol. Figure 10 tracks the decline in expression of specific stem cell-related genes, indicating that the cells transition away from a stem cell state. The markers included are: NANOG (brown line), OCT4 (grey line), SOX2 (pink line), LIN28 (turquoise line). Each gene's expression level decreases significantly over time, indicating that these stem cell markers are downregulated as the differentiation progresses. By Day 25, all markers show minimal or nearly absent expression, which aligns with the expected loss of stem cell characteristics as cells differentiate into cardiac fibroblasts.

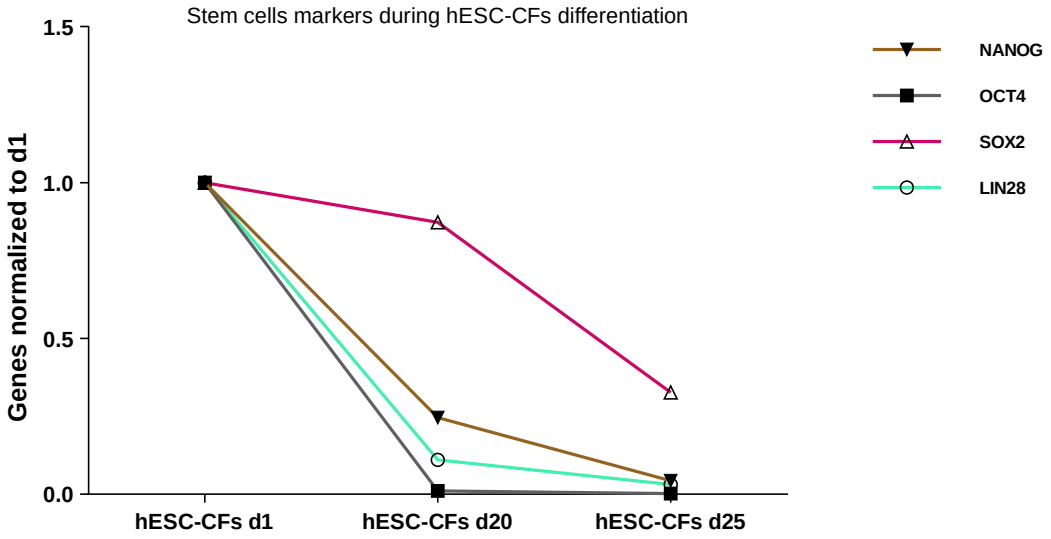

Figure 10. Expression levels of stem cell markers (NANOG, OCT4, SOX2 and LIN28) in hESC-CFs cultures during Differentiation Protocol at Day 1 (d1), Day 20 (d20) and Day 25 (d25). RT-qPCR analysis shows a progressive decline in the expression of these markers, indicating the loss of pluripotency as the cells differentiate. Gene expression is normalized for Day 1 of differentiation.

Cardiac fibroblast markers

We also analyzed the gene expression of some cardiac fibroblast markers during the differentiation process at Day 1 (d1), Day 20 (d20) and Day 25 (d25). The genes analyzed are: *POSTN* (blue line), *VIM* (green line), *COL1A1* (red line) and *CTGF* (black line). Each gene's expression level increases significantly over time, indicating the progressive expression of cardiac fibroblast-specific genes as differentiation advances, with *POSTN* exhibiting the most pronounced increase (Figure 11).

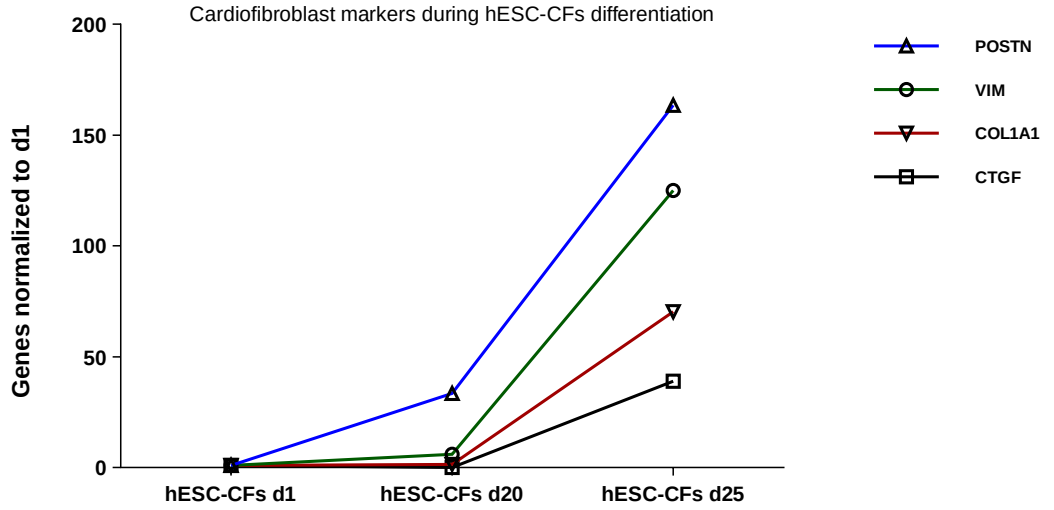

Figure 11. Expression levels of cardiac fibroblast markers (POSTN, VIM, *COL1A1* and *CTGF*) during hESC-CFs differentiation at Day 1 (d1), Day 20 (d20) and Day 25 (d25). Gene expression is normalized for Day 1 of differentiation.

Pro-inflammatory Genes Baseline Expression

To evaluate the basal expression level of target genes, cardiac fibroblasts (30,000 cells/cm^2 in 12-well plate), after a period in culture with CFGM, were incubated in serum-free medium containing vitamin C and gentamycin for 28 hours and 48 hours. Some studies have previously reported that the expression levels of genes involved in extracellular matrix remodeling increased in isolated fibroblasts after serum deprivation (Leicht et al., 2001). In this study, we also measured the expression of genes not involved in matrix remodeling but in inflammatory processes to assess any differences at these two timepoints. The basal expression was measured by RT-qPCR in 4 separate hESC-CFs differentiations (PSC018, PSC019, PSC020, PSC021).

At 28 hours, *CCL2* expression varies significantly across the cell lines: PSC018 exhibits the highest expression values; in contrast, PSC020 and PSC021 show much lower values. At 48 hours, the expression of *CCL2* changes in the different cell lines: PSC018 continues to show high levels of *CCL2*; PSC019 exhibits some increase compared to 28 hours while PSC020 and PSC021 show relatively stable levels (Figure 12, A).

We proceeded by measuring the basal expression level of another pro-inflammatory marker, *IL-6* (Figure 12, B). At 28 hours, there are noticeable differences in *IL-6* expression across the different cell lines. PSC018 shows the highest expression levels, followed by PSC020 while PSC019 and PSC021 show lower expression. At 48 hours, *IL-6* expression increases in all cell lines. The expression of *IL-6* is lower than that of *CCL2* in all cell lines and at both timepoints.

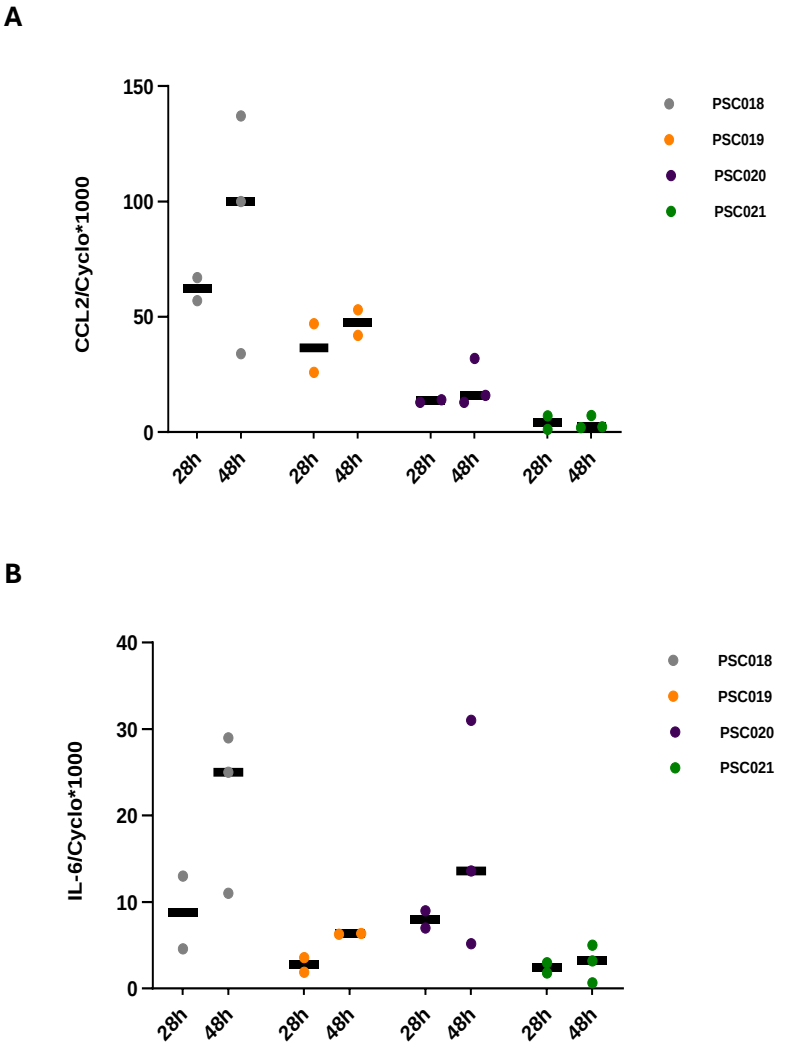

Figure 12. Pro-inflammatory Genes Baseline Expression in four fibroblast lines (PSC018, PSC019, PSC020 and PSC021) measured at 28 and 48 hours in serum-free medium. **(A)** Baseline expression levels of *CCL2*. *CCL2* expression varied between cell lines, with PSC018 showing the highest expression at both timepoints, and a notable increase from 28 to 48 hours. PSC019 exhibited moderate expression at both timepoints, while PSC020 and PSC021 displayed low basal expression. **(B)** Baseline expression levels of *IL-6*. At 28 hours, PSC018 exhibits the highest *IL-6* expression, followed by PSC020, while PSC019 and PSC021 show lower expression. At 48 hours, *IL-6* expression increases in PSC018, with moderate increases in PSC019 and PSC020. PSC021 maintains low *IL-6* expression throughout both timepoints. Expression levels were normalized for Cyclophilin A and calculated using the comparative threshold cycle method (ΔCt*1000).

Profibrotic Genes Baseline Expression

In this part of the characterization, we evaluated the expression level of some fibrotic markers such as *ACTA2* (known as α-smooth muscle actin), a contractile protein that is expressed in fibroblasts during their differentiation into myofibroblasts. As shown in Figure 13 (A), PSC019 demonstrates the highest expression of *ACTA2* across both timepoints (28 hours and 48 hours). PSC018 shows moderate expression with an increase at 48 hours, while PSC020 shows a slight decrease in *ACTA2* expression. PSC021, although having low expression at 28 hours, shows a notable increase in *ACTA2* at 48 hours, suggesting a delayed response in myofibroblast activation. This variability in *ACTA2* levels could reflect differences in the timing and extent of fibroblast activation into myofibroblasts.
We also measured the basal expression level of *CTGF* (Connective Tissue Growth Factor), a protein that plays a significant role in tissue repair, fibrosis and extracellular matrix production. As shown in Figure

13 (B), at the 28 hours, PSC018 and PSC019 display the highest *CTGF* expression. This could suggest an early activation of *CTGF* in these two cell lines. At 48 hours, *CTGF* expression increases significantly in all cell lines, indicating a time-dependent response.

Expression of *COL1A1* (Collagen Type I Alpha 1 Chain), resulting in synthesizing type I collagen, which is a major component of the extracellular matrix (ECM) was also evaluated (Figure 13, C). At both timepoints an increase expression was highlighted. This data seems to be in line with what was demonstrated previously: increased expression of the *COL1A1* gene in fibroblasts during prolonged culture, often in response to factors such as stress and changing microenvironment (Chen Jet al., 2023; Pan et al., 2013). In our model, with some variability, all four cell lines showed an increase in collagen levels after 48 hours in culture. The observed increase in *COL1A1* expression across all cell lines after 48 hours in culture suggests that the fibroblasts are responding to the culture environment, possibly as part of an early adaptation phase or stress response.

The last fibrotic marker evaluated was *TGFβ* (Transforming Growth Factor β), important for driving the activation of fibroblasts into myofibroblasts. Unlike other fibrotic markers, as shown in Figure 13 (D) the expression level decreases in all cell lines after 48 hours, except for PSC021. PSC018 line has the highest initial expression of *TGFβ*, while PSC020 has the lowest expression at both timepoints. These patterns suggest that *TGFβ* expression in hESC-CFs may vary depending on the specific line and the timing of differentiation.

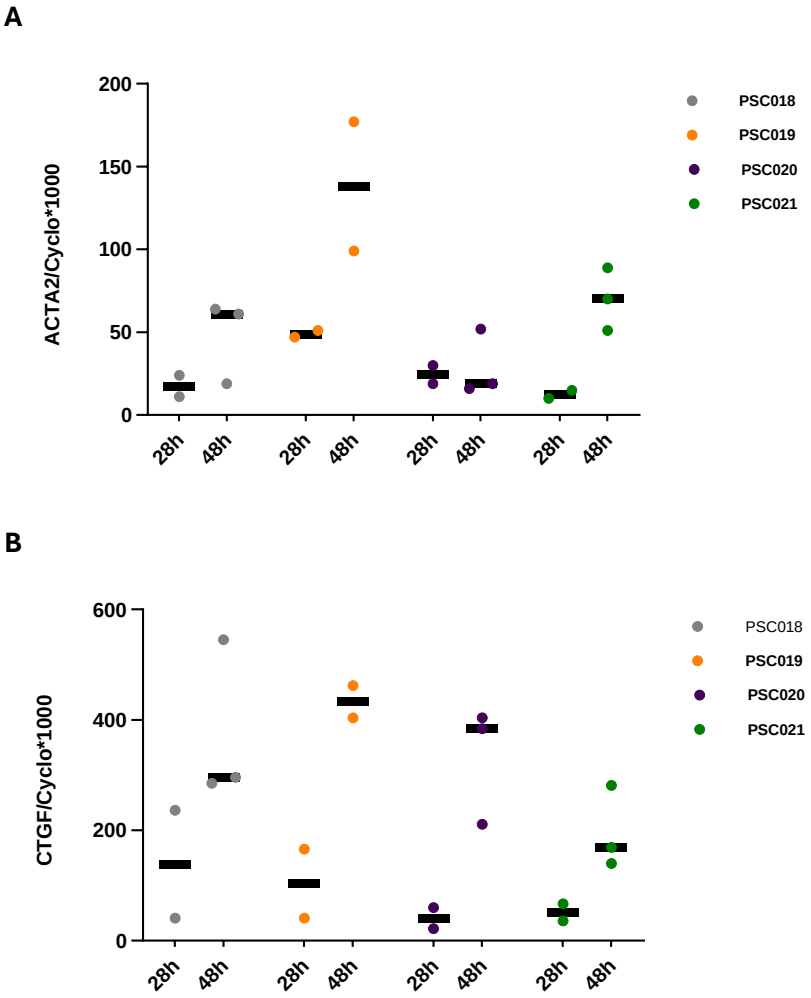

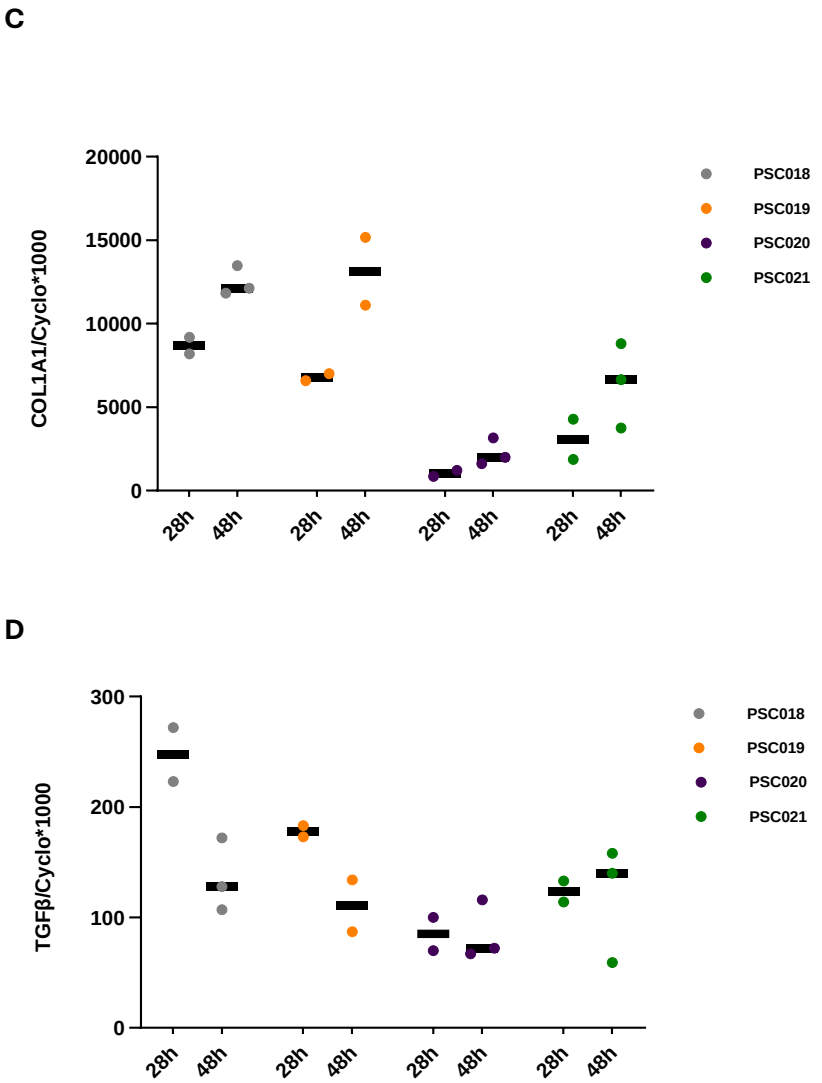

Figure 13. Profibrotic Genes Baseline Expression in four fibroblast lines (PSC018, PSC019, PSC020 and PSC021) measured at 28 and 48 hours in serum-free medium. **(A)** Baseline expression levels of *ACTA2*. At 28 hours, PSC019 exhibits the highest expression of *ACTA2*. At 48 hours, PSC019 maintains the highest expression, with a significant increase compared to the 28 hours timepoint. PSC018 also shows an increase in expression at 48 hours, while PSC020 demonstrates a decrease in *ACTA2* expression. **(B)** Baseline expression levels of *CTGF*. At 28 hours, PSC018 and PSC019 exhibit higher *CTGF* expression compared to PSC020 and PSC021. By 48 hours, all cell lines show a marked increase in *CTGF* expression. **(C)** Baseline expression levels of *COL1A1*. All cell lines exhibit an increase in *COL1A1* expression at 48 hours compared to 28 hours, though initial baseline levels vary significantly across lines. **(D)** Baseline expression levels of *TGFβ*. At 28 hours, PSC018 shows the highest expression. By 48 hours, PSC018, PSC019 and PSC020 show a decrease in *TGFβ* expression, while PSC021 displays a more sustained expression. Expression levels were normalized for Cyclophilin A and calculated using the comparative threshold cycle method (ΔCt).

PAR Receptors Genes Baseline Expression

Following the characterization of the baseline expression of certain marker genes in these four cell lines, we measured the expression of the PAR receptors. As previously shown, coagulation factors appear to exert their non-hemostatic effects on these receptors (D'Alessandro et al., 2021), making it crucial to understand the baseline expression levels of the PAR receptors in our hESC-CFs model. Specifically, we assessed the expression of *F2R* (*PAR1*) and *F2RL1* (*PAR2*), which are predominantly expressed at the cardiac level. As indicated in Figure 14 (A), the expression of *F2R* is highest in PSC020, with a significant increase over time, whereas PSC018 shows a decrease. PSC018 and PSC019 maintain relatively stable

expression at both timepoints. These results indicate that the *F2R* gene expression is variable across the different hESC-CFs lines, with PSC020 showing the most dynamic response over time. We measured the *F2RL1* expression in the same hESC-CFs lines. At 28 hours, PSC018 shows the highest expression while PSC021 has a consistently low expression compared to other cell lines. The lower expression of *F2RL1* in these hESC-CFs lines is comparable to primary cardiac fibroblasts and further supports the notion that *F2RL1* is a less abundant receptor in comparison to *F2R* in this cell type (D'Alessandro et al., 2021).

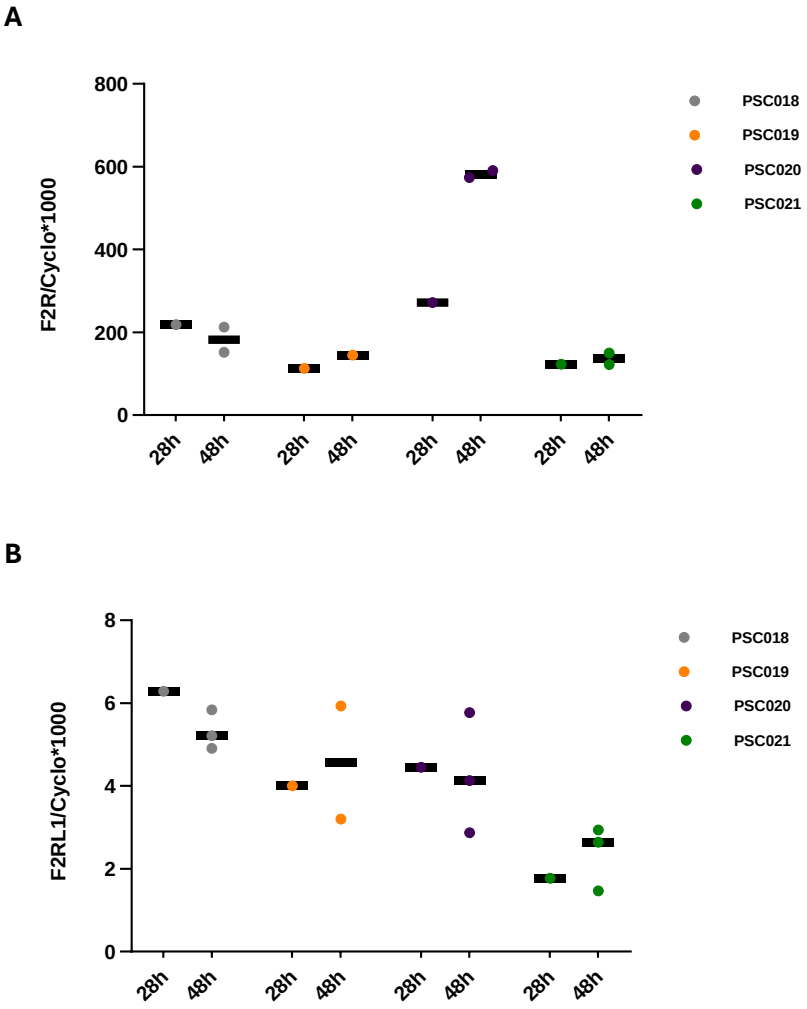

Figure 14. PAR Receptors Genes Baseline Expression. **(A)** Baseline expression levels of *F2R*. At 28 hours, PSC020 exhibits the highest expression of *F2R*, followed by PSC018. PSC021 and PSC019. At 48 hours, PSC020 shows a significant increase in *F2R* expression, while PSC018 shows relatively slightly decreased levels. PSC018 and PSC019 maintain moderate expression at both timepoints. **(B)** Baseline expression levels of *F2RL1*. At 28 hours, PSC018 shows the highest expression of *F2RL1*, followed by PSC020 and PSC019, with PSC021 exhibiting the lowest expression. At 48 hours, PSC021 continues to exhibit the lowest expression. Expression levels were normalized for Cyclophilin A and calculated using the comparative threshold cycle method (ΔCt * 1000).

3.1.2 Effect of *TGFβ* on hESC-CFs

Effect of TGFβ on pro-inflammatory genes

TGFβ is a well-known immunosuppressive anti-inflammatory factor. After 4 hours and 24 hours of incubation with *TGFβ* (1 ng/mL), we performed RT-qPCR to measure the expression of pro-inflammatory markers such as *CCL2* and *IL-6*. As shown in Figure 15 (A), at 4 hours of incubation, the data indicate a significant increase in *CCL2* expression (±1.5-fold) in the samples incubated with *TGFβ* compared to the control group (Ctrl) at the same timepoint. This effect was previously observed after 6 hours of incubation with *TGFβ* (van Nieuwenhoven et al., 2013). However, after 24 hours, *TGFβ* exerts an anti-inflammatory effect on hESC-CFs: *CCL2* levels are significantly lower than the control group (±0.5-fold, decrease). As shown in Figure 15 (B) after 4 hours of incubation, *TGFβ* doesn't have any significant response on *IL-6* expression, however it's possible to appreciate a slightly anti-inflammatory trend compared to control condition. Conversely, after 24 hours of incubation *TGFβ* significantly down-regulates *IL-6* expression (±0.5-fold, decrease). These data suggest that *TGFβ* has a time-dependent regulatory effect on pro-inflammatory and anti-inflammatory response in hESC-CFs culture, with an early activation followed by a suppressive phase, which may reflect the dual role of *TGFβ* in modulating inflammation.

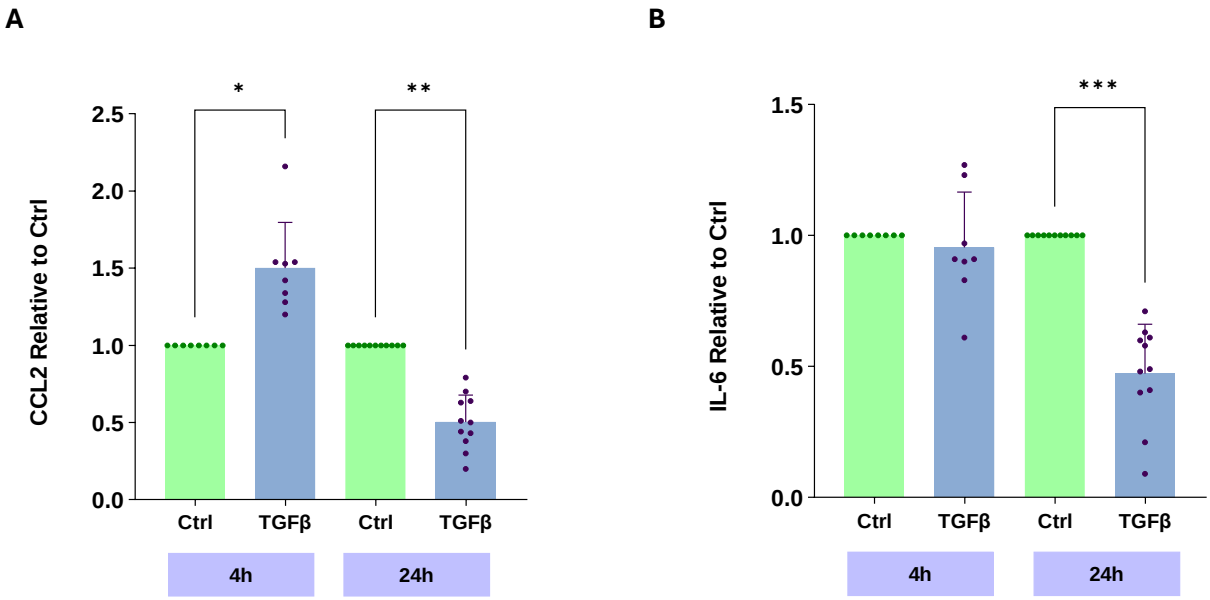

Figure 15. Effect of *TGFβ* on pro-inflammatory genes. **(A)** Pro-inflammatory effect of *TGFβ* (1ng/mL) on *CCL2* expression in hESC-CFs cultures after 4 hours (n=8) and 24 hours (n=11) of incubation. At 4 hours, *TGFβ* treatment significantly increases *CCL2* expression compared to the control. However, after 24 hours, *TGFβ* strongly down-regulates *CCL2* expression levels compared to the control group. **(B)** Pro-inflammatory effect of *TGFβ* (1ng/mL) on *IL-6* expression in hESC-CFs cultures after 4 hours (n=8) and 24 hours (n=11) of incubation. At 4 hours, *TGFβ* doesn't have any significant response on *IL-6* expression, however it's possible to appreciate a slightly anti-inflammatory trend compared to control condition. After 24 hours *TGFβ* significantly down-regulates *IL-6* expression. Gene expression was measured by RT-qPCR after 4 hours and 24 hours of incubation. Results are expressed as fold-change relative to control, with dots indicating separate experiments and error bars indicating SD. Statistical analysis was performed using the non-parametric Kruskal-Wallis test with Dunn's multiple comparison *post-hoc* test (*p<0.05, ** p<0.01, *** p<0.001, **** p<0.0001).

Effect of TGFβ on PAR Receptor and profibrotic genes

We measured the expression level of two isoform of PAR Receptor family after exposure to *TGFβ* for 4 and 24 hours and as shown in the Figure 16 we found no significant effects on *F2R* and *F2RL1* genes. Regarding profibrotic genes at 4 hours, *TGFβ* seems to have no impact on *ACTA2* expression. Conversely, at 24 hours, *ACTA2* expression is notably higher (±2-fold) in the *TGFβ* group compared to the control group (Figure 17, A). The graph suggests that *TGFβ* does not immediately affect *ACTA2* expression at 4 hours but leads to a significant increase by 24 hours, indicating a delayed but robust response. As indicated in Figure 17 (B), *TGFβ* is also able to regulate the *CTGF* expression. From our study it emerged that *TGFβ* determined a statistically significant up-regulation on *CTGF* expression after 4 hours (±2.5-fold) and at 24 hours expression (±2-fold). We also evaluated the expression of two other known fibrosis markers, *COL1A1* and *TGFβ* at the same timepoints. As shown in Figure 17 (C) after 4 hours of incubation, *TGFβ* doesn't have any significant response on *COL1A1* expression, however it's possible to appreciate a slightly increase trend compared to control condition. Conversely, after 24 hours of incubation *TGFβ* has a strong impact on *COL1A1* expression increasing significantly the expression of this gene (±2.5-fold). Furthermore, we measured the expression of the *TGFβ* itself and we observed that this factor can induce significant overexpression of its gene at 4 hours (±1.5-fold) and 24 hours of incubation (±2.5-fold) (Figure 17, D).

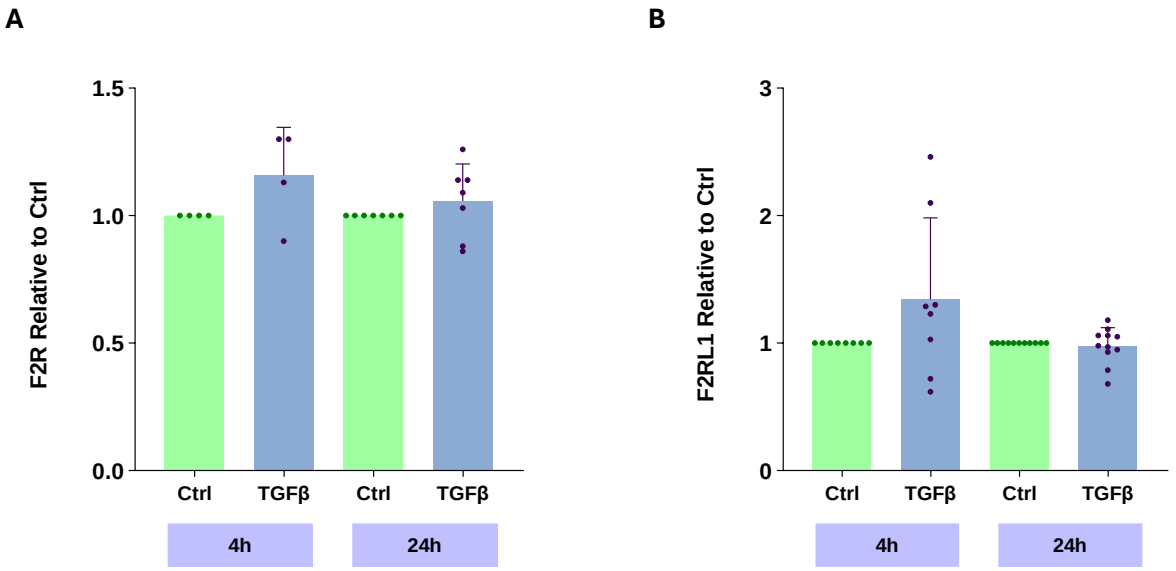

Figure 16. Effect of *TGFβ* on PAR Receptors genes. **(A)** Effect of *TGFβ* (1ng/mL) on *F2R* expression in hESC-CFs cultures after 4 hours (n=4) and 24 hours (n=7) of incubation. No statistically significant differences were observed between *TGFβ* -treated and control groups at either timepoint. **(B)** Effect of *TGFβ* (1ng/mL) on *F2RL1* expression in hESC-CFs cultures after 4 hours (n=8) and 24 hours (n=11) of incubation. No statistically significant differences were observed between *TGFβ*-treated and control groups at either timepoint. Gene expression was measured by RT-qPCR after 4 hours and 24 hours of incubation. Results are expressed as fold-change relative to control, with dots indicating separate experiments and error bars indicating SD. Statistical analysis was performed using the non-parametric Kruskal-Wallis test with Dunn's multiple comparison *post-hoc* test (*p<0.05, ** p<0.01, *** p<0.001, **** p<0.0001).

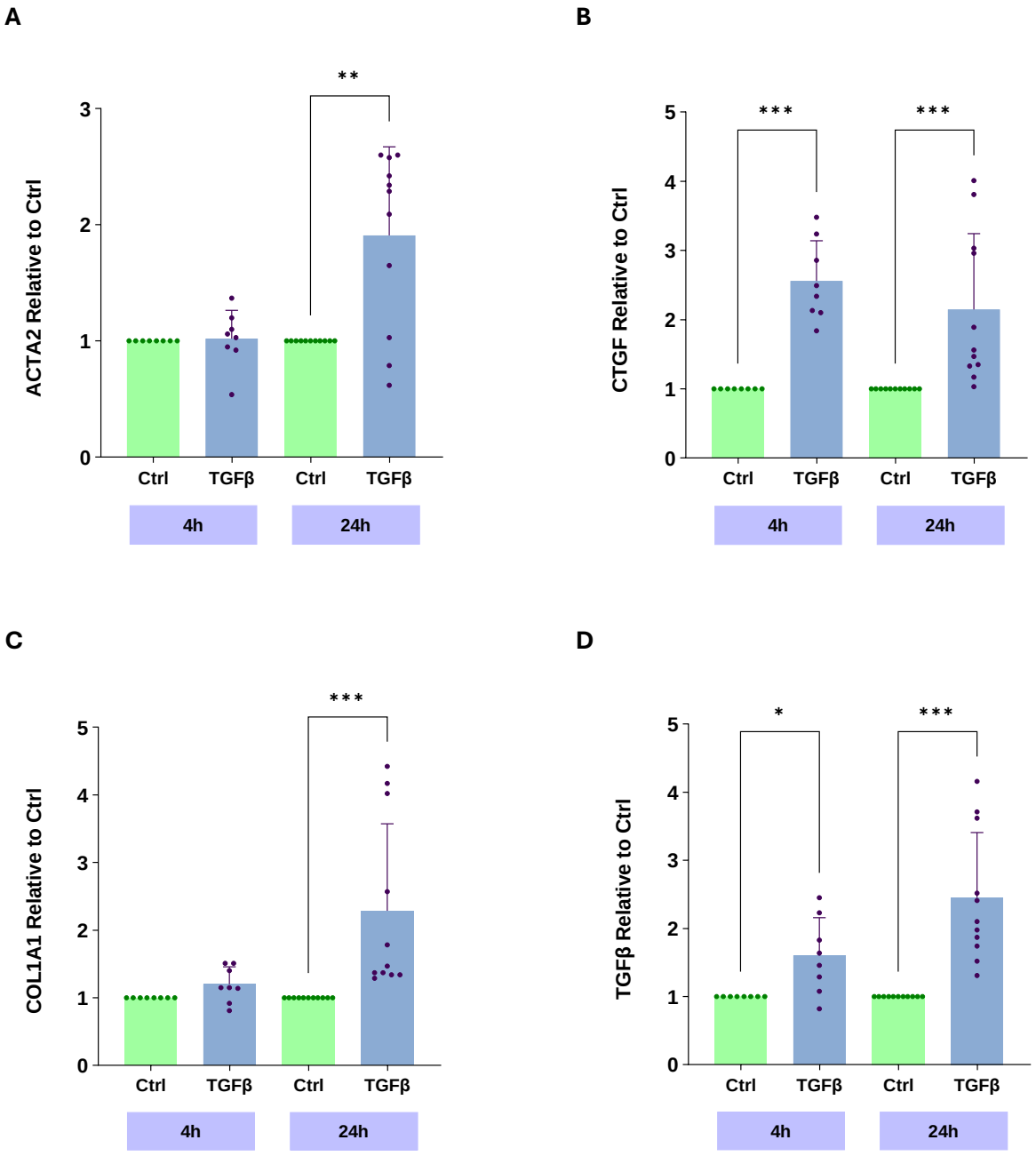

Figure 17. Effect of *TGFβ* on profibrotic genes. **(A)** Profibrotic effect of *TGFβ* (1ng/mL) on *ACTA2* expression in hESC-CFs cultures after 4 hours (n=8) and 24 hours (n=11) of incubation. At 4 hours, *TGFβ* treatment doesn't have any significant response on *ACTA2* expression. However, after 24 hours, *TGFβ* strongly up-regulates *ACTA2* expression levels compared to the control group. **(B)** Profibrotic effect of *TGFβ* (1ng/mL) on *CTGF* expression in hESC-CFs cultures after 4 hours (n=8) and 24 hours (n=11) of incubation. *TGFβ* significantly up-regulates *CTGF* expression after 4 hours and 24 hours of incubation. **(C)** Profibrotic effect of *TGFβ* (1ng/mL) on *COL1A1* expression in hESC-CFs cultures after 4 hours (n=8) and 24 hours (n=11) of incubation. At 4 hours, *TGFβ* treatment doesn't have any significant response on *COL1A1* expression. However, after 24 hours, *TGFβ* strongly up-regulates *COL1A1* expression levels compared to the control. **(D)** Profibrotic effect of *TGFβ* (1ng/mL) on *TGFβ* expression in hESC-CFs cultures after 4 hours (n=8) and 24 hours (n=11) of incubation. *TGFβ* significantly up-regulates *TGFβ* expression after 4 hours and 24 hours of incubation. Gene expression was measured by RT-qPCR after 4 hours and 24 hours of incubation. Results are expressed as fold-change relative to control, with dots indicating separate experiments and error bars indicating SD. Statistical analysis was performed using the non-parametric Kruskal-Wallis test with Dunn's multiple comparison *post-hoc* test (*p<0.05, ** p<0.01, *** p<0.001, **** p<0.0001).

3.2 Role of Coagulation Factors in inflammatory and fibrotic processes in hESC-CFs

3.2.1 Effect of FIIa on pro-inflammatory genes

To evaluate the pro-inflammatory effect of Thrombin, hESC-CFs were incubated with CFGM and human FIIa (0.008 nM) at two different timepoints (4 hours and 24 hours). *CCL2*, known for its role in promoting inflammation, was measured relative to the control (Ctrl). As shown in Figure 18 (A), after 4 hours of incubation Thrombin induces a statistically significant up-regulation of *CCL2* (±2-fold). This effect suggests that FIIa has an immediate and strong pro-inflammatory effect on *CCL2* expression within the first few hours of incubation. The pro-inflammatory effect of FIIa on *CCL2* appears to decrease after 24 hours of incubation. As indicated in the Figure 18 (B), the incubation with Thrombin, after 4 hours, induces a statistically significant up-regulation of *IL-6* (±2.5-fold). After 24 hours, the effect of FIIa on *IL-6* expression appears reduced compared to the 4-hour timepoint. In summary, FIIa induces a significant increase in *IL-6* expression at 4 hours, but this effect diminishes at 24 hours, this could indicate an acute, early inflammatory response. This experiment shows that the hESC-CFs show similar pro-inflammatory responses to FIIa as seen in primary cell culture of human cardiac fibroblasts (D'Alessandro et al., 2021).

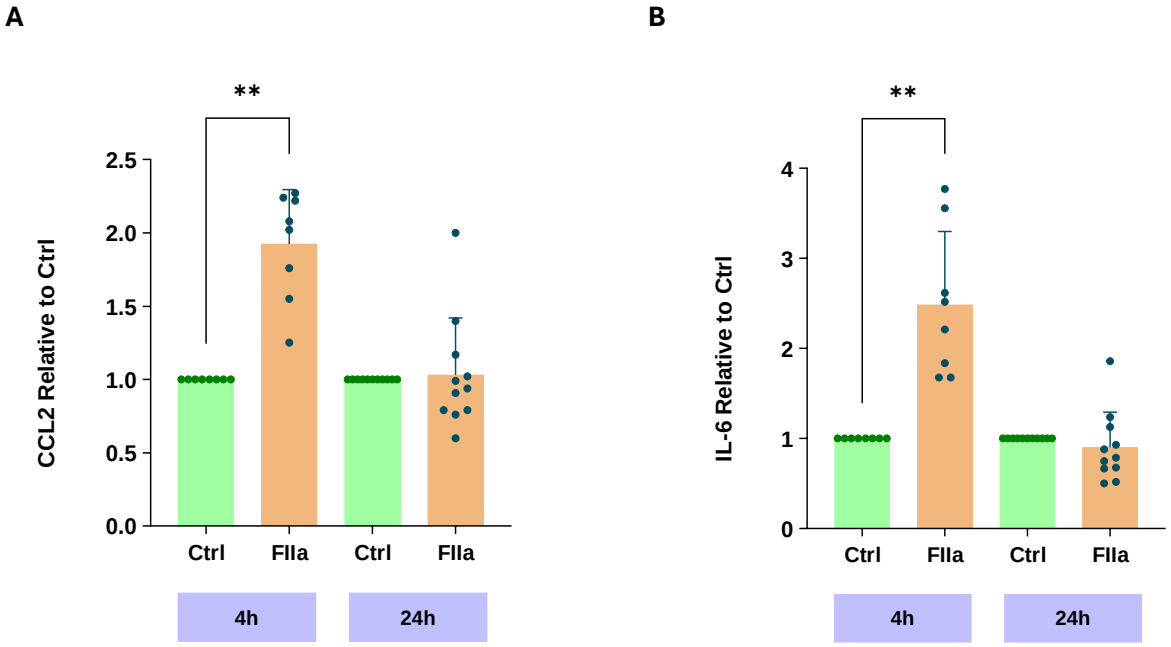

Figure 18. Effect of FIIa on pro-inflammatory genes. **(A)** Pro-inflammatory effect of FIIa (0.008 nM) on *CCL2* expression in hESC-CFs cultures after 4 hours (n=8) and 24 hours (n=11) of incubation. At 4 hours, FIIa treatment significantly increases *CCL2* expression compared to the control. However, this effect is not observed at 24 hours, suggesting an early pro-inflammatory response. **(B)** Pro-inflammatory effect of FIIa (0.008 nM) on *IL-6* expression in hESC-CFs cultures after 4 hours (n=8) and 24 hours (n=11) of incubation. At 4 hours, FIIa treatment significantly increases *IL-6* expression compared to the control. However, this effect is not observed at 24 hours, suggesting a transient pro-inflammatory response. Gene expression was measured by RT-qPCR after 4 hours and 24 hours of incubation. Results are expressed as fold-change relative to control, with dots indicating separate experiments and error bars indicating SD. Statistical analysis was performed using the non-parametric Kruskal-Wallis test with Dunn's multiple comparison *post-hoc* test (*p<0.05, ** p<0.01, *** p<0.001, **** p<0.0001).

3.2.2 Effect of FIIa on profibrotic genes

FIIa appears to have no effect on the expression of *ACTA2* at both timepoint (Figure 19, A) while after 4 hours of incubation with FIIa, the expression level of *CTGF* increases (±3.5 -fold), representing high statistical significance. This effect is not detectable after 24 hours of incubation with FIIa (Figure 19, B). This could indicate that an early regulation of *CTGF* gene promoted by FIIa. Other two profibrotic markers, *COL1A1* and *TGFβ*, are also evaluated. As shown in Figure 19 (C), after 4 and 24 hours of

incubation FIIa does not induce a profibrotic response in terms of *COL1A1* expression at this two timepoints. As reported in Figure 19 (D), the expression level of *TGFβ*, a well-known profibrotic factor, seems slightly increased after 4 hours and 24 hours in the FIIa-treated group, but this increase is not statistically significant in both cases.

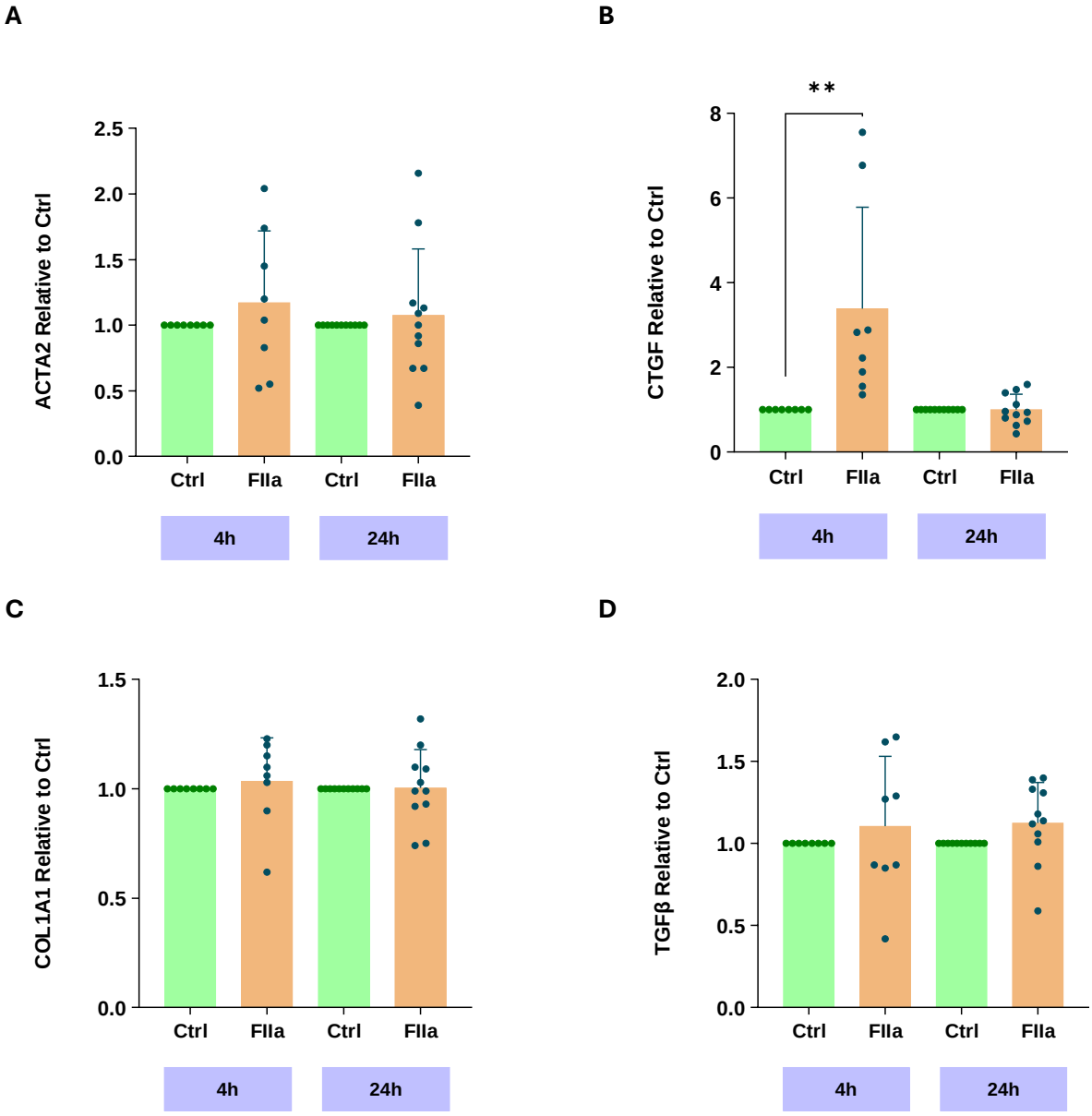

Figure 19. Effect of FIIa on profibrotic genes. **(A)** Profibrotic effect of FIIa (0.008 nM) on *ACTA2* expression in hESC-CFs cultures after 4 hours (n=8) and 24 hours (n=11) of incubation. No statistically significant differences were observed between FIIa-treated and control groups at either timepoint. **(B)** Profibrotic effect of FIIa (0.008 nM) on *CTGF* expression in hESC-CFs cultures after 4 hours (n=8) and 24 hours (n=11) of incubation. At 4 hours, FIIa treatment significantly increases *CTGF* expression compared to the control. However, this effect is not observed at 24 hours. **(C)** Profibrotic effect of FIIa (0.008 nM) on *COL1A1* expression in hESC-CFs cultures after 4 hours (n=8) and 24 hours (n=11) of incubation. No statistically significant differences were observed between FIIa-treated and control groups at either timepoint. **(D)** Profibrotic effect of FIIa (0.008 nM) on *TGFβ* expression in hESC-CFs cultures after 4 hours (n=8) and 24 hours (n=11) of incubation. At 4 hours and 24 hours of incubation, FIIa seems slightly up-regulate the expression of *TGFβ*, but this increase is not statistically significant in both cases. Gene expression was measured by RT-qPCR after 4 hours and 24 hours of incubation. Results are expressed as fold-change relative to control, with dots indicating separate experiments and error bars indicating SD. Statistical analysis was performed using the non-parametric Kruskal-Wallis test with Dunn's multiple comparison *post-hoc* test (*p<0.05, ** p<0.01, *** p<0.001, **** p<0.0001).

3.2.3 Effect of FIIa on PAR Receptors

As shown in Figure 20 (A), there appears to be a slight increase in *F2R* expression after 4 hours of incubation with FIIa, but this change is not statically significant. On the contrary, after 24 hours of incubation with the FIIa, it is possible to appreciate a reduction in the expression of *F2R* expression, also in this case not statistically significant. The same pattern can be observed in Figure 20 (B) in which the expression of *F2RL1* was evaluated, even in this case the slight variations induced by the treatment with FIIa are not statistically significant.

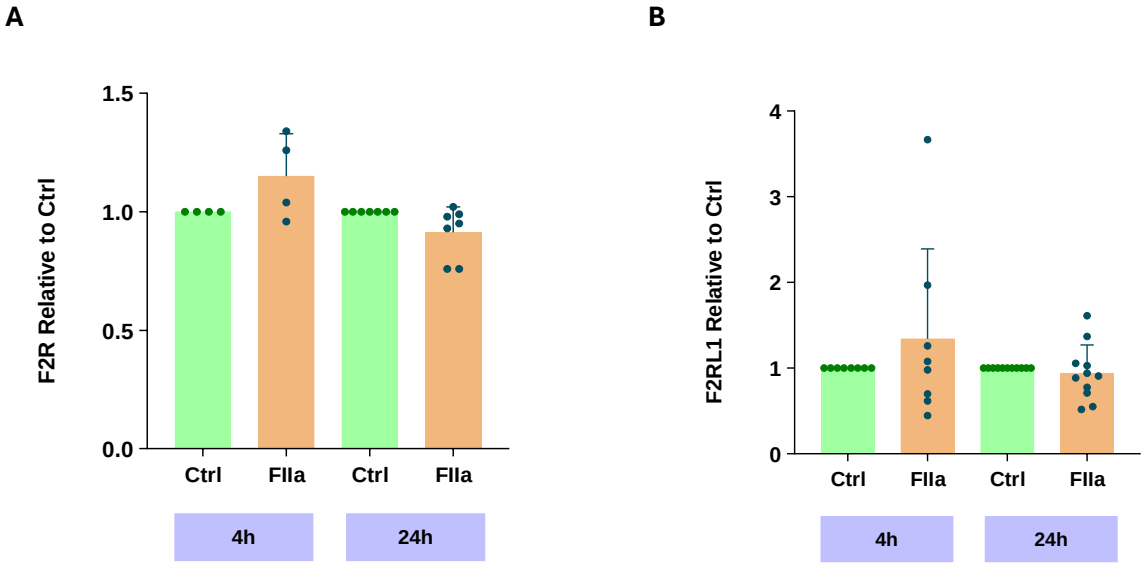

Figure 20. Effect of FIIa on PAR Receptors genes. **(A)** Effect of FIIa (0.008 nM) on *F2R* expression in hESC-CFs cultures after 4 hours (n=4) and 24 hours (n=7) of incubation. No statistically significant differences were observed between FIIa-treated and control groups at either timepoint. **(B)** Effect of FIIa (0.008 nM) on *F2RL1* expression in hESC-CFs cultures after 4 hours (n=8) and 24 hours (n=11) of incubation. No statistically significant differences were observed between FIIa-treated and control groups at either timepoint. Gene expression was measured by RT-qPCR after 4 hours and24 hours of incubation. Results are expressed as fold-change relative to control, with dots indicating separate experiments and error bars indicating SD. Statistical analysis was performed using the non-parametric Kruskal-Wallis test with Dunn's multiple comparison *post-hoc* test (*p<0.05, ** p<0.01, *** p<0.001, **** p<0.0001).

3.2.4 Effect of FXa on pro-inflammatory genes

To verify the effect of hFXa on pro-inflammatory genes, we incubated hESC-CFs at two different concentrations (10nM and 50nM) and then we measured the expression level using RT-qPCR. The incubations were carried out at two different timepoints, 4 hours and 24 hours. As shown in Figure 21 (A and B), 4 hours of incubation with FXa (10 nM) up-regulates the mRNA expression of the *CCL2* (±2-fold) and *IL-6* (±2.5-fold). Similarly, exposure after 4 hours to FXa (50nM) strongly up-regulated the mRNA expression of *CCL2* (±3-fold) and *IL-6* (±4-fold). Furthermore, it is possible to see that in the group treated with high concentration of FXa (50nM) the up-regulation of *CCL2* and *IL-6* is stronger compared to the group incubated with low concentration of FXa (10nM). This suggests a dose-dependent effect exerted by this coagulation factor on hESC-CFs cultures. The exposure at FXa at 24 hours does not appear to have a significant effect on *CCL2* and *IL-6* expression at both concentrations, but an increasing trend can be appreciated. These findings suggest that FXa may play a direct role in promoting pro-inflammatory responses in hESC-CFs line.

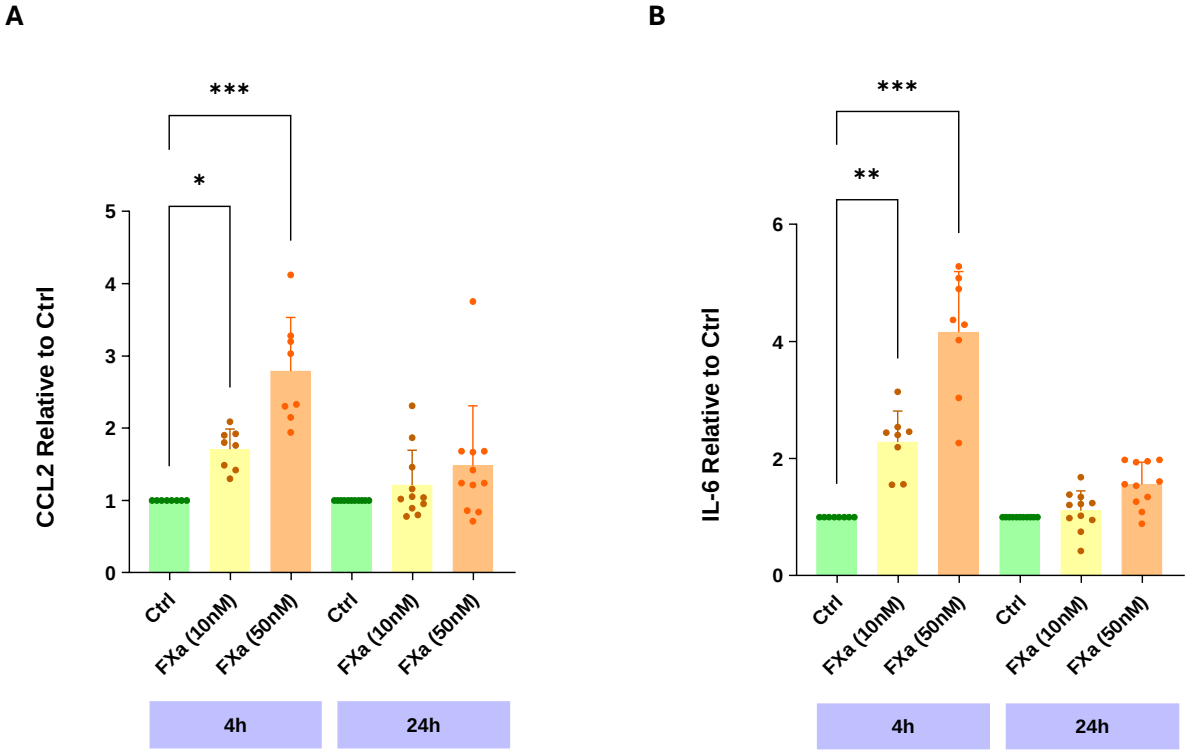

Figure 21. Effect of FXa on pro-inflammatory genes. **(A)** Pro-inflammatory effect of FXa (10nM and 50nM) on *CCL2* expression in hESC-CFs cultures after 4 hours (n=8) and 24 hours (n=11) of incubation. At 4 hours, FXa (10nM and 50 nM) treatment significantly increases *CCL2* expression compared to the control in dose-dependent manner. At 24 hours incubation, no statistical significance was observed between FXa-treated and control groups at either concentration. **(B)** Pro-inflammatory effect of FXa (10nM and 50nM) on *IL-6* expression in hESC-CFs cultures after 4 hours (n=8) and 24 hours (n=11) of incubation. At 4 hours, FXa (10nM and 50 nM) treatment significantly increases *IL-6* expression compared to the control in dose-dependent manner. At 24 hours incubation, no statistical significance was observed between FXa-treated and control groups at either concentration. Gene expression was measured by RT-qPCR after 4 hours and24 hours of incubation. Results are expressed as fold-change relative to control, with dots indicating separate experiments and error bars indicating SD. Statistical analysis was performed using the non-parametric Kruskal-Wallis test with Dunn's multiple comparison *post-hoc* test (*p<0.05, ** p<0.01, *** p<0.001, **** p<0.0001).

3.2.5 Effect of FXa on profibrotic genes

Previous studies have shown that FXa can regulate the expression of genes involved in extracellular matrix remodeling and fibrotic processes in adult rat CFs (D'Alessandro et al., 2021). In this context, we evaluated the effects of this factor on hESC-CFs culture. As shown in Figure 22 (A), no statistically significant effect on *ACTA2* gene is visible after 4 hours of incubation at both concentrations (10 nM and 50n M). On the contrary, after 24 hours of treatment, the higher concentration of FXa (50 nM) strongly up-regulates the expression of *ACTA2* (±3.5-fold) compared to control condition. The up-regulation is also statistically significant between the two groups incubated with FXa at different concentration (10nM vs. 50nM ±3.5-fold). This effect suggests the late regulation promoted by FXa on *ACTA2* gene. We also measured *CTGF* gene expression: after 4 hours, as evident in Figure 22 (B), FXa (10 nM and 50 nM) induces a strong up-regulation of *CTGF* (±4-fold; ±5.2-fold respectively compared to control condition). At 24 hours of incubation, exposure to FXa (50nM) strongly up-regulated the expression of *CTGF* (±2-fold).

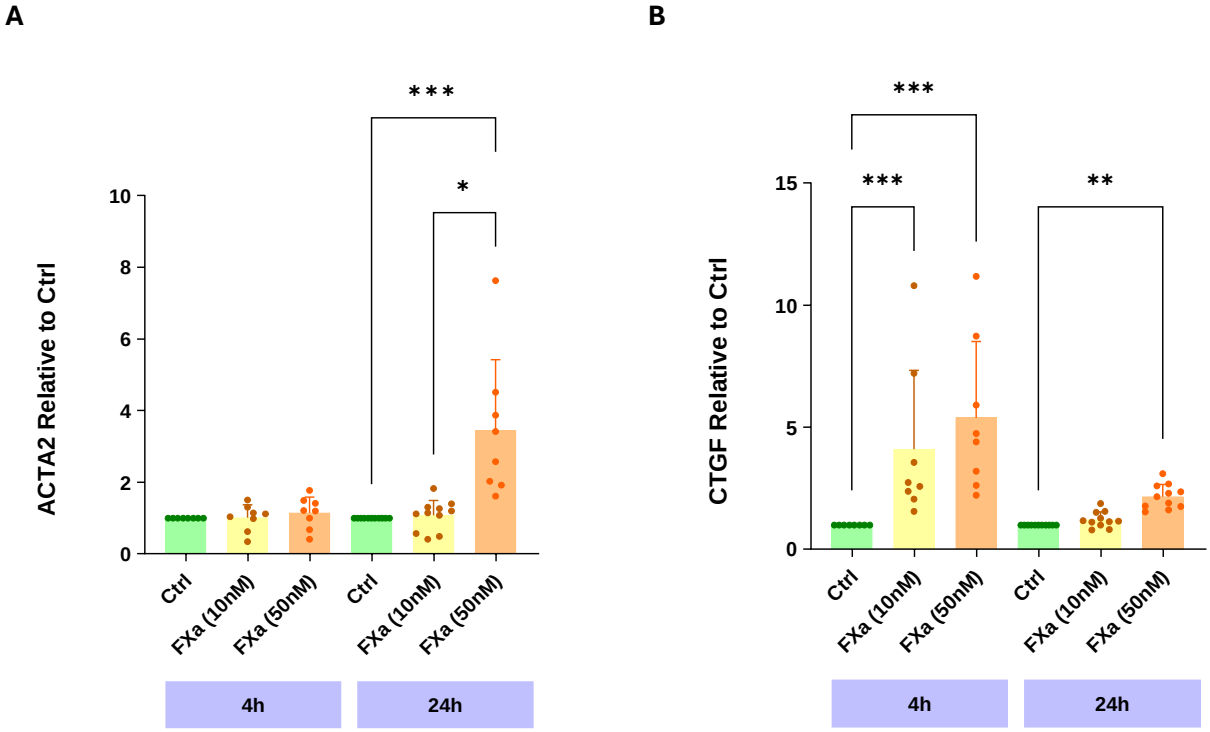

Figure 22. Effect of FXa on profibrotic genes. **(A)** Profibrotic effect of FXa (10nM and 50nM) on *ACTA2* expression in hESC-CFs cultures after 4 hours (n=8) and 24 hours (n=8) of incubation. At 4 hours no statistically significant differences were observed between FXa-treated and control group at either concentrations. At 24 hours incubation, FXa (50 nM) strongly up-regulates the expression of *ACTA2* compared to control condition. **(B)** Profibrotic effect of FXa (10nM and 50nM) on *CTGF* expression in hESC-CFs cultures after 4 hours (n=8) and 24 hours (n=11) of incubation. At 4 hours, FXa (10 nM and 50nM) treatment significantly increases *CTGF* expression compared to the control. At 24 hours *CTGF* up-regulation is statistically significant at the highest concentration of FXa (50nM). Gene expression was measured by RT-qPCR after 4 hours and24 hours of incubation. Results are expressed as fold-change relative to control, with dots indicating separate experiments and error bars indicating SD. Statistical analysis was performed using the non-parametric Kruskal-Wallis test with Dunn's multiple comparison *post-hoc* test (*p<0.05, ** p<0.01, *** p<0.001, **** p<0.0001).

Analyzing the expression of *COL1A1* in hESC-CFs incubated with FXa, no significant increase was observed at either timepoint, indicating that FXa does not appear to strongly influence *COL1A1* expression in this model (Figure 23, A). As shown in Figure 23 (B), after 4 hours of treatment, no significant differences were observed between the control and either FXa concentration in *TGFβ* expression. After 24 hours, a statistically significant increase in *TGFβ* levels (±1.5-fold) is evident in the samples incubated with the highest concentration of FXa (50nM) compared to the control. This suggests that higher concentrations of FXa may induce *TGFβ* expression over extended exposure times.

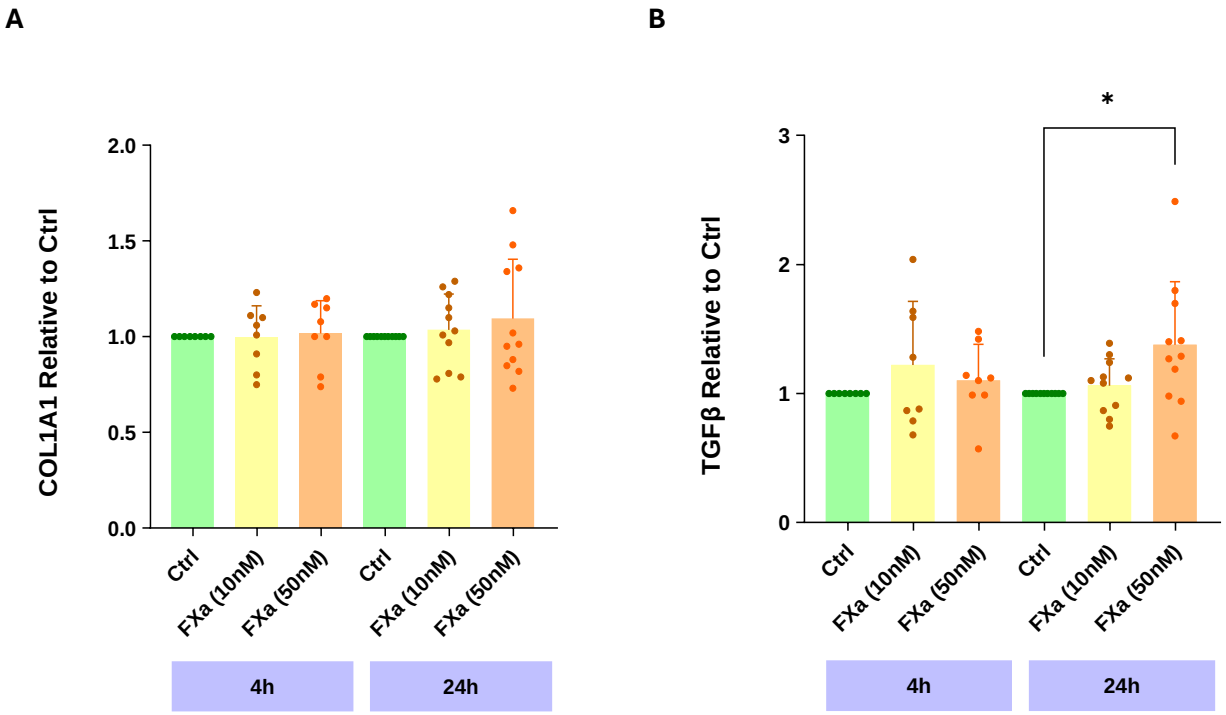

Figure 23. Effect of FXa on profibrotic genes. **(A)** Profibrotic effect of FXa (10nM and 50nM) on *COL1A1* expression in hESC-CFs cultures after 4 hours (n=8) and 24 hours (n=11) of incubation. At 4 hours and 24 hours no statistically significant differences were observed between FXa-treated and control group at either concentration. **(B)** Profibrotic effect of FXa (10nM and 50nM) on *TGFβ* expression in hESC-CFs cultures after 4 hours (n=8) and 24 hours (n=9) of incubation. At 4 hours, no significant differences were observed between the control and either FXa concentration. At 24 hours *TGFβ* up-regulation is statistically significant at the highest concentration of FXa (50nM). Gene expression was measured by RT-qPCR after 4 hours and24 hours of incubation. Results are expressed as fold-change relative to control, with dots indicating separate experiments and error bars indicating SD. Statistical analysis was performed using the non-parametric Kruskal-Wallis test with Dunn's multiple comparison *post-hoc* test (*p<0.05, ** p<0.01, *** p<0.001, **** p<0.0001).

3.2.6 Effect of FXa on PAR Receptors

As we did previously for Thrombin, we evaluated the expression levels of PAR receptors to elucidate their role in this process. In the study by Elisa et al., a statistically significant increase in the levels of PAR1 and *PAR2* was observed after exposure to Thrombin and FXa at 4 hours of incubation (D'Alessandro et al., 2021) suggesting the existence of a positive feedback loop on PAR expression upon their activation. In our case, we did not obtain statistically significant results, although a slight increasing trend in the mRNA expression of these two receptors was visible after 4 hours of incubation (Figure 24).

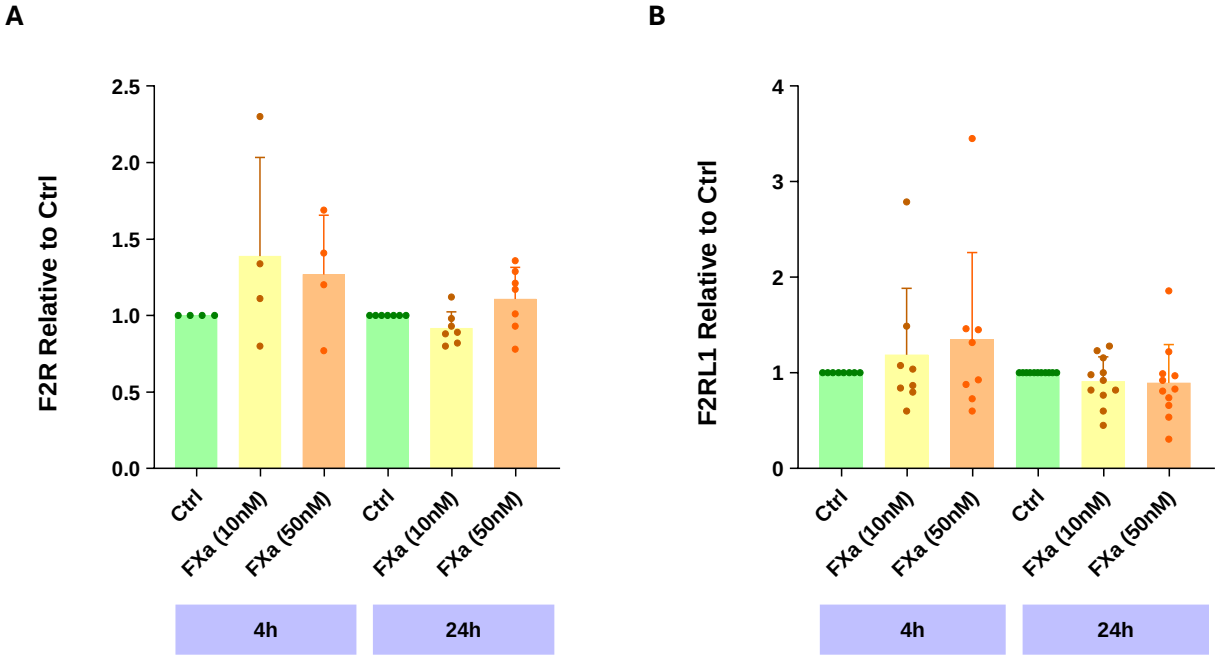

Figure 24. Effect of FXa on PAR Receptors genes. **(A)** Effect of FXa (10nM and 50nM) on *F2R* expression in hESC-CFs cultures after 4 hours (n=4) and 24 hours (n=7) of incubation. No statistically significant differences were observed between FXa-treated and control groups at either timepoint. **(B)** Effect of FXa (10nM and 50nM) on *F2RL1* expression in hESC-CFs cultures after 4 hours (n=8) and 24 hours (n=11) of incubation. No statistically significant differences were observed between FXa-treated and control groups at either timepoint. Gene expression was measured by RT-qPCR after 4 hours and24 hours of incubation. Results are expressed as fold-change relative to control, with dots indicating separate experiments and error bars indicating SD. Statistical analysis was performed using the non-parametric Kruskal-Wallis test with Dunn's multiple comparison *post-hoc* test (*p<0.05, ** p<0.01, *** p<0.001, **** p<0.0001).

3.3 Discussion

Characterization of the hESC-CFs Cellular Model: Molecular and Functional Analyses

The development of new cellular model requires an initial phase of characterization to validate its reliability for subsequent experimental applications. In this study, the hESC-CFs model was employed using a differentiation protocol based on modulation of the WNT signaling (Zhang et al., 2019). The characterization of this model was primarily performed at the molecular level through gene expression analysis at different timepoints post-differentiation, a method widely used in stem cell research (Chan et al., 2016; Takahashi and Yamanaka, 2016). This approach allowed for an assessment of the expression dynamics of stem cells markers and genes associated with mature cardiac fibroblasts.

The observed trends indicate a progressive downregulation of stem cells markers (e.g., NANOG, OCT4), accompanied by an upregulation of CFs specific markers (e.g., *COL1A1*, POSTN) as the days post-differentiation increase. Furthermore, four cell lines (PSC018, PSC019, PSC020, PSC021) derived from the same differentiation protocol were analyzed in terms of baseline gene expression to investigate potential intrinsic variations. Despite originating from the same protocol, differences in basal gene expression levels were observed among the lines after 28 hours and 48 hours of serum-free incubation. A high level of heterogeneity within the cardiac fibroblast population has been reported in the mammalian heart (Pinto et al., 2016). Single-cell analysis revealed the induction of CFs *in vivo* arise from a myogenic and non-myogenic lineage (Mononen et al., 2020). Also *in vitro* studies, using single cell transcriptomics, has showed that the hiPSC-derived organoid fibroblast population displays a high degree of heterogeneity that approximates the heterogeneity of populations in both normal and diseased human heart (Fernandes et al., 2023). In addition to intrinsic variability, extrinsic factors related to culture conditions may also contribute to the heterogeneity observed *in vitro*. In particular, it is well established that fibroblasts cultured on stiff substrates, such as conventional tissue culture plastic, tend to undergo spontaneous activation, acquiring a myofibroblast-like phenotype even in the absence of specific stimuli (Huang et al., 2012). This phenomenon can confound the interpretation of experimental *data*, especially in early-stage model characterization. To mitigate this effect, alternative strategies such as culturing cells on softer substrates that better mimic the physiological stiffness of cardiac tissue (approx. 10 kPa) or the use of TGFβ pathway inhibitors can be employed (Chaudhuri et al., 2016; van Putten et al., 2020). These approaches help preserve a more quiescent fibroblast phenotype, thereby improving the reliability and reproducibility of the model.

The use of serum-free culture medium allows control over culture conditions. In this case, serum deprivation at 48 hours considerably increased the expression levels of pro-inflammatory markers. A similar trend was observed for the expression of profibrotic genes, with the notable exception of *TGFβ*, which exhibited a reduction at this timepoint. It is possible that serum deprivation triggers a pro-inflammatory and profibrotic cellular response due to oxidative stress (White et al., 2020).

In this study, we also evaluated the expression levels of genes encoding for *PAR1* and *PAR2* receptors. PARs are receptors located on the cell surfaces of CMs, CFs, endothelial cells, vascular smooth muscle cells and other kind of cells. Research showed that FIIa and FXa can activate these receptors (Posma et al., 2016). From our results it emerged that in hESC-CFs model, *PAR1* receptor is more abundantly expressed compared to *PAR2* receptor, this is in line with previously findings in CFs from primary culture (D'Alessandro et al., 2022).

A crucial aspect of the characterization involved the investigation of *TGFβ* effects on pro-inflammatory and profibrotic genes in hESC-CFs at 4 hours or 24 hours of incubation. During early incubation phases, *TGFβ* induced a pro-inflammatory response as previously described (van Nieuwenhoven et al., 2013). On the contrary, this effect is completely reversed after late incubation at 24 hours showing an anti-inflammatory effect. As a well-known profibrotic factor (Chen et al., 2000), in our experiment *TGFβ* caused a strong increase on profibrotic genes, especially after 24 hours of incubation. Furthermore, our data confirmed the profibrotic effect of *TGFβ* through a positive feedback mechanism, leading to the

upregulation of its own gene expression and enhancing the transition to myofibroblasts. This transition is mediated via *TGFβ* receptors on the CFs cell surface triggering Smad intracellular signalling (Moustakas, 2002).

Role of Coagulation Factors in inflammatory and fibrotic processes in hESC-CFs

Only a limited number of studies have explored the potential impact of activated coagulation factors on cardiac remodeling; these studies were mainly conducted on atrial fibroblasts from rats, but also in primary atrial fibroblasts from humans (D'Alessandro et al., 2021; Spronk et al., 2017).

From this study we observed that both coagulation factors, FXa and FIIa, can regulate pro-inflammatory and profibrotic genes. It emerged that Thrombin has a strong effect on *IL-6* at 4 hours of incubation, while FXa positively regulates the expression of *CCL2* and *IL-6* at both timepoints. This implies that pro-inflammatory genes are regulated early by FIIa and FXa. In this study it was not demonstrated that the effect of the coagulation factors is *PAR1*-mediated as previously shown (D'Alessandro et al., 2021). Further experiments using *PAR1* agonists and antagonists will need to be conducted. However, we have observed that in this new cellular model *PAR1* and *PAR2* are expressed, so we can hypothesize that the effect is PAR-mediated. In our case, it was not possible to observe a positive feedback mechanism of *PAR1* and *PAR2* expression levels after exposure to Thrombin and FXa, as previously demonstrated in other cardiac fibroblast models (D'Alessandro et al., 2021; Spronk et al., 2017), although an increasing trend was observed, especially after 4 hours of exposure.

A regulation by coagulation factors of the genes involved in the fibrotic process (activation of fibroblasts into myofibroblasts) has emerged. Thrombin appears to exert a significant effect on *CTGF*, a gene associated with fibrotic processes (Rebolledo et al., 2021), in the early incubation phase (4 hours); while this effect is no longer visible at 24 hours. Contrary to what was demonstrated by D'Alessandro et al. on primary adult rat CFs (D'Alessandro et al., 2021), our data showed that *ACTA2* and *TGFβ* expression does not appear to be statistically regulated by Thrombin in the early stages of incubation although an increasing trend is quite visible. A similar pattern is observed for *COL1A1* expression. However, incubation with FXa induces a significant, dose-dependent increase in *ACTA2* levels at 24 hours, suggesting its role in fibroblast activation and differentiation towards a myofibroblast phenotype. This aligns with previous studies demonstrating FXa's involvement in profibrotic signaling pathways (D'Alessandro et al., 2021). *CTGF* expression shows a rapid and robust increase at 4 hours following FXa exposure, but its sustained upregulation at 24 hours occurs only in cells treated with higher FXa concentrations. This suggests an early fibrotic response that is reinforced under prolonged and intensified FXa stimulation. In contrast, *COL1A1* expression does not show a significant response to FXa. However, *TGFβ* expression increases only after 24 hours at most FXa concentrations, suggesting a delayed fibrotic signaling response. This aligns with the role of *TGFβ* as a key regulator of fibrosis that is often activated downstream of initial inflammatory and fibrotic cues (Moustakas, 2002). These findings highlight FXa's potential role in modulating fibroblast activation and fibrotic responses, supporting its involvement in cardiac structural remodeling.

Chapter 4

Results and Discussion

Activated Coagulation Factors FXa and Thrombin induce prohypertrophic response in human stem-cell derived cardiomyocytes (hiPSC-CMs) through stimulation of protease activated receptor 1 (*PAR1*)

4.1 Characterization of the hiPSC-CMs Cellular Model: Molecular and Functional Analyses

Gene expression of stem cells markers from RT-qPCR

To verify the differentiation status of hiPSC-CMs line compared to stem cells, we measured the expression dynamics of pluripotency-associated genes of SOX2, OCT4, NANOG and LIN28 after the differentiation protocol at Day 1 (d1) and Day 7 (d7) and compared it to levels in stem cells. These genes, central regulators of stem cell pluripotency, show a marked downregulation during differentiation. Their expression levels drop significantly at day 1 and remain low at day 7 (Figure 25). This trend indicates a loss of the pluripotent state and a successful initiation of differentiation. According to studies, the effective silencing of OCT4 and NANOG correlates with the efficiency of differentiation protocols, serving as a benchmark for assessing the quality of stem cell-derived models (Yu et al. 2007).

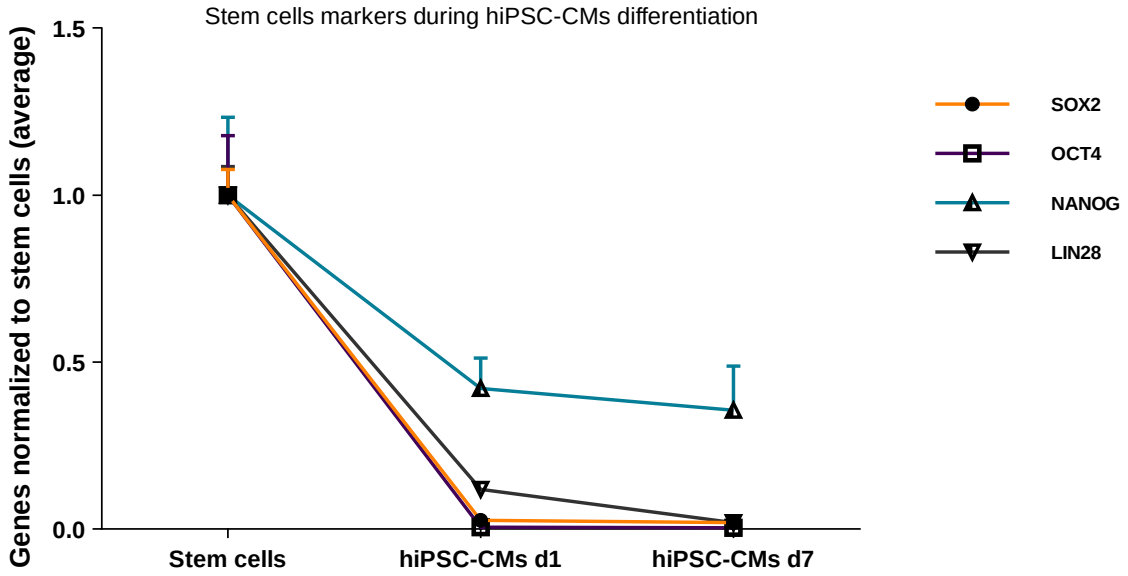

Figure 25. Expression levels of stem cell markers (SOX2, OCT4, NANOG and LIN28) in stem cells and hiPSC-CMs cultures after Differentiation Protocol at Day 1 (d1) and Day 7 (d7). RT-qPCR analysis shows significant downregulation over time, indicating the transition from a pluripotent state to a differentiated cardiomyocyte lineage. The y-axis represents the normalized gene expression (relative to stem cells). Error bars represent standard deviation.

Gene expression of cardiomyocyte markers from RT-qPCR

The Figure 26 illustrates the expression dynamics of cardiomyocyte marker genes (*NPPB*, *NPPA*, *TNNI3, MYH7, TNNT2, MYH6* and *HCN4*) after the differentiation process of hiPSC-CMs at Day 1 (d1) and Day 7 (d7). The data highlights a progression from a pluripotent stem cell state to differentiated cardiomyocytes. *TNNT2, TNNI3, MYH6, MYH7* and *NPPA* show steep and consistent increases in expression from day 1 to day 7, reflecting robust structural and functional maturation of cardiomyocytes. In contrast to the sharp increases seen with most other markers, *NPPB* displays a gradual increase from day 1 to day 7 and HCN4 shows a decreasing trend during differentiation. HCN4 is highly expressed on day 1 of differentiation, but its levels significantly decrease by day 7. HCN4 is known to play a pivotal role in pacemaker cells of the sinoatrial node, where it governs the funny current (I_f), critical for initiating and regulating heart rhythms. Its expression is typically prominent in the early stages of differentiation and gradually declines as the cardiomyocytes mature. This decline in HCN4 expression could suggest a shift from an atrial-like or pacemaker-like phenotype to ventricular cardiomyocytes, which rely less on HCN4-mediated pacemaker activity.

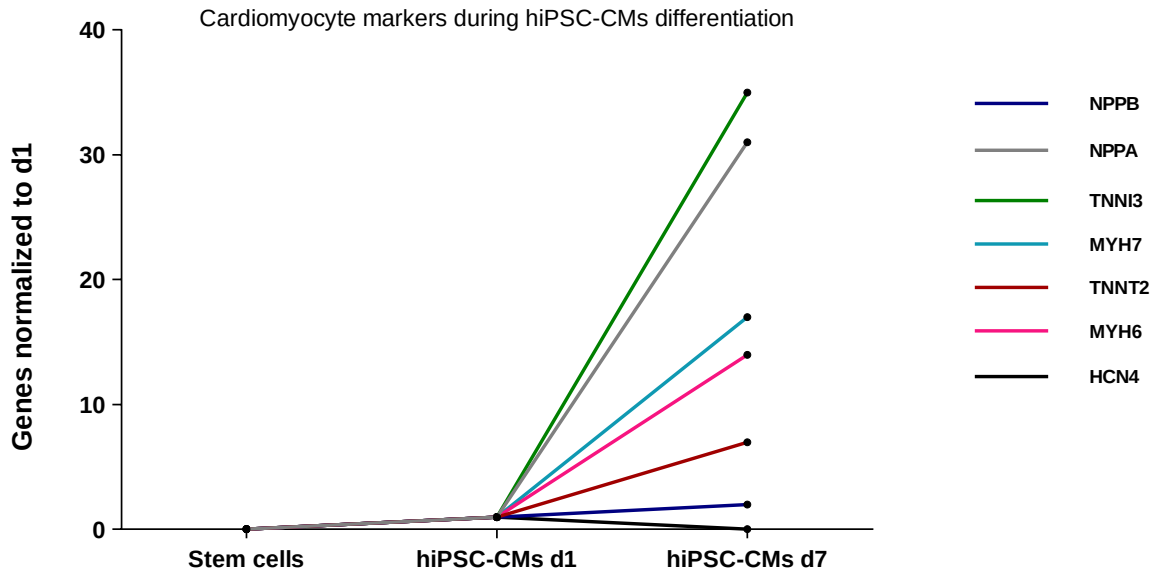

Figure 26. Expression levels of cardiomyocyte markers (*NPPB, NPPA, TNNI3, MYH7, TNNT2, MYH6* and *HCN4*) in stem cells and hiPSC-CMs cultures after Differentiation Protocol at Day 1 (d1) and Day 7 (d7). Almost all cardiac genes show a marked increase from d1 to d7, reflecting progressive cardiomyocyte maturation. In contrast, HCN4 peaks at d1 and decreases by d7, indicating its role in early differentiation while *NPPB* demonstrates a gradual rise compared to other sharply increasing markers. The y-axis represents the normalized gene expression (relative to d1).

Cardiomyocyte markers from Immunocytochemistry

To understand the maturation state of hiPSC-CMs, a monolayer of beating cells was cultured on a 4-well culture slide for immunocytochemistry (ICC) experiments. The images below show immunofluorescence results highlighting the structural organization of hiPSC-CMs. Hoechst dye (blue) stains the cell nuclei, Actin (green) labels the actin filaments and cardiac Troponin I (cTnI) (green) identifies a key contractile protein specific to cardiomyocytes. The Figure 27 shows the distribution and morphology of hiPSC-CMs stained with Actin and Troponin I at different magnifications. Interestingly, we identified binucleated cardiomyocytes that is a hallmark of mature phenotype. From confocal microscopy it was possible to visualize the sarcomeric structure (Figure 28) with an evident striated pattern, reflecting the organization of mature sarcomeres. Overall, the ICC images show that hiPSC-CMs express key structural and contractile proteins essential for cardiomyocyte function.

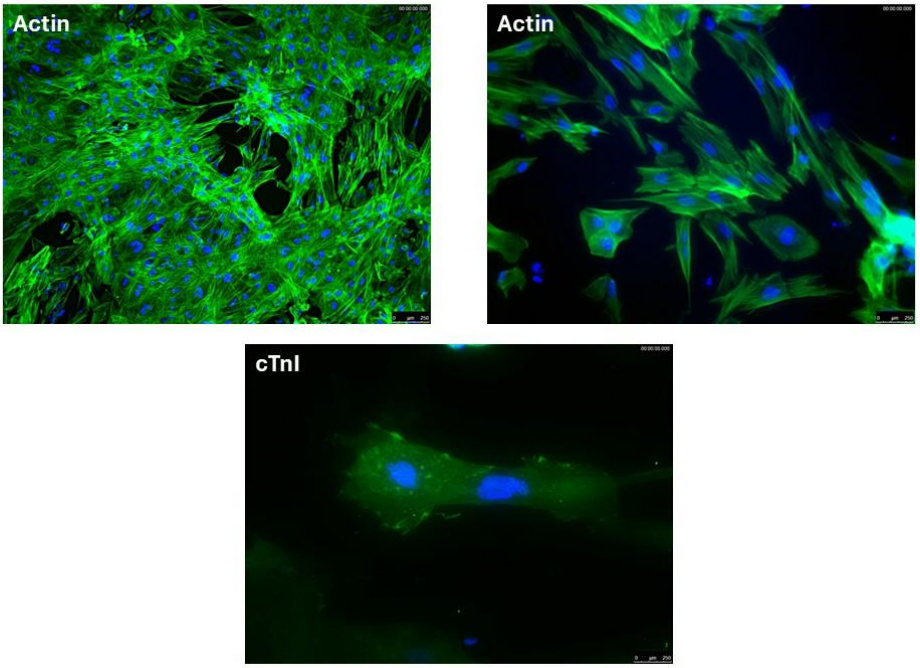

Figure 27. Structural organization in hiPSC-derived cardiomyocytes. Immunofluorescence images show actin filaments (top panels) and cardiac Troponin I (bottom panel) during hiPSC-CMs maturation.

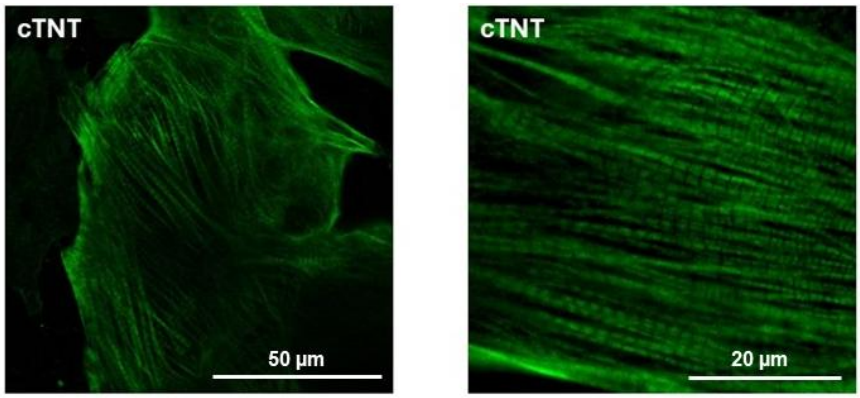

Figure 28. Sarcomere organization in iPSC-derived cardiomyocytes. Immunofluorescence images showing cardiac troponin T (cTNT) staining in cardiomyocytes.

4.2 Role of Coagulation Factors in hypertrophic processes in hiPSC-CMs

4.2.1 Effect of FIIa on pro-hypertrophic and pro-inflammatory genes

After the characterization of hiPSC-CMs model, we evaluated the effect of coagulation factors on pro-hypertrophic genes (*NPPA* and *NPPB*) and pro-inflammatory gene (*CCL2*). As shown in Figure 29, incubation of hiPSC-CMs with Thrombin (0.008 nM) leads to a significant increase of *NPPB* (±10-fold), *NPPA* (±2-fold) and *CCL2* (±5-fold) expression compared to control. While when hiPSC-CMs were exposed to Dabigatran (350ng/mL), a direct Thrombin Inhibitor, there was a significant reduction in the FIIa-induced upregulation of *NPPB* (±10-fold decrease) and *NPPA* expression (±2-fold decrease). This effect is not significant in the case of *CCL2*, but a strong reduction is evident (Figure 29, C).

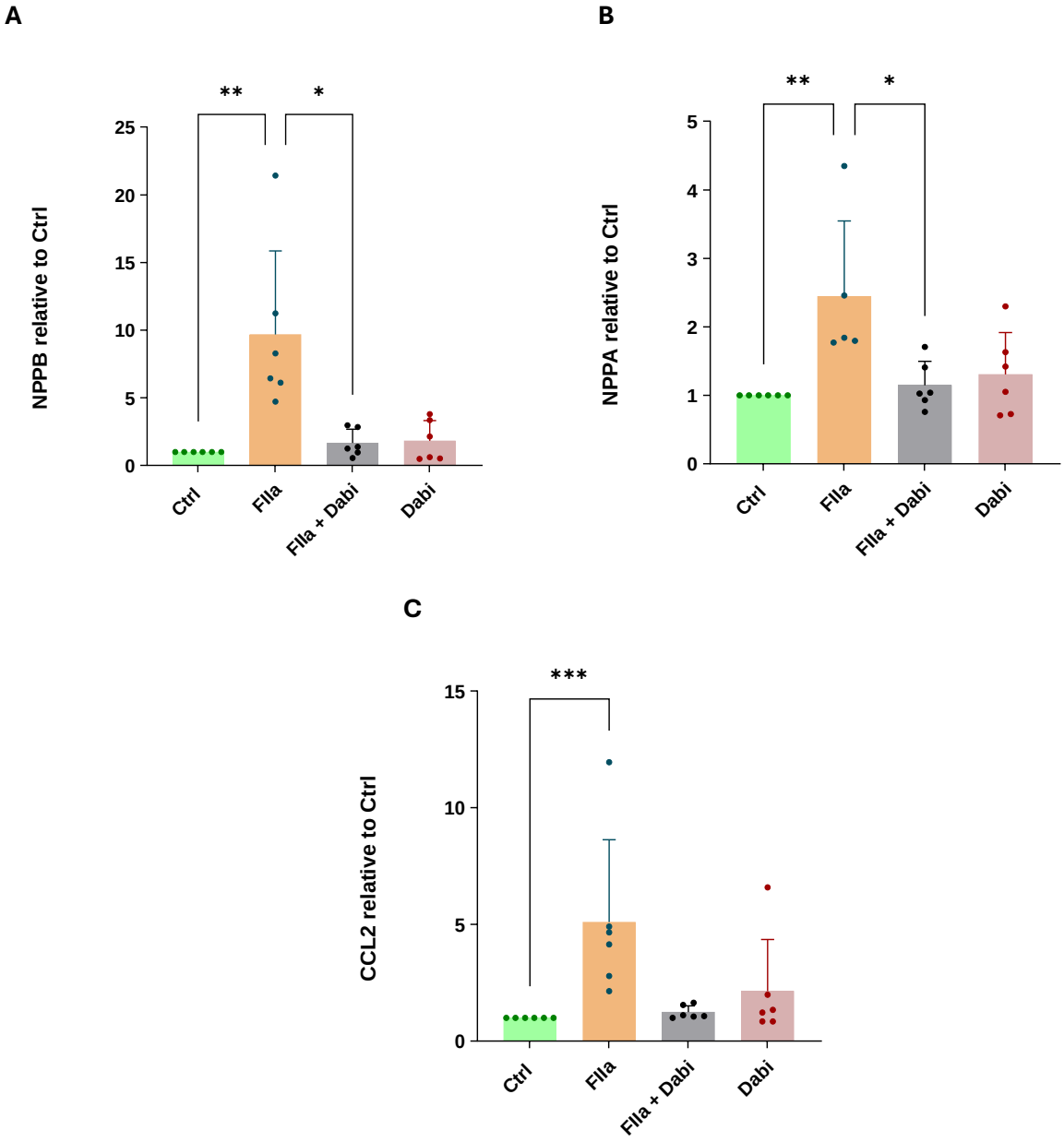

Figure 29. Effect of FIIa on hiPSC-CMs model. **(A - B)** Effect of FIIa (0.008 nM) on pro-hypertrophic genes after 24 hours of incubation (n=6) and **(C)** pro-inflammatory gene in the presence and absence of Dabigatran (350ng/mL). FIIa treatment significantly increases *NPPB*, *NPPA* and *CCL2* expression compared to the control. This effect is significantly prevented in *NPPB* and *NPPA* expression when hiPSC-CMs are incubated with Dabigatran (in presence or absence of FIIa), this effect is not significant in the case of *CCL2*, but a strong reduction is evident. Results are expressed as fold-change relative to control, with dots indicating different iPSC-CM experiments and error bars

indicating SD. Statistical analysis was performed using the non-parametric Kruskal-Wallis test with Dunn's multiple comparison *post-hoc* test (*p<0.05, ** p<0.01, *** p<0.001, **** p<0.0001).

4.2.2 Effect of FIIa on PAR Receptors

FIIa treatment does not significantly affect the mRNA levels of PAR receptors. A small increase in *F2R* expression was found, which has reverted with Dabigatran (Figure 30, A). In contrast, the *F2RL1* expression was reduced by FIIa compared to control (Figure 30, B). These differences don't reach statistical significance, possibly due to high variation and limited number of experiments.

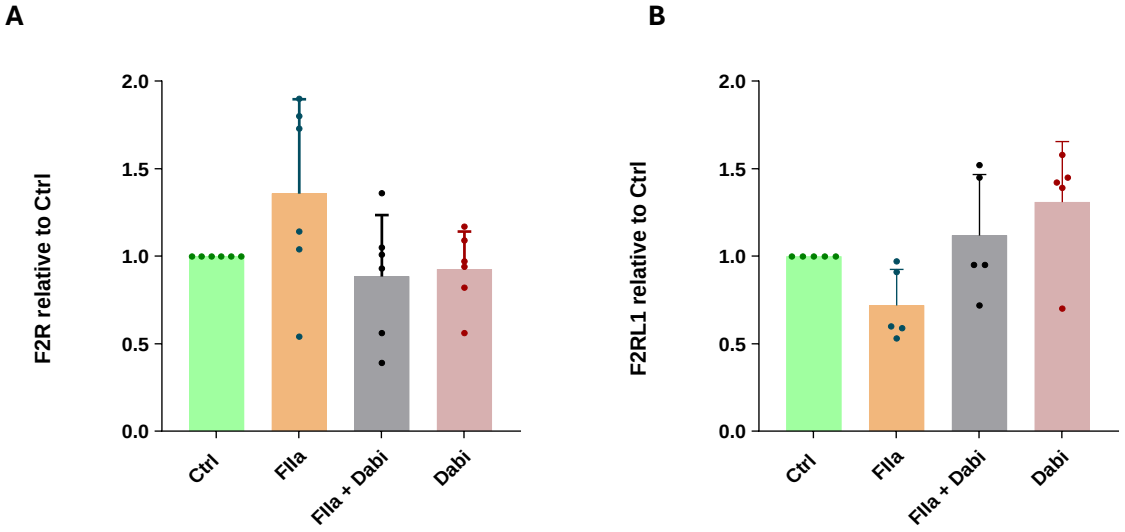

Figure 30. Effect of FIIa on PAR Receptors genes. **(A)** Effect of FIIa (0.008 nM) with or without Dabigatran (350ng/mL) on *F2R* expression in hiPSC-CMs cultures after 24 hours of incubation (n=6). No statistically significant differences were observed between FIIa-treated and control groups at either timepoint. **(B)** Effect of FIIa (0.008 nM)) with or without Dabigatran (350ng/mL) on *F2RL1* expression in hiPSC-CMs cultures after 24 hours (n=5). No statistically significant differences were observed between FIIa-treated and control groups at either timepoint. Results are expressed as fold-change relative to control, with dots indicating separate experiments and error bars indicating SD. Statistical analysis was performed using the non-parametric Kruskal-Wallis test with Dunn's multiple comparison *post-hoc* test (*p<0.05, ** p<0.01, *** p<0.001, **** p<0.0001).

4.2.3 Effect of FXa and *PAR1* Agonist on pro-hypertrophic and pro-inflammatory genes

We conducted experiments using FXa (50 nM) and its inhibitor Rivaroxaban (400ng/mL) to clarify the involvement of this coagulation factor in the molecular mechanisms underlying cardiac hypertrophy and the potential protective effect of its inhibitor. Furthermore, to evaluate whether the effect is *PAR1* mediated we used a selective *PAR1* agonist, TRAP14 (100 µM). As shown in Figure 31, direct activation of *PAR1* by the agonist TRAP14 significantly upregulates the mRNA expression of the hypertrophic genes *NPPB* (±6.5-fold) and *NPPA* (±2-fold) and pro-inflammatory gene *CCL2* (±3-fold) compared to control. These findings suggest that *PAR1* activation plays a direct role in promoting pro-hypertrophic and pro-inflammatory responses in cardiomyocytes. Similarly, exposure of iPSC-CM to FXa strongly upregulates the mRNA expression of *NPPB* (±6-fold), *NPPA* (±2-fold) and *CCL2* (±3.5-fold). Surprisingly, direct inhibition of FXa via Rivaroxaban doesn't downregulate the effect of FXa on gene expression in hiPSC-CMs.

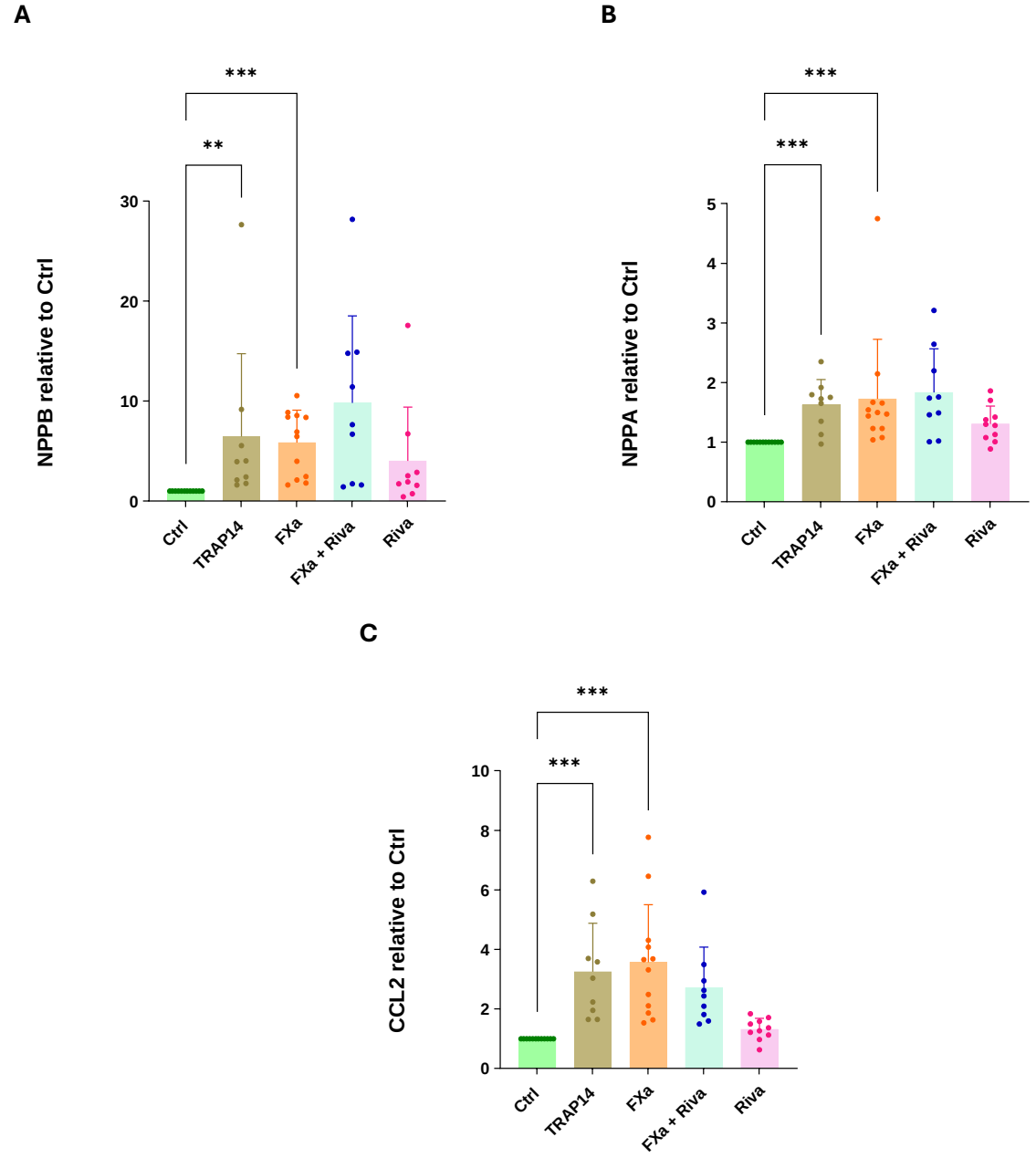

Figure 31. Effect of FXa and *PAR1* activation on pro-hypertrophic and pro-inflammatory genes. Cells incubated with TRAP14 (100 µM) or FXa (50 nM) significantly express pro-hypertrophic and pro-inflammatory genes compared to control. On the contrary, direct inhibition of FXa via Rivaroxaban (400 ng/mL) doesn't downregulate the effect of FXa on gene expression in hiPSC-CMs model. Gene expression was measured by RT-qPCR after 24 hours of incubation.

Results are expressed as fold-change relative to control, with dots indicating separate experiments and error bars indicating SD. Statistical analysis was performed using the non-parametric Kruskal-Wallis test with Dunn's multiple comparison *post-hoc* test (*p<0.05, ** p<0.01, *** p<0.001, **** p<0.0001).

A possible explanation for the lack of effect of Rivaroxaban is that the FXa we used in these experiments is purified FXa from human blood, so it's possible that there is a contamination with Thrombin. From our studies it emerged that a lower concentration of FIIa (0.008 nM) is sufficient to have a significant effect on the gene expression in cardiomyocytes and cardiac fibroblasts. Consequently, given the low concentrations of Thrombin (0.008 nM) and relatively high concentration of FXa (50nM) used in the present study, the pro-hypertrophic and inflammatory effect observed with FXa appears to be primarily caused by activation of *PAR1* via Thrombin. For this reason, we conducted a set of experiments incubating FXa (50 nM) with Dabigatran (350ng/mL) together. As shown in Figure 32, already at 4 hours of incubation, Dabigatran completely prevented the upregulation of *CCL2* triggered by FXa and reduced the FXa-induced overexpression of *NPPB* (±2-fold decrease). Furthermore, it's possible to appreciate a slightly reduction of *NPPA* expression level after incubation with Dabigatran.

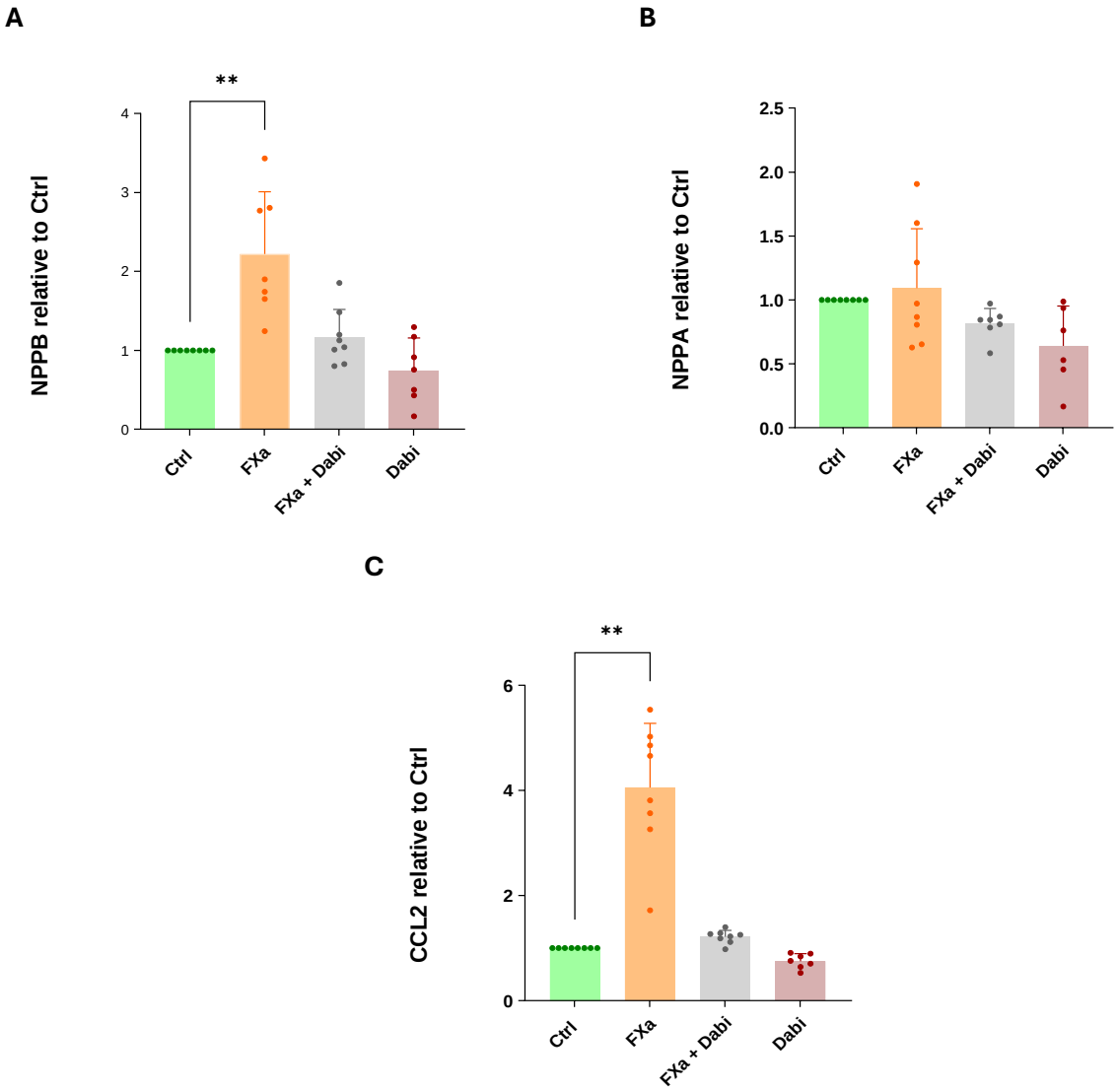

Figure 32. Effect of FXa inhibition via Dabigatran on *NPPB*, *NPPA* and *CCL2* gene expression in hiPSC-CMs model. Cells were incubated with FXa (50nM) with and without Dabigatran (350ng/mL). Gene expression was measured by RT-qPCR after 4 hours of incubation. Results are expressed as fold-change relative to control, with dots indicating different hiPSC-CM experiments and error bars indicating SD. Statistical analysis was performed using the non-parametric Kruskal-Wallis test with Dunn's multiple comparison *post-hoc* test (*p<0.05, ** p<0.01, *** p<0.001, **** p<0.0001).

4.2.4 Effect of FXa and *PAR1* Antagonist on pro-hypertrophic and pro-inflammatory genes

The co-treatment of FXa with the *PAR1* antagonist (SCH79797; 1µM) reduces *NPPB* (±2-fold decrease), *NPPA* (±1-fold decrease) and *CCL2* (±2-fold decrease) mRNA expression levels compared to FXa alone, indicating that the hypertrophic effects of FXa are at least partially mediated by *PAR1* signaling (Figure 33).

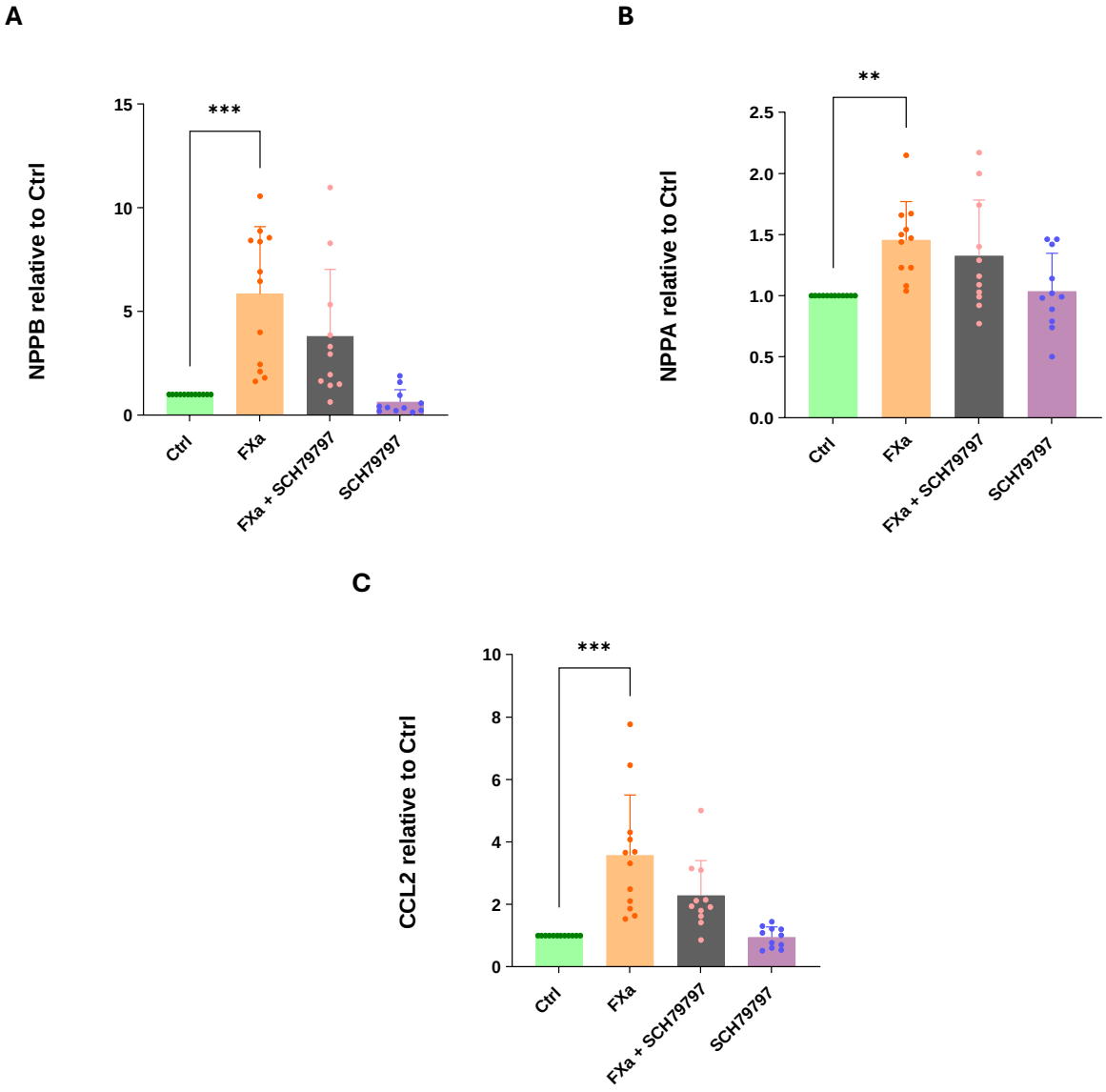

Figure 33. Effect of FXa and *PAR1* deactivation on pro-hypertrophic and pro-inflammatory genes. Exposure to FXa (50 nM) significantly upregulates the expression of *NPPB*, *NPPA* and *CCL2* compared to the untreated control. Co-treatment with the *PAR1* antagonist SCH79797 (1µM) attenuates the FXa-induced upregulation, suggesting a *PAR1*-dependent mechanism. SCH79797 alone does not significantly alter the expression of these markers compared to the control. Gene expression was measured by RT-qPCR after 24 hours of incubation. Results are expressed as fold-change relative to control, with dots indicating separate experiments and error bars indicating SD. Statistical analysis was performed using the non-parametric Kruskal-Wallis test with Dunn's multiple comparison *post-hoc* test (*p<0.05, ** p<0.01, *** p<0.001, **** p<0.0001).

4.2.5 Effect of Coagulation Factors on sarcomere genes

We evaluate the expression of the sarcomere genes, *MYH6* and *MYH7*, without identifying any statistically significant variation after treatment with FIIa or with FIIa + Dabigatran (FIIa + Dabi) (Figure 34, A and B). However, we reveal an interesting trend: incubation with Thrombin seems to reduce the

levels of *MYH6* compared to the control values. This trend is reversed by treatment with Dabigatran (Figure 34, C). This trend is especially fascinating as it closely matches the findings of the Kurabayashi study (Kurabayashi et al., 1990) in cardiac overload conditions. In such conditions, the α myosin heavy chain (gene name: *MYH6*) isoform typically decreases, while the β myosin heavy chain (gene name: *MYH7*) isoform increases.

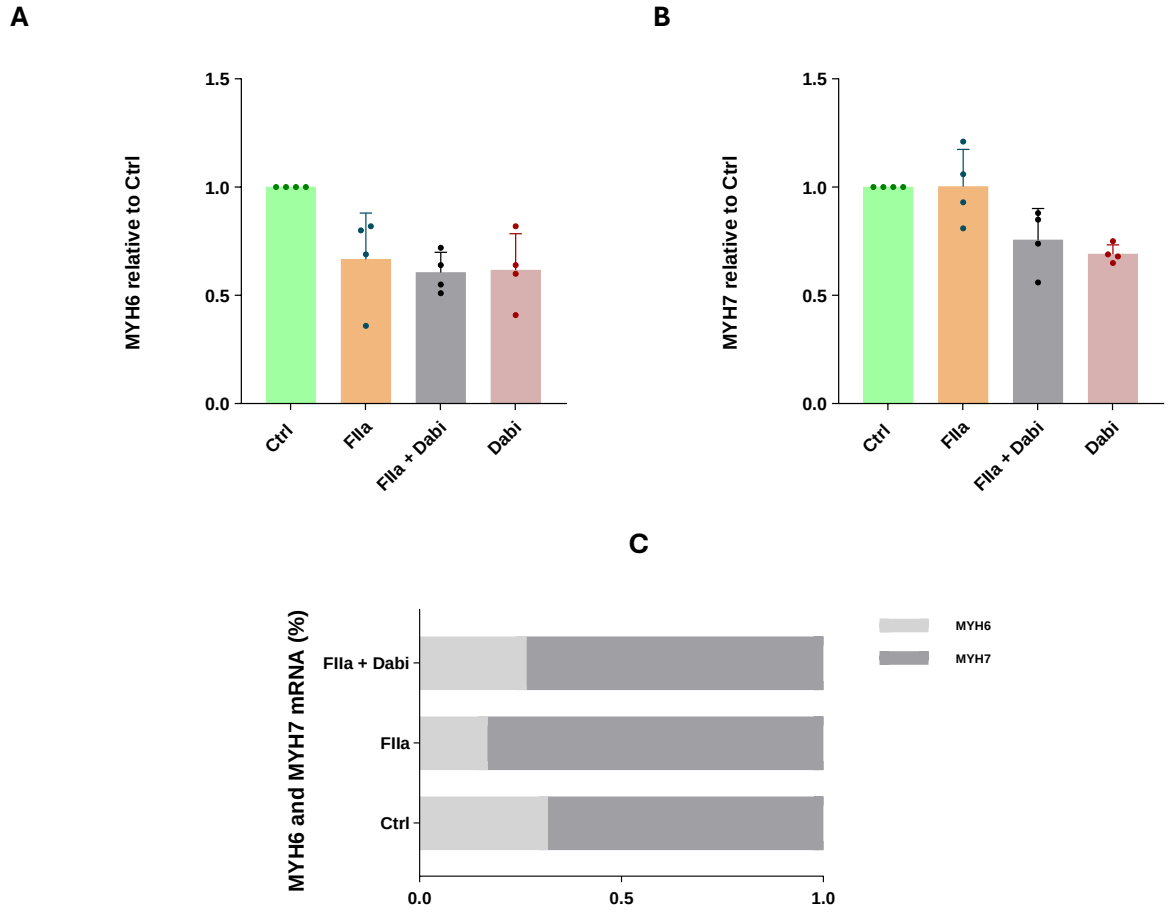

Figure 34. (A-B). Effect of FIIa on sarcomere genes. The graph illustrates the relative expression levels of *MYH6* and *MYH7* after incubation with FIIa (0.008 nM) and Dabigatran (350ng/mL) with o without FIIa. No statistically significant differences are observed, although a trend toward decreased *MYH6* levels is evident after all incubations. In contrast, a reduction in *MYH7* expression levels is observed only after incubation with Dabigatran (with or without FIIa). Results are expressed as fold-change relative to control, with dots indicating separate experiments and error bars indicating SD. Statistical analysis was performed using the non-parametric Kruskal-Wallis test with Dunn's multiple comparison *post-hoc* test (*p<0.05, ** p<0.01, *** p<0.001, **** p<0.0001). **(C).** Relative expression of *MYH6* and *MYH7* mRNA in control, FIIa and FIIa + Dabigatran treatment. The FIIa group shows reduced *MYH6* levels (lighter grey bar) and increased *MYH7* levels (darker grey bar) compared to the control group. In the FIIa + Dabigatran group, the *MYH6* and *MYH7* levels are comparable to the control group.

Incubation with TRAP14 (100 μM) or FXa (50 nM) decrease *MYH6* and *MYH7* expression levels, however the data is statistically significant only in the incubation with FXa for *MYH6* expression. Incubation with Rivaroxaban (400 ng/mL), whether alone or combined with FXa, shows no significant changes in *MYH6* and *MYH7* levels (Figure 35, A and B). In this case a possible shift between the *MYH6* (pink bar) and *MYH7* (sky blue bar) isoforms is not very pronounced (Figure 35, C).

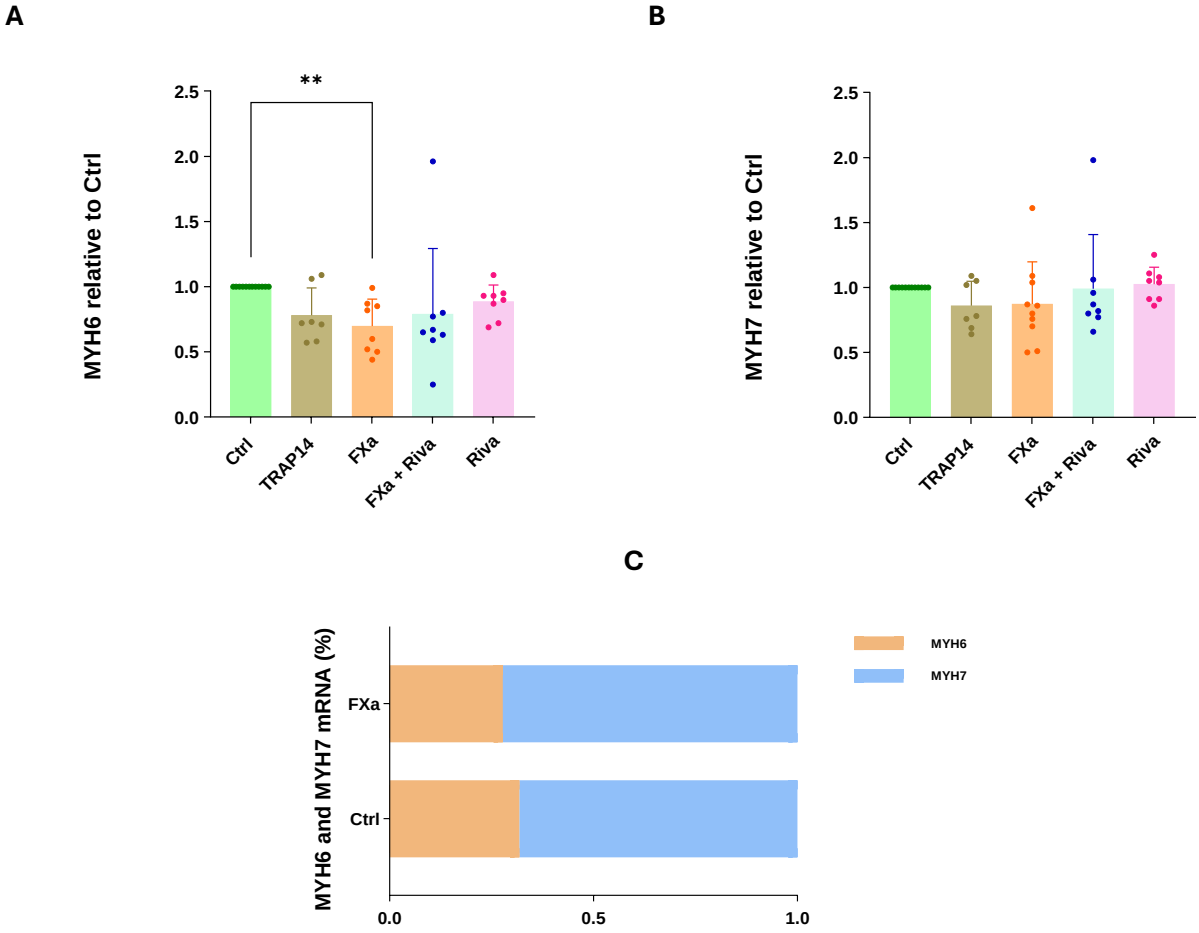

Figure 35. (A - B) Effect of FXa and *PAR1* activation on sarcomere genes. The graph illustrates the relative expression levels of *MYH6* and *MYH7* after incubation with TRAP14 (100 μM), FXa (50 nM), or Rivaroxaban (400 ng/mL) with or without FXa. Treatment with TRAP14 and FXa reduce *MYH6* and *MYH7* expression. In contrast, Rivaroxaban, whether administered alone or with FXa, doesn't affect *MYH6* or *MYH7* levels. Results are expressed as fold-change relative to control, with dots indicating separate experiments and error bars indicating SD. Statistical analysis was performed using the non-parametric Kruskal-Wallis test with Dunn's multiple comparison *post-hoc* test (*p<0.05, ** p<0.01, *** p<0.001, **** p<0.0001). **(C).** Relative expression of *MYH6* and *MYH7* mRNA in control condition and during incubation with FXa.

4.3 BNP ELISA Results

The Figure 36 represents the levels of circulating BNP (B Natriuretic Peptide) detected in the incubation medium of hiPSC-CMs cultures after 24 hours of incubation with different factors. BNP is a protein typically secreted under hypertrophic conditions, so its presence is an indirect indicator of hypertrophic stress in the cells. FXa, FIIa and TRAP14 incubation show higher BNP levels compared to the control. Co-treatment FXa + SCH79797 shows a reduction in BNP levels. Statistical significance can not be proven, because of the low number of experiments. However, these results indicate that, similar to *NPPB* gene expression, also BNP protein levels are increased by coagulation factors FXa and FIIa through *PAR1* activation.

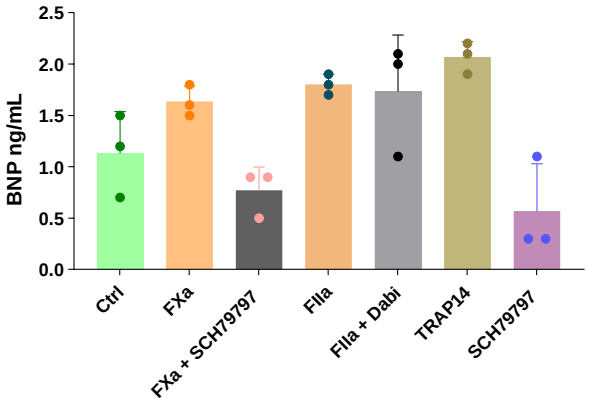

Figure 36. Levels of BNP (B Natriuretic Peptide) measured in the culture medium of hiPSC-derived cardiomyocytes after 24 hours of treatment with different factors. BNP secretion, a hallmark of cardiac hypertrophy, is increased by FXa, FIIa, and TRAP14 treatments. Co-treatment with SCH79797 or Dabigatran reduces BNP levels induced by FXa and FIIa, respectively, suggesting their inhibitory effects. SCH79797 alone significantly lowers BNP secretion. Data represent mean ± SD, with individual data points shown.

4.4 Discussion

Characterization of the hiPSC-CMs Cellular Model: Molecular and Functional Analyses

The advent of cellular reprogramming with the discovery of the hiPSC-CMs model has revolutionized the scientific community and transformed the way basic research is conducted. Among the many practical advantages, the use of this model would allow for a drastic reduction in the employment of animal models, which are still widely used in biomedical research despite ethical concerns and physiological differences that can limit their translational relevance to human biology. Furthermore, this model has a wide range of potential applications, as the differentiated cells can be directly derived from the patient and, after appropriate manipulation, re-implanted without the risk of rejection. However, the effective use of hiPSC-CMs remains challenging, primarily due to their structural immaturity (Koivumäki et al., 2018) and incomplete electrophysiological properties (Goversen et al., 2017).

In our study, to assess the degree of maturation of hiPSC-CMs, they were characterized through both molecular and structural analyses. Structural analysis was performed using advanced imaging techniques, including confocal and fluorescence microscopy, to examine sarcomere organization and overall cellular architecture. Since long-term culture has been suggested as a strategy to promote cardiomyocyte maturation (Jiang et al., 2018), we selected two distinct post-differentiation timepoints day 1 and day 7, to assess the baseline expression levels of both cardiac-specific and pluripotency markers. By day 7, cardiomyocytes exhibited a significant upregulation of cardiac-specific markers compared to day 1, while pluripotency markers, already markedly reduced at day 1, showed a further decline, indicating progressive maturation. Interesting *NPPA* exhibits a steep and consistent increase in expression from day 1 to day 7, while *NPPB* does not show increased expression levels between the two timepoints. This trend aligns with postnatal expression patterns, where *NPPB* is generally expressed at lower levels than *NPPA* throughout the heart. Meanwhile *NPPA* becomes restricted to the atria, with some residual expression in the peripheral ventricular conduction system (Houweling et al., 2005). This could indicate that post-differentiation cardiomyocytes present a more atrial-like phenotype.

HiPSC-CMs exhibit spontaneous contractile activity, similar to sinoatrial node cells, primarily due to the funny current mediated by the HCN4 channel. In our study, in addition to assessing HCN4 expression levels, we performed structural imaging to evaluate sarcomeric organization. Sarcomere formation begins during the cardiomyocyte differentiation process and then continues into the early postnatal phase. Subsequently, the structure acquired at this level is maintained throughout life (Ahmed et al.,

2022). To assess the maturation level of sarcomeres from hiPSC-CMs, we analyzed images obtained through confocal microscopy. From a morphological standpoint, we observed that the sarcomeres were positioned in a parallel and aligned manner. Subsequently, we measured the length of the sarcomeres using ImageJ, and it was found that the average length of the sarcomeres was around 2 µm, which is consistent with mature sarcomeres phenotype (Bird et al., 2003).
Despite these findings, hiPSC-CMs remain immature compared to adult cardiomyocytes. Strategies such as metabolic conditioning (e.g., fatty acid supplementation), extended culture duration, and electrical stimulation have been shown to promote maturation (Yang et al., 2019; Ronaldson-Bouchard et al., 2018). Moreover, 3D culture systems like engineered heart tissues or cardiac organoids further enhance structural and functional maturation by better mimicking the native cardiac environment (Giacomelli et al., 2020).

Role of Coagulation Factors in hypertrophic processes in hiPSC-CMs
The effects of coagulation factors on cardiac remodeling are not only limited to the context of cardiac fibrosis but also appear to extend to induced hypertrophy in cardiomyocytes. To date, no studies have specifically characterized the effect of coagulation factors such as Thrombin and FXa on hiPSC-CMs model. Our results provide new insights into this area indicating that hFXa is capable of significantly upregulating the expression of hypertrophic (*NPPA* and *NPPB*) and proinflammatory (*CCL2*) genes in this model. This regulation appears to be mediated by *PAR1* activation, as incubation of the cells with the selective *PAR1* antagonist SCH79797 resulted in a notable reduction in gene expression, which returned to control levels. Conversely, treatment with the selective *PAR1* agonist, TRAP14, induced an upregulation of gene expression, comparable to the effect observed with FXa incubation.
At the same time, we stimulated human iPSC-CMs with the FXa specific inhibitor, Rivaroxaban. Surprisingly, in cells treated with Rivaroxaban, the FXa induced upregulation was not inhibited. Additionally, BNP secretion was not suppressed in the culture medium of samples treated with both FXa and Rivaroxaban (*data not shown*). The lack of inhibition from Rivaroxaban on FXa could be explained by the fact that we used purified human FXa, which may contain traces of Thrombin. From our experiment, we noticed that a very low concentration of Thrombin is sufficient to have significant upregulation of hypertrophic genes because Thrombin is the most potent activator of *PAR1*. Since Rivaroxaban is a specific inhibitor of FXa and has no direct effects on Thrombin, it may have only partially modulated the FXa-mediated hypertrophic response. This suggests that Thrombin contamination in the FXa preparation may have mediated the observed effects. On the contrary the effect of FIIa on hypertrophic and proinflammatory genes is prevented using its selective antagonist, Dabigatran. Because Thrombin mediated expression of hypertrophic genes was comparable to that induced by FXa, and very low concentrations of Thrombin were sufficient to trigger a notable hypertrophic response, we exposed human iPSC-CMs to FXa with and without Dabigatran to test for possible Thrombin contamination in the FXa preparation. Our experiments showed that Dabigatran completely inhibited the effect of FXa, confirming that, in these contexts, Thrombin (acting through *PAR1*) is the main mediator of the hypertrophic response observed in human iPSC cardiomyocytes.

Chapter 5

Results and Discussion

3D Engineered Heart Tissue (EHT)

5.1 Characterization of 3D EHT Rings in Different Culture Conditions

5.1.1 Surface Area of 3D hESC-CFs 3D EHT Rings

To assess and compare the stability of hESC-CFs 3D rings in terms of morphology, stiffness, cell distribution and variations in gene expression; the rings were cultured for 14 days in different culture media. In particular, the 3D rings were kept in culture using specific cardiac fibroblast medium (CFGM supplemented with serum 1% and CFGM supplemented with serum 10% respectively) and specific cardiomyocyte medium (CM RPMI: RPMI medium 1640(1x) + GlutaMAX™ #61870 Gibco Thermofisher + B27™ supplement (50x) (#17504044, 17504001 Gibco Thermofisher) + Penicillin/Streptomycin (Gibco)). The graphs below (Figure 37) highlight a clear trend of surface area reduction (in mm^2): initially, most rings start with a larger surface area (up to 80 mm^2), but there is a rapid surface decrease, due to collagen compaction, during the first few days of culture. This reduction stabilizes after day 7, with most rings maintaining a surface area between 10 and 20 mm^2 (corresponding to ring thickness of approximately 1mm) until day 14 (Figure 37, A). The graph B shows the trend of the cell surface of hESC-CFs 3D rings in different culture conditions: CFGM 1%, CFGM 10% and CM RPMI medium. Interestingly, the difference between CFGM 1% and CFGM 10% is almost none, but when cultured in CM RPMI the average ring surface area seems larger. In specific cardiac fibroblast medium, there is a significant reduction in surface area from day 1 to day 7 and maintain a small, stable surface area until day 14. In CM RPMI medium, rings exhibit the highest variability, with a generally larger surface area compared to the CFGM groups, especially at day 7. This could indicate that CM RPMI promotes less compaction, possibly due to differences in nutrient composition. These data demonstrate that the degree of ring compaction is medium-dependent, with the most significant compaction occurring during the initial phase of culture. This might also be a consequence of differences in fibroblast phenotype, with cells in CFGM likely adopting a more myofibroblast-like phenotype, known for their stronger contractile activity. Myofibroblasts are characterized by increased contractility, which could explain the pronounced compaction observed in the CFGM groups.

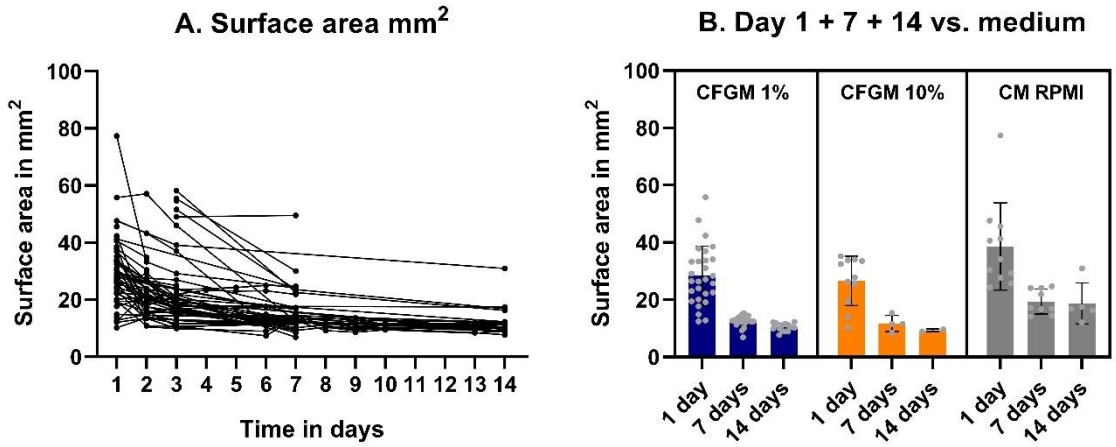

Figure 37. The course of compaction of the 3D rings consists of hESC-CFs only. The surface area (in mm^2) is measured daily via ImageJ. These surface areas include the center post area which has a surface area of 3.14 mm^2. **(A)** All measured surface area per day. **(B)** Surface area categorized by medium type and selected by day 1, 7, and 14. Bar indicates mean.

5.1.2 ESC-CFs Distribution throughout 3D Rings

To evaluate the distribution of cardiac fibroblasts throughout the matrix, several hESC-CFs 3D rings (after 14 days of culturing) were fixed in 4% paraformaldehyde and embedded in paraffin. Embedded rings were sectioned into 4 µm thick paraffin tissue slices using a Slee™ Aquatec microtome. After a

series of rehydration in ethanol, staining with Hematoxylin and Eosin (H&E), followed by series of dehydration in ethanol. The Figure 38 illustrates a histological cross-section of one hESC-CFs 3D ring. The high magnification inset (on the right) shows a non-homogeneous distribution of the cell's nuclei (Hematoxylin, purple dots) which are mainly distributed along the external and internal edges of the ring, while the central part is mainly made up of extracellular matrix (Eosin, pink stains).

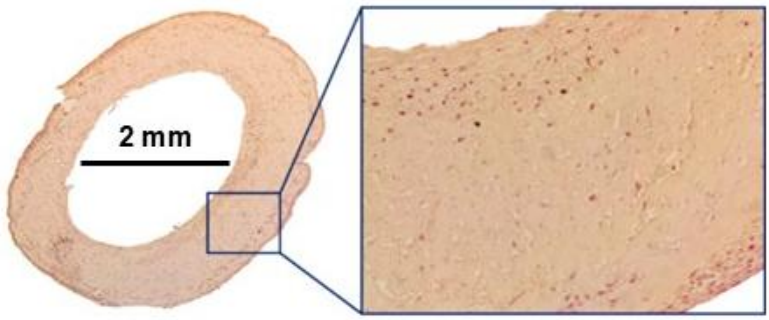

Figure 38. H&E staining of hESC-CFs 3D rings after 14 days of culturing. Pictures are taken at 4x magnification and a 10x magnification. The dark purple stains are nuclei whereas the lighter pink stain is matrix. The stained samples showed how the hESC-CFs are distributed in the matrix. Based on the purple stains this EHT ring suggests that the cells are mainly found at the outer layer.

Cellular distribution was also investigated through immunofluorescent staining. Three different staining were used: Hoechst (blue) for cell nuclei, Vimentin (green) for CFs cells and WGA (red) for plasma membrane. The pictures below (Figure 39; magnitude: 10x) show the rings after 14 days of incubation with CFGM medium. As already seen for the section stained with Hematoxylin and Eosin, a non-homogeneous distribution of the cells, mainly distributed on the external and internal sides of the ring, has emerged (Hoechst staining: Figure 39 A and Vimentin staining: Figure 39 B). The use of Vimentin indicates that the nuclei marked by Hoechst belong to fibroblasts. Unfortunately, the WGA marker (Figure 39, C) was less specific than expected and marked the entire ring structure. Picture 39, D shows merged signals (blue, green, and red) underlining the integration of cells and ECM components.

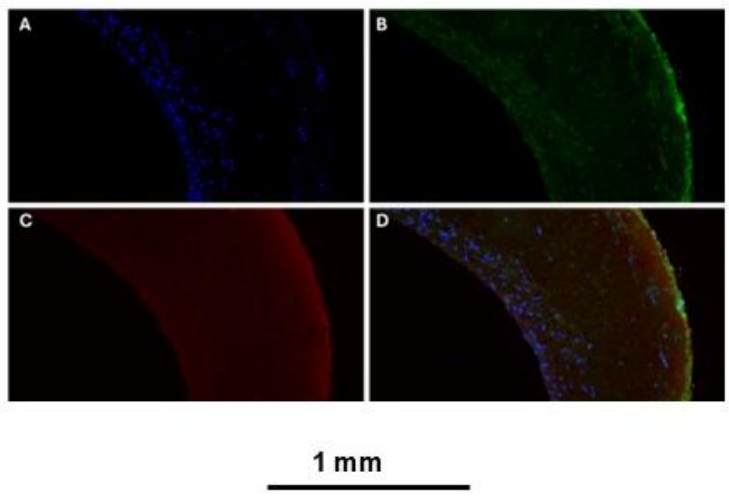

Figure 39. Fluorescence staining of hESC-CFs 3D Ring after 14 days of incubation in CFGM medium (magnification: 10x). **(A)** Hoechst staining (blue) highlights cell nuclei, **(B)** Vimentin staining (green) identifies CFs cells, **(C)** WGA staining (red) identifies plasma membrane, **(D)** Merged image (blue, green, and red) integrates signals from Hoechst, Vimentin, and WGA. Pictures made by Leica® DFC350 FX fluorescent microscope.

The cellular distribution in the rings cultured with CM RPMI is rather nonhomogeneous. It should be underlined that the CM RPMI rings show a larger diameter so at the same magnification (10x) it was

not possible to appreciate the entire section of the ring. In this case a weak compaction of the ring was highlighted (Figure 40).

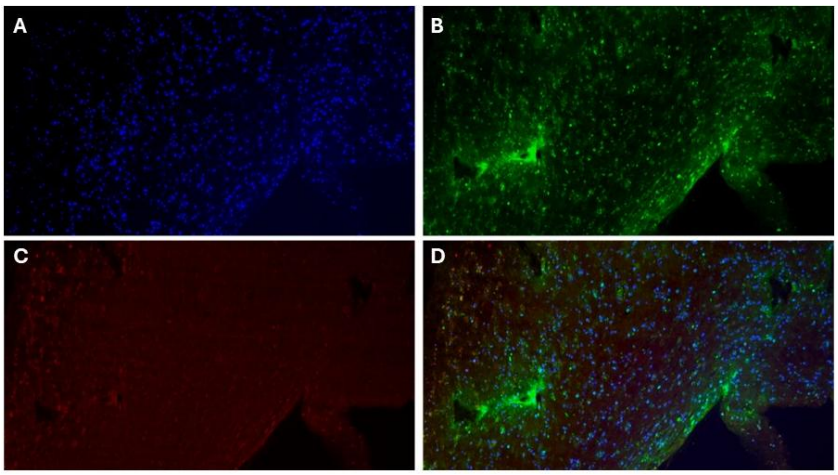

Figure 40. Fluorescence staining of hESC-CFs 3D Ring after 14 days of incubation in CM RPMI medium (magnification: 10x). **(A)** Hoechst staining (blue) highlights cell nuclei, **(B)** Vimentin staining (green) identifies CFs cells, **(C)** WGA staining (red) identifies the plasma membrane. **(D)** Merged image (blue, green, and red) integrates signals from Hoechst, Vimentin, and WGA. Pictures made by Leica® DFC350 FX fluorescent microscope.

5.2 HESC-CFs hESC-CMs Co-culture Engineering 3D Rings

5.2.1 Gene expression in hESC-CFs hESC-CMs 3D Rings

A part of this study was dedicated to the development of 3D model of co-cultures hESC-CFs and hESC-CMs, provided from the Department of Molecular Genetics of Maastricht University. Each ring consisted of 1 million hESC-CFs and 3 million hESC-CMs. After mixing hydrogel with hESC-CFs and hESC-CMs, and polymerization, the EHT co-culture rings were cultured in CM RPMI + vitamin C medium for 2 or 7 days. The rings showed rhythmical contractility indicating the contractile activity of the cardiomyocyte: at these two timepoints (Day 2 (d2) and Day 7 (d7)) rings were harvested for RT-qPCR measurements. Figure 41, A shows the percentage expression of specific CFs marker genes (*ACTA2*, *COL1A1* and VIM) and specific markers for CMs (*TNNT2*, *TNNI3*, *MYH6* and *MYH7*). For the first two genes (*ACTA2* and *COL1A1*) there is a slightly induction after 7 days in culture compared with day 2, while *VIM* is less expressed after one week of incubation. Cardiomyocytes markers are most expressed on day 2 while they undergo a consistent reduction in expression level after 7 days in culture. This finding could indicate either a greater proliferation rate of cardiac fibroblasts compared to cardiomyocytes, or a reduction in the number of cardiomyocytes induced by the culture conditions. It is interesting to note that in the starting conditions the cellular concentration of CMs was three times higher than that of CFs. Relative expression for each individual gene is specified in the graphs in Figure 41, B. Please note that the various genes have very different basal expressions.

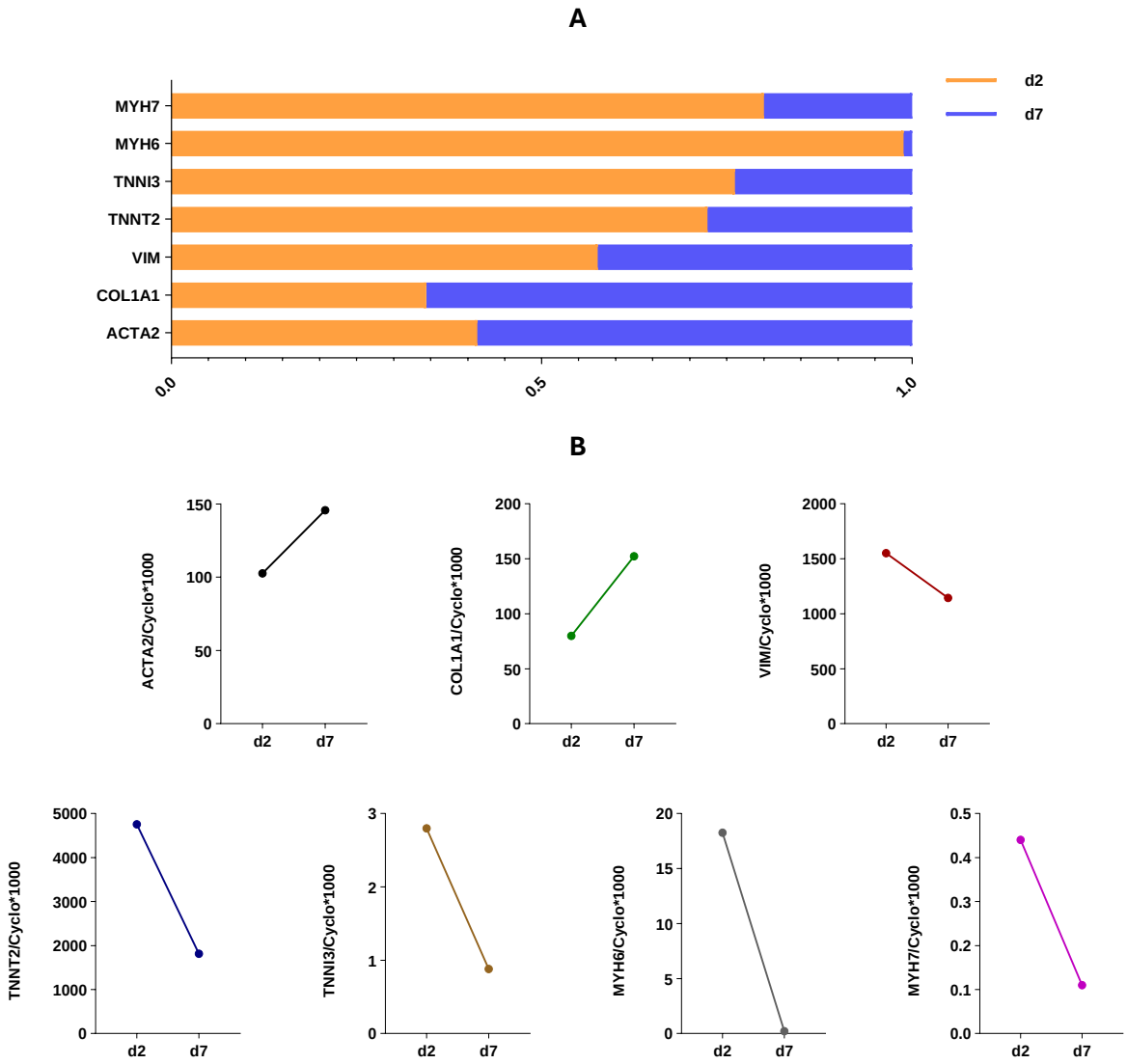

Figure 41. (A) Percentage expression levels of gene markers in a 3D co-culture of cardiac fibroblasts (CFs) and cardiomyocytes (CMs) at day 2 (d2, orange) and day 7 (d7, blue). The first three markers (*ACTA2*, *COL1A1*, and VIM) are specific to CFs. The last four markers (*TNNT2*, *TNNI3*, *MYH6* and *MYH7*) are specific to CMs. These data, expressed as percentages, highlight the dynamic interaction between CFs and CMs within the 3D co-culture rings. **(B)** Expression levels of different genes at day 2 (d2) and day 7 (d7). The bar plots represent gene expression values. Different colors highlight different genes, showing trends of upregulation or downregulation over time.

5.2.2 Distribution of hESC-CFs hESC-CMs Co-colture in 3D Rings

The pictures below (Figure 42) display results of hESC-CFs hESC-CMs EHT co-culture from immunohistochemical staining. Three different staining were used: Hoechst (blue) for cell nuclei, α-actinin (red) for cardiomyocyte sarcomere proteins and Vimentin (green) for cardiac fibroblasts. The merged images (blue, green and red) provide a composite view of the co-culture. The first row represents the outer part of the ring in which a higher density of cells is visible, as seen by the intense Hoechst (blue) staining. Similarly, sections close to the center post of the ring (third row) also show a higher cell density. However, the inner part (second row) of the ring displays reduced fluorescence intensity, indicating fewer cells in these areas, possibly due to limited diffusion of nutrients and oxygen. The overlap between α-actinin (red) and vimentin (green) in outer layer of the rings suggests regions where fibroblasts and cardiomyocytes are more concentrated, while the center has fewer cells. Based on these findings it might be that the diffusion of nutrients and/or oxygen through the ring might be less effective.

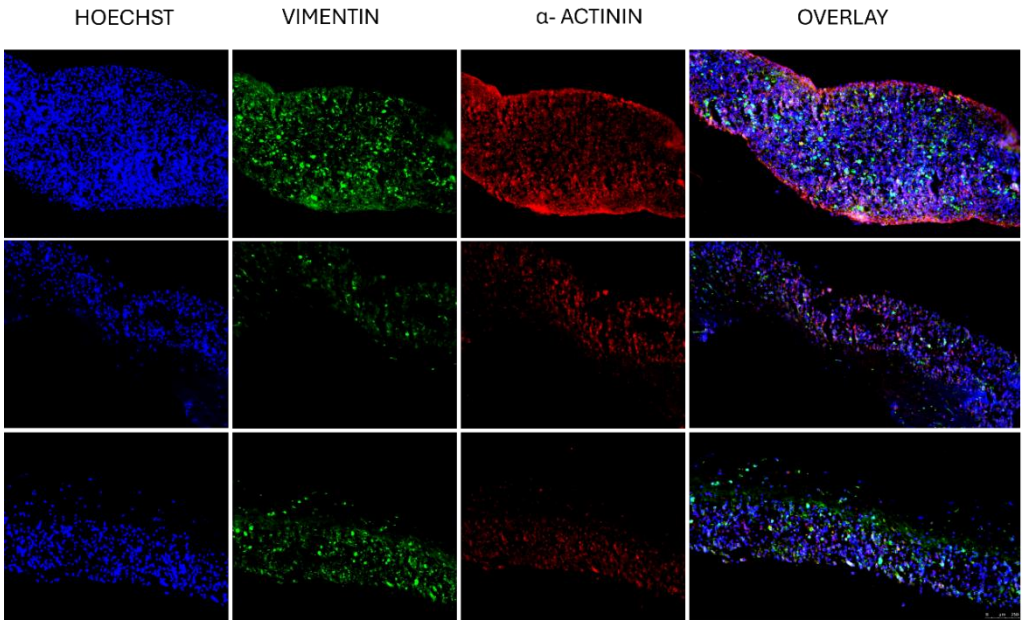

Figure 42. Hoechst, α -actinin, vimentin staining. Magnitude: 10x. Frontal sections of the 3D co-culture EHT ring after 7 days of culture. First row: outer layer section. Second row: center section. Third row: section close to the center post. The pictures are made by Leica® DFC350 FX fluorescent microscope.

5.3 Discussion

Although 2D cultures represent a valid *in vitro* model capable of performing cellular functions and properties, they also present limitations in terms of reproducibility of the environmental conditions and cellular interactions that occur *in vivo*. The aim of 3D cultures is primarily to faithfully reproduce the complex network of cell-cell and cell-matrix interactions. In the cardiac field, numerous 3D models, known as engineered heart tissues (EHTs), have been developed to date (Zimmermann et al., 2002). Despite significant progress, EHTs still face notable challenges, one of which is their neonatal-like structural and functional characteristics, distinct from those of mature heart tissue. Several approaches have been proposed to enhance the maturity of EHTs, such as long-term culture (Lewandowski et al., 2018) and co-culturing with different cell types (Beauchamp et al., 2020).

The adult mammalian heart is composed of various cell types, with the most abundant being cardiomyocytes (CMs), cardiac fibroblasts (CFs), endothelial cells (ECs), and perivascular cells (Tang et al., 2009). In particular, CMs and CFs, vary in proportion during developmental stages or in response to pathological conditions (Banerjee et al., 2007). In our first set of experiments, EHTs containing only cardiac fibroblasts were cultured simultaneously in different media, including cardiac fibroblast medium (CFGM with two different serum concentrations) and cardiomyocyte medium (CM RPMI). Tissues cultured in CM RPMI demonstrated significantly lower cellular compaction compared to those cultured in CFGM, suggesting that the degree of ring compaction is medium-dependent. A possible explanation for the pronounced compaction observed in the CFGM groups might be the fibroblast phenotype, with cells in CFGM adopting a more myofibroblast-like phenotype, which is known for its stronger contractile activity (Noom et al., 2024).

For the development of co-cultures, it has been observed in the literature that different *ratios* of cardiomyocytes to cardiac fibroblasts are used. In one study, the 1:1 *ratio* was found to be more favorable for the contractile properties of cardiomyocytes compared to other *ratios* analyzed (Mostert et al., 2022), while in another study, the recommended CM:CF *ratio* was 4:1 to avoid mimicking a fibrotic state (Beauchamp et al., 2020). We chose a 1:3 *ratio* to balance the contractile properties of cardiomyocytes with the support and functionality of fibroblasts, considering that fibroblasts play an important role in extracellular matrix organization and in providing structural support to cardiomyocytes (Hall et al., 2021).

Spontaneous beating EHTs were maintained in culture for a maximum of 7 days. We observed a significant reduction in cardiomyocyte markers from day 2 to day 7, while those of cardiac fibroblasts increased. This could indicate either a rapid proliferation of CFs or an increase in CMs cell apoptosis possible due to the culture conditions. Several factors may contribute to this loss, including cell compaction and the limitations of oxygen (O_2) and nutrient diffusion within the tissue. In 3D cultures, core anoxia is common due to the increased diffusion distance. One strategy proposed to enhance oxygen diffusion is to culture tissues in an incubator with elevated pO_2 levels (Tse et al., 2021). However, this method may induce prolonged exposure to high oxygen levels, which can lead to the formation of toxic free radical species (Martens et al., 2005).

Cell loss due to compaction is another key issue that affects the quality of 3D cardiac cultures. In this study, compaction was intentionally induced by creating a collagen-rich matrix that allowed the hESC-CFs to perform their compactible functions. However, this compaction can trigger apoptotic cell responses, which are highly dependent on both the cell type and culture conditions (Valon and Levayer, 2019). Other possible improvement of the model could be to decrease the starting volume and cell number of the hydrogel mix, to decrease the diameter of the EHT-ring. This would decrease the diffusion distance and possibly allow survival and further maturation of the cells in our EHT model.

3D cultures present promising opportunities for cardiovascular research by providing *in vitro* cardiac models that can mimic heart function and contractility. These advanced models are crucial for discovering more effective treatments for cardiovascular diseases. Additionally, the development of

such models is especially significant from an ethical standpoint, as they offer a viable alternative to animal models in cardiovascular research. By reducing the need for animal experimentation, these human-based models not only improve the relevance and accuracy of research but also help address the increasing ethical concerns surrounding the use of animals in scientific studies.

Chapter 6

Conclusions

6.1 General Conclusion

Through our investigations, we aimed to provide a functional analysis of two-dimensional and three-dimensional *in vitro* models to enhance our understanding of cellular behavior in the context of cardiac remodeling.

Based on the data discussed in **Chapter 3**, we observed that human embryonic stem cell-derived cardiac fibroblasts (hESC-CFs) consistently responded to experimental *stimuli*, such as the well-known profibrotic factor *TGFβ*, in a similar manner to primary cardiac fibroblasts. This finding underscores the reliability and reproducibility of the hESC-CFs model, highlighting its potential as a valuable alternative to primary cell cultures for studying cardiac fibrosis. In **Chapter 4**, we focused on the maturation process of human induced pluripotent stem cell-derived cardiomyocytes (hiPSC-CMs). Our molecular and structural studies demonstrated that, by the end of the differentiation process, hiPSC-CMs expressed typical markers of mature cardiomyocytes, with a significant reduction in stem cell markers. Additionally, we observed the arrangement of the sarcomere structure along the cardiomyocytes, starting from a beating monolayer.
In these two chapters, we evaluated the non-hemostatic effects of coagulation factors on cardiac fibroblast and cardiomyocyte cultures. Our findings provided new insights into the role of Thrombin (FIIa) and activated Factor X (FXa) in mediating hypertrophic and fibrotic responses in the human heart. Specifically, we observed that activated coagulation factors induce a hypertrophic response in hiPSC-CMs through the activation of protease-activated receptor 1 (*PAR1*). This investigation is particularly relevant because modulating *PAR1* activity with agonists and antagonists allows for the specific assessment of coagulation-related signaling in cardiomyocyte hypertrophy, helping to identify potential therapeutic targets for preventing pathological cardiac remodeling.

Chapter 5 was dedicated to the characterization of engineered heart tissues (EHTs), which have gained significant attention as promising *in vitro* models for studying cardiac function and disease. While EHTs provide a more physiologically relevant environment compared to traditional two-dimensional cultures, challenges remain in replicating the complexity and functional maturity of native heart tissue. Factors such as tissue stiffness, cellular composition, oxygen and nutrient diffusion, and cell viability during culture play crucial roles in determining the success and applicability of these 3D cardiac models.

In conclusion, this study has demonstrated the potential of *in vitro* models ranging from hESC-CFs and hiPSC-CMs to engineered heart tissues, as valuable tools for investigating human cardiogenesis, cardiac disease mechanisms and the impact of coagulation factors on pathological remodeling.

6.2 Study Limitations and Future Prospectives

In the four human embryonic stem cell-derived cardiac fibroblast cell lines used in this study (PSC018, PSC019, PSC020, and PSC021), we assessed the basal expression levels of genes encoding for the *PAR1* and *PAR2* receptors. However, we did not evaluate whether the profibrotic and pro-inflammatory effects induced by coagulation factors are PAR-mediated. This is an important aspect to consider, as PAR receptors play a critical role in mediating cellular responses to coagulation factors. To further elucidate this relationship, future experiments utilizing *PAR1* and *PAR2* antagonists and agonists would be necessary to determine their specific involvement in the observed effects.

Although gene expression analysis via qPCR is a fundamental and widely used approach for characterizing cellular models, it presents inherent limitations. The quantification of mRNA levels provides only a partial view and does not account for regulatory mechanisms occurring post-transcriptionally, such as post-translational modifications (PTMs) of the encoded proteins. These modifications, including phosphorylation, acetylation, glycosylation, and ubiquitination can

significantly influence protein function, subcellular localization, stability, and protein–protein interactions (Walsh et al., 2005). To achieve a more comprehensive understanding of the molecular mechanisms involved, it is essential to complement qPCR data with additional analytical approaches, such as Western blotting, immunofluorescence, proteomics, and phosphoproteomics, to detect actual protein levels and functional modifications (Gstaiger & Aebersold, 2009). An integrated multi-omic strategy thus represents a more robust and informative framework to validate transcriptional data and uncover dynamic, functional insights into the cellular pathways under investigation.

Regarding the cardiomyocyte cell lines derived from human stem cell differentiation protocols established in Florence and Maastricht, we observed some variations in terms of baseline expression of cardiac markers as well as morphological differences. These discrepancies highlight the need for careful selection of cell lines with similar characteristics to ensure the validity and consistency of experimental results. Therefore, only those cell lines exhibiting comparable parameters were included in this study.

An additional limitation of our study lies in the inability to fully define the exclusive role of activated Factor X and its inhibitor, Rivaroxaban, in the observed outcomes. FXa used in our experiments was purified, but it is presumed that it might have been contaminated with Thrombin. This potential contamination could have contributed more significantly to the hypertrophic effects observed, given that FIIa is the primary activator of *PAR1*. Consequently, for future experiments, it would be ideal to use synthetic FXa to unequivocally assess the specific contribution of this factor in cardiac hypertrophy.

In the final part of this study, a preliminary characterization of 3D co-culture models was provided. The future goal is to identify an optimal culture condition that ensures adequate survival of these two cell lines, while minimizing apoptosis due to hypoxic conditions (especially in the central regions of the rings) and nutrient deprivation. Furthermore, investigating the effects of coagulation factors within this 3D model could yield important insights into how these factors influence cellular processes in a more physiologically relevant setting.

References

Ahmed RE, Tokuyama T, Anzai T, Chanthra N, Uosaki H. Sarcomere maturation: function acquisition, molecular mechanism, and interplay with other organelles. Philos Trans R Soc Lond B Biol Sci. 2022 Nov 21;377(1864):20210325. doi: 10.1098/rstb.2021.0325. Epub 2022 Oct 3. PMID: 36189811; PMCID: PMC9527934.

Alberelli MA, De Candia E. Functional role of protease activated receptors in vascular biology. Vascul Pharmacol. 2014 Aug;62(2):72-81. doi: 10.1016/j.vph.2014.06.001. Epub 2014 Jun 9. PMID: 24924409.

Allessie M, Ausma J, Schotten U. Electrical, contractile and structural remodeling during atrial fibrillation. Cardiovasc Res. 2002 May;54(2):230-46. doi: 10.1016/s0008-6363(02)00258-4. PMID: 12062329.

Anker SD, von Haehling S. Inflammatory mediators in chronic heart failure: an overview. Heart. 2004 Apr;90(4):464-70. doi: 10.1136/hrt.2002.007005. PMID: 15020532; PMCID: PMC1768165.

Antar SA, Ashour NA, Marawan ME, Al-Karmalawy AA. Fibrosis: Types, Effects, Markers, Mechanisms for Disease Progression, and Its Relation with Oxidative Stress, Immunity, and Inflammation. Int J Mol Sci. 2023 Feb 16;24(4):4004. doi: 10.3390/ijms24044004. PMID: 36835428; PMCID: PMC9963026.

Atienza F, Martins RP, Jalife J. Translational research in atrial fibrillation: a quest for mechanistically based diagnosis and therapy. Circ Arrhythm Electrophysiol. 2012 Dec;5(6):1207-15. doi: 10.1161/CIRCEP.111.970335. Epub 2012 Sep 27. PMID: 23022707; PMCID: PMC3535065.

Bae JS, Kim IS, Rezaie AR. Thrombin down-regulates the TGF-beta-mediated synthesis of collagen and fibronectin by human proximal tubule epithelial cells through the EPCR-dependent activation of PAR1. J Cell Physiol. 2010 Oct;225(1):233-9. doi: 10.1002/jcp.22249. PMID: 20506163; PMCID: PMC3957190.

Banerjee I, Fuseler JW, Price RL, Borg TK, Baudino TA. Determination of cell types and numbers during cardiac development in the neonatal and adult rat and mouse. Am J Physiol Heart Circ Physiol. 2007 Sep;293(3):H1883-91. doi: 10.1152/ajpheart.00514.2007. Epub 2007 Jun 29. PMID: 17604329.

Bartelds B, Gratama JW, Knoester H, Takens J, Smid GB, Aarnoudse JG, Heymans HS, Kuipers JR. Perinatal changes in myocardial supply and flux of fatty acids, carbohydrates, and ketone bodies in lambs. Am J Physiol. 1998 Jun;274(6):H1962-9. doi: 10.1152/ajpheart.1998.274.6.H1962. PMID: 9841523.

Bartelds B, Knoester H, Smid GB, Takens J, Visser GH, Penninga L, van der Leij FR, Beaufort-Krol GC, Zijlstra WG, Heymans HS, Kuipers JR. Perinatal changes in myocardial metabolism in lambs. Circulation. 2000 Aug 22;102(8):926-31. doi: 10.1161/01.cir.102.8.926. PMID: 10952964.

Battistoni A, Rubattu S, Volpe M. Circulating biomarkers with preventive, diagnostic and prognostic implications in cardiovascular diseases. Int J Cardiol. 2012 May 31;157(2):160-8. doi: 10.1016/j.ijcard.2011.06.066. Epub 2011 Jul 16. PMID: 21763018.

Beauchamp P, Jackson CB, Ozhathil LC, Agarkova I, Galindo CL, Sawyer DB, Suter TM, Zuppinger C. 3D Co-culture of hiPSC-Derived Cardiomyocytes With Cardiac Fibroblasts Improves Tissue-Like Features of Cardiac Spheroids. Front Mol Biosci. 2020 Feb 14;7:14. doi: 10.3389/fmolb.2020.00014. PMID: 32118040; PMCID: PMC7033479.

Beecroft SJ, van de Locht M, de Winter JM, Ottenheijm CA, Sewry CA, Mohammed S, Ryan MM, Woodcock IR, Sanders L, Gooding R, Davis MR, Oates EC, Laing NG, Ravenscroft G, McLean CA, Jungbluth H. Recessive MYH7-related myopathy in two families. Neuromuscul Disord. 2019 Jun;29(6):456-467. doi: 10.1016/j.nmd.2019.04.002. Epub 2019 Apr 12. PMID: 31130376.

Beqqali A, Kloots J, Ward-van Oostwaard D, Mummery C, Passier R. Genome-wide transcriptional profiling of human embryonic stem cells differentiating to cardiomyocytes. Stem Cells. 2006 Aug;24(8):1956-67. doi: 10.1634/stemcells.2006-0054. Epub 2006 May 4. PMID: 16675594.

Bers DM. Calcium fluxes involved in control of cardiac myocyte contraction. Circ Res. 2000 Aug 18;87(4):275-81. doi: 10.1161/01.res.87.4.275. PMID: 10948060.

Bers DM. Cardiac excitation-contraction coupling. Nature. 2002 Jan 10;415(6868):198-205. doi: 10.1038/415198a. PMID: 11805843.

Bird SD, Doevendans PA, van Rooijen MA, Brutel de la Riviere A, Hassink RJ, Passier R, Mummery CL. The human adult cardiomyocyte phenotype. Cardiovasc Res. 2003 May 1;58(2):423-34. doi: 10.1016/s0008-6363(03)00253-0. PMID: 12757876.

Bosma GC, Custer RP, Bosma MJ. A severe combined immunodeficiency mutation in the mouse. Nature. 1983 Feb 10;301(5900):527-30. doi: 10.1038/301527a0. PMID: 6823332.

Boyd AS, Rodrigues NP, Lui KO, Fu X, Xu Y. Concise review: Immune recognition of induced pluripotent stem cells. Stem Cells. 2012 May;30(5):797-803. doi: 10.1002/stem.1066. PMID: 22419544.

Brette F, Orchard C. T-tubule function in mammalian cardiac myocytes. Circ Res. 2003 Jun 13;92(11):1182-92. doi: 10.1161/01.RES.0000074908.17214.FD. PMID: 12805236.

Brown HF, DiFrancesco D, Noble SJ. How does adrenaline accelerate the heart? Nature. 1979 Jul 19;280(5719):235-6. doi: 10.1038/280235a0. PMID: 450140.

Brundel BJJM, Ai X, Hills MT, Kuipers MF, Lip GYH, de Groot NMS. Atrial fibrillation. Nat Rev Dis Primers. 2022 Apr 7;8(1):21. doi: 10.1038/s41572-022-00347-9. PMID: 35393446.

Burchfield JS, Xie M, Hill JA. Pathological ventricular remodeling: mechanisms: part 1 of 2. Circulation. 2013 Jul 23;128(4):388-400. doi: 10.1161/CIRCULATIONAHA.113.001878. PMID: 23877061; PMCID: PMC3801217.

Burridge PW, Matsa E, Shukla P, Lin ZC, Churko JM, Ebert AD, Lan F, Diecke S, Huber B, Mordwinkin NM, Plews JR, Abilez OJ, Cui B, Gold JD, Wu JC. Chemically defined generation of human cardiomyocytes. Nat Methods. 2014 Aug;11(8):855-60. doi: 10.1038/nmeth.2999. Epub 2014 Jun 15. PMID: 24930130; PMCID: PMC4169698.

Camm AJ, Lip GYH, De Caterina R, et al. Atrial fibrillation: pathophysiology and management. Heart. 2012 Nov;98(22):1651-1659. doi: 10.1136/heartjnl-2012-302349. PMID: 23041962.

Carreño JE, Apablaza F, Ocaranza MP, Jalil JE. Hipertrofia cardiaca: eventos moleculares y celulares [Cardiac hypertrophy: molecular and cellular events]. Rev Esp Cardiol. 2006 May;59(5):473-86. Spanish. PMID: 16750145.

Catalán V, Frühbeck G, Gómez-Ambrosi J. Chapter 8 - Inflammatory and Oxidative Stress Markers in Skeletal Muscle of Obese Subjects, Editor(s): Amelia Marti del Moral, Concepción María Aguilera García, Obesity, Academic Press, 2018, Pages 163-189, ISBN 9780128125045, https://doi.org/10.1016/B978-0-12-812504-5.00008-8. (https://www.sciencedirect.com/science/article/pii/B9780128125045000088)

Chan SS, Hagen HR, Swanson SA, Stewart R, Boll KA, Aho J, Thomson JA, Kyba M. Development of Bipotent Cardiac/Skeletal Myogenic Progenitors from MESP1+ Mesoderm. Stem Cell Reports. 2016 Jan 12;6(1):26-34. doi: 10.1016/j.stemcr.2015.12.003. PMID: 26771351; PMCID: PMC4719188.

Chaudhuri O, Cooper-White J, Janmey PA, Mooney DJ, Shenoy VB. Effects of extracellular matrix viscoelasticity on cellular behaviour. Nature. 2020 Aug;584(7822):535-546. doi: 10.1038/s41586-020-2612-2. Epub 2020 Aug 26. PMID: 32848221; PMCID: PMC7676152.

Chaudhry R, Usama SM, Babiker HM. Physiology, Coagulation Pathways. In: StatPearls [Internet]. Treasure Island (FL): StatPearls Publishing; 2023 [cited 2023 Sep 8]. Available from: http://www.ncbi.nlm.nih.gov/books/NBK482253/

Chen J, Wang J, Hart DA, Zhou Z, Ackermann PW, Ahmed AS. Complement factor D regulates collagen type I expression and fibroblast migration to enhance human tendon repair and healing outcomes. Front Immunol. 2023 Sep 6;14:1225957. doi: 10.3389/fimmu.2023.1225957. PMID: 37744351; PMCID: PMC10512081.

Chen MM, Lam A, Abraham JA, Schreiner GF, Joly AH. CTGF expression is induced by TGF- beta in cardiac fibroblasts and cardiac myocytes: a potential role in heart fibrosis. J Mol Cell Cardiol. 2000 Oct;32(10):1805-19. doi: 10.1006/jmcc.2000.1215. PMID: 11013125.

Chien KR, Zhu H, Knowlton KU, Miller-Hance W, van-Bilsen M, O'Brien TX, Evans SM. Transcriptional regulation during cardiac growth and development. Annu Rev Physiol. 1993;55:77-95. doi: 10.1146/annurev.ph.55.030193.000453. PMID: 8466192.

Chung E, Leinwand LA. Pregnancy as a cardiac stress model. Cardiovasc Res. 2014 Mar 15;101(4):561-70. doi: 10.1093/cvr/cvu013. Epub 2014 Jan 20. PMID: 24448313; PMCID: PMC3941597.

Cohen DE, Melton D. Turning straw into gold: directing cell fate for regenerative medicine. Nat Rev Genet. 2011 Apr;12(4):243-52. doi: 10.1038/nrg2938. Epub 2011 Mar 9. PMID: 21386864.

Cohn JN, Ferrari R, Sharpe N. Cardiac remodeling--concepts and clinical implications: a consensus paper from an international forum on cardiac remodeling. Behalf of an International Forum on Cardiac Remodeling. J Am Coll Cardiol. 2000 Mar 1;35(3):569-82. doi: 10.1016/s0735-1097(99)00630-0. PMID: 10716457.

Cowan CA, Klimanskaya I, McMahon J, Atienza J, Witmyer J, Zucker JP, Wang S, Morton CC, McMahon AP, Powers D, Melton DA. Derivation of embryonic stem-cell lines from human blastocysts. N Engl J Med. 2004 Mar 25;350(13):1353-6. doi: 10.1056/NEJMsr040330. Epub 2004 Mar 3. PMID: 14999088.

Cumberland MJ, Euchner J, Azad AJ, T N Vo N, Kirchhof P, Holmes AP, Denning C, Gehmlich K. Generation of a human iPSC-derived cardiomyocyte/fibroblast engineered heart tissue model. F1000Res. 2024 Feb 12;12:1224. doi: 10.12688/f1000research.139482.1. PMID: 38298530; PMCID: PMC10828555.

D'Alessandro E, Posma JJN, Spronk HMH, Ten Cate H. Tissue factor (Factor VIIa) in the heart and vasculature: More than an envelope. Thromb Res. 2018 Aug; 168:130-137. doi: 10.1016/j.thromres.2018.06.020. Epub 2018 Jun 28. PMID: 30064684.

D'Alessandro E, Scaf B, Munts C, van Hunnik A, Trevelyan CJ, Verheule S, Spronk HMH, Turner NA, Ten Cate H, Schotten U, van Nieuwenhoven FA. Coagulation Factor Xa Induces Proinflammatory Responses in Cardiac Fibroblasts via Activation of Protease-Activated Receptor-1. Cells. 2021 Oct 30;10(11):2958. doi: 10.3390/cells10112958. PMID: 34831181; PMCID: PMC8616524.

D'Alessandro E, Winters J, van Nieuwenhoven FA, Schotten U, Verheule S. The Complex Relation between Atrial Cardiomyopathy and Thrombogenesis. Cells. 2022 Sep 22;11(19):2963. doi: 10.3390/cells11192963. PMID: 36230924; PMCID: PMC9563762.

de Lange WJ, Farrell ET, Kreitzer CR, Jacobs DR, Lang D, Glukhov AV, Ralphe JC. Human iPSC-engineered cardiac tissue platform faithfully models important cardiac physiology. Am J Physiol Heart Circ Physiol. 2021 Apr 1;320(4):H1670-H1686. doi: 10.1152/ajpheart.00941.2020. Epub 2021 Feb 19. PMID: 33606581; PMCID: PMC8260387.

Denham NC, Pearman CM, Caldwell JL, Madders GWP, Eisner DA, Trafford AW, Dibb KM. Calcium in the Pathophysiology of Atrial Fibrillation and Heart Failure. Front Physiol. 2018 Oct 4;9:1380. doi: 10.3389/fphys.2018.01380. PMID: 30337881; PMCID: PMC6180171.

Devalla HD, Schwach V, Ford JW, Milnes JT, El-Haou S, Jackson C, Gkatzis K, Elliott DA, Chuva de Sousa Lopes SM, Mummery CL, Verkerk AO, Passier R. Atrial-like cardiomyocytes from human pluripotent stem cells are a robust preclinical model for assessing atrial-selective pharmacology. EMBO Mol Med. 2015 Apr;7(4):394-410. doi: 10.15252/emmm.201404757. PMID: 25700171; PMCID: PMC4403042.

Dirkx E, da Costa Martins PA, De Windt LJ. Regulation of fetal gene expression in heart failure. Biochim Biophys Acta. 2013 Dec;1832(12):2414-24. doi: 10.1016/j.bbadis.2013.07.023. Epub 2013 Sep 10. PMID: 24036209.

Dzeshka MS, Lip GY, Snezhitskiy V, Shantsila E. Cardiac Fibrosis in Patients With Atrial Fibrillation: Mechanisms and Clinical Implications. J Am Coll Cardiol. 2015 Aug 25;66(8):943-59. doi: 10.1016/j.jacc.2015.06.1313. PMID: 26293766.

Ellerström C, Strehl R, Moya K, Andersson K, Bergh C, Lundin K, Hyllner J, Semb H. Derivation of a xeno-free human embryonic stem cell line. Stem Cells. 2006 Oct;24(10):2170-6. doi: 10.1634/stemcells.2006-0130. Epub 2006 Jun 1. PMID: 16741223.

Ellison GM, Waring CD, Vicinanza C, Torella D. Physiological cardiac remodelling in response to endurance exercise training: cellular and molecular mechanisms. Heart. 2012 Jan;98(1):5-10. doi: 10.1136/heartjnl-2011-300639. Epub 2011 Aug 31. PMID: 21880653.

Evans SM, Yelon D, Conlon FL, Kirby ML. Myocardial lineage development. Circ Res. 2010 Dec 10;107(12):1428-44. doi: 10.1161/CIRCRESAHA.110.227405. PMID: 21148449; PMCID: PMC3073310.

Fabiato A. Calcium-induced release of calcium from the cardiac sarcoplasmic reticulum. Am J Physiol. 1983 Jul;245(1):C1-14. doi: 10.1152/ajpcell.1983.245.1.C1. PMID: 6346892.

Fernandes I, Funakoshi S, Hamidzada H, Epelman S, Keller G. Modeling cardiac fibroblast heterogeneity from human pluripotent stem cell-derived epicardial cells. Nat Commun. 2023 Dec 11;14(1):8183. doi: 10.1038/s41467-023-43312-0. PMID: 38081833; PMCID: PMC10713677.

Fisher DJ, Heymann MA, Rudolph AM. Myocardial oxygen and carbohydrate consumption in fetal lambs in utero and in adult sheep. Am J Physiol. 1980 Mar;238(3):H399-405. doi: 10.1152/ajpheart.1980.238.3.H399. PMID: 7369385.

Frangogiannis NG. Cardiac fibrosis: Cell biological mechanisms, molecular pathways and therapeutic opportunities. Mol Aspects Med. 2019 Feb;65:70-99. doi: 10.1016/j.mam.2018.07.001. Epub 2018 Aug 2. PMID: 30056242.

Frey N, Richardson JA, Olson EN. Calsarcins, a novel family of sarcomere calcineurin-binding proteins. Proc Natl Acad Sci U S A. 2000 Dec 19;97(26):14632-7. doi: 10.1073/pnas.260501097. PMID: 11114196; PMCID: PMC18970.

Fu X, Xu Y. Self-renewal and scalability of human embryonic stem cells for human therapy. Regen Med. 2011 May;6(3):327-34. doi: 10.2217/rme.11.18. PMID: 21548738.

Gallagher MP, Kelly PJ, Jardine M, Perkovic V, Cass A, Craig JC, Eris J, Webster AC. Long-term cancer risk of immunosuppressive regimens after kidney transplantation. J Am Soc Nephrol. 2010 May;21(5):852-8. doi: 10.1681/ASN.2009101043. Epub 2010 Apr 29. PMID: 20431040; PMCID: PMC2865745.

Garry DJ, Olson EN. A common progenitor at the heart of development. Cell. 2006 Dec 15;127(6):1101-4. doi: 10.1016/j.cell.2006.11.031. PMID: 17174889.

Giacomelli E, Meraviglia V, Campostrini G, Cochrane A, Cao X, van Helden RWJ, Krotenberg Garcia A, Mircea M, Kostidis S, Davis RP, van Meer BJ, Jost CR, Koster AJ, Mei H, Míguez DG, Mulder AA, Ledesma-Terrón M, Pompilio G, Sala L, Salvatori DCF, Slieker RC, Sommariva E, de Vries AAF, Giera M, Semrau S, Tertoolen LGJ, Orlova VV, Bellin M, Mummery CL. Human-iPSC-Derived Cardiac Stromal Cells Enhance Maturation in 3D Cardiac Microtissues and Reveal Non-cardiomyocyte Contributions to Heart Disease. Cell Stem Cell. 2020 Jun 4;26(6):862-879.e11. doi: 10.1016/j.stem.2020.05.004. Epub 2020 May 26. PMID: 32459996; PMCID: PMC7284308.

Gibb AA, Lazaropoulos MP, Elrod JW. Myofibroblasts and Fibrosis: Mitochondrial and Metabolic Control of Cellular Differentiation. Circ Res. 2020 Jul 17;127(3):427-447. doi: 10.1161/CIRCRESAHA.120.316958. Epub 2020 Jul 16. PMID: 32673537; PMCID: PMC7982967.

Gieseler F, Ungefroren H, Settmacher U, Hollenberg MD, Kaufmann R. Proteinase-activated receptors (PARs) - focus on receptor-receptor-interactions and their physiological and pathophysiological impact. Cell Commun Signal. 2013 Nov 11;11:86. doi: 10.1186/1478-811X-11-86. PMID: 24215724; PMCID: PMC3842752.

Goldfracht I, Protze S, Shiti A, Setter N, Gruber A, Shaheen N, Nartiss Y, Keller G, Gepstein L. Generating ring-shaped engineered heart tissues from ventricular and atrial human pluripotent stem cell-derived cardiomyocytes. Nat Commun. 2020 Jan 7;11(1):75. doi: 10.1038/s41467-019-13868-x. PMID: 31911598; PMCID: PMC6946709.

Goodwin GW, Taylor CS, Taegtmeyer H. Regulation of energy metabolism of the heart during acute increase in heart work. J Biol Chem. 1998 Nov 6;273(45):29530-9. doi: 10.1074/jbc.273.45.29530. PMID: 9792661.

Goversen B, van der Heyden MAG, van Veen TAB, de Boer TP. The immature electrophysiological phenotype of iPSC-CMs still hampers in vitro drug screening: Special focus on IK1. Pharmacol Ther. 2018 Mar;183:127-136. doi: 10.1016/j.pharmthera.2017.10.001. Epub 2017 Oct 3. PMID: 28986101.

Gstaiger M, Aebersold R. Applying mass spectrometry-based proteomics to genetics, genomics and network biology. Nat Rev Genet. 2009 Sep;10(9):617-27. doi: 10.1038/nrg2633. PMID: 19687803.

Gupta MP. Factors controlling cardiac myosin-isoform shift during hypertrophy and heart failure. J Mol Cell Cardiol. 2007 Oct;43(4):388-403. doi: 10.1016/j.yjmcc.2007.07.045. Epub 2007 Jul 21. PMID: 17720186; PMCID: PMC2701247.

Hall C, Gehmlich K, Denning C, Pavlovic D. Complex Relationship Between Cardiac Fibroblasts and Cardiomyocytes in Health and Disease. J Am Heart Assoc. 2021 Feb;10(5):e019338. doi: 10.1161/JAHA.120.019338. Epub 2021 Feb 15. PMID: 33586463; PMCID: PMC8174279.

Hall JE and Michael EH. Guyton and Hall Textbook of Medical Physiology. 14th ed. Elsevier, 2021.

Heijman J, Voigt N, Nattel S, Dobrev D. Cellular and molecular electrophysiology of atrial fibrillation initiation, maintenance, and progression. Circ Res. 2014 Apr 25;114(9):1483-99. doi: 10.1161/CIRCRESAHA.114.302226. PMID: 24763466.

Heineke J, Molkentin JD. Regulation of cardiac hypertrophy by intracellular signalling pathways. Nat Rev Mol Cell Biol. 2006 Aug;7(8):589-600. doi: 10.1038/nrm1983. PMID: 16936699.

Hertzberg M. Biochemistry of factor X. Blood Rev. 1994 Mar;8(1):56-62. doi: 10.1016/0268-960x(94)90007-8. PMID: 8205010.

Hindricks G, Potpara T, Dagres N, Arbelo E, Bax JJ, Blomström-Lundqvist C, Boriani G, Castella M, Dan GA, Dilaveris PE, Fauchier L, Filippatos G, Kalman JM, La Meir M, Lane DA, Lebeau JP, Lettino M, Lip GYH, Pinto FJ, Thomas GN, Valgimigli M, Van Gelder IC, Van Putte BP, Watkins CL; ESC Scientific Document Group. 2020 ESC Guidelines for the diagnosis and management of atrial fibrillation developed in collaboration with the European Association for Cardio-Thoracic Surgery (EACTS): The Task Force for the diagnosis and management of atrial fibrillation of the European Society of Cardiology (ESC) Developed with the special contribution of the European Heart Rhythm Association (EHRA) of the ESC. Eur Heart J. 2021 Feb 1;42(5):373-498. doi: 10.1093/eurheartj/ehaa612. Erratum in: Eur Heart J. 2021 Feb 1;42(5):507. doi: 10.1093/eurheartj/ehaa798. Erratum in: Eur Heart J. 2021 Feb 1;42(5):546-547. doi: 10.1093/eurheartj/ehaa945. Erratum in: Eur Heart J. 2021 Oct 21;42(40):4194. doi: 10.1093/eurheartj/ehab648. PMID: 32860505.

Hochman JS, Bulkley BH. Expansion of acute myocardial infarction: an experimental study. Circulation. 1982 Jun;65(7):1446-50. doi: 10.1161/01.cir.65.7.1446. PMID: 7074800.

Hoshijima M. Mechanical stress-strain sensors embedded in cardiac cytoskeleton: Z disk, titin, and associated structures. Am J Physiol Heart Circ Physiol. 2006 Apr;290(4):H1313-25. doi: 10.1152/ajpheart.00816.2005. PMID: 16537787; PMCID: PMC3241960.

Houweling AC, van Borren MM, Moorman AF, Christoffels VM. Expression and regulation of the atrial natriuretic factor encoding gene NPPA during development and disease. Cardiovasc Res. 2005 Sep 1;67(4):583-93. doi: 10.1016/j.cardiores.2005.06.013. PMID: 16002056.

Hovatta O, Stojkovic M, Nogueira M, Varela-Nieto I. European scientific, ethical, and legal issues on human stem cell research and regenerative medicine. Stem Cells. 2010 Jun;28(6):1005-7. doi: 10.1002/stem.436. PMID: 20533567.

Huang X, Yang N, Fiore VF, Barker TH, Sun Y, Morris SW, Ding Q, Thannickal VJ, Zhou Y. Matrix stiffness-induced myofibroblast differentiation is mediated by intrinsic mechanotransduction. Am J Respir Cell Mol Biol. 2012 Sep;47(3):340-8. doi: 10.1165/rcmb.2012-0050OC. Epub 2012 Mar 29. PMID: 22461426; PMCID: PMC3488695.

Hutschalik T, Özgül O, Casini M, Szabó B, Peyronnet R, Bártulos Ó, Argenziano M, Schotten U, Matsa E. Immune response caused by M1 macrophages elicits atrial fibrillation-like phenotypes in coculture model with isogenic hiPSC-derived cardiomyocytes. Stem Cell Res Ther. 2024 Sep 4;15(1):280. doi: 10.1186/s13287-024-03814-0. PMID: 39227896; PMCID: PMC11373469.

Inoue K, Sakamoto T, Yuge S, Iwatani H, Yamagami S, Tsutsumi M, Hori H, Cerra MC, Tota B, Suzuki N, Okamoto N, Takei Y. Structural and functional evolution of three cardiac natriuretic peptides. Mol Biol Evol. 2005 Dec;22(12):2428-34. doi: 10.1093/molbev/msi243. Epub 2005 Aug 24. PMID: 16120806.

Ivey MJ, Tallquist MD. Defining the Cardiac Fibroblast. Circ J. 2016 Oct 25;80(11):2269-2276. doi: 10.1253/circj.CJ-16-1003. Epub 2016 Oct 14. PMID: 27746422; PMCID: PMC5588900.

Jiang Y, Park P, Hong SM, Ban K. Maturation of Cardiomyocytes Derived from Human Pluripotent Stem Cells: Current Strategies and Limitations. Mol Cells. 2018 Jul 31;41(7):613-621. doi: 10.14348/molcells.2018.0143. Epub 2018 Jun 12. PMID: 29890820; PMCID: PMC6078855.

Kannel WB, Dannenberg AL, Levy D. Population implications of electrocardiographic left ventricular hypertrophy. Am J Cardiol. 1987 Dec 14;60(17):85I-93I. doi: 10.1016/0002-9149(87)90466-8. PMID: 2961250.

Karakikes I, Senyei GD, Hansen J, Kong CW, Azeloglu EU, Stillitano F, Lieu DK, Wang J, Ren L, Hulot JS, Iyengar R, Li RA, Hajjar RJ. Small molecule-mediated directed differentiation of human embryonic stem cells toward ventricular cardiomyocytes. Stem Cells Transl Med. 2014 Jan;3(1):18-31. doi: 10.5966/sctm.2013-0110. Epub 2013 Dec 9. PMID: 24324277; PMCID: PMC3902291.

Kattman SJ, Witty AD, Gagliardi M, Dubois NC, Niapour M, Hotta A, Ellis J, Keller G. Stage-specific optimization of activin/nodal and BMP signaling promotes cardiac differentiation of mouse and human pluripotent stem cell lines. Cell Stem Cell. 2011 Feb 4;8(2):228-40. doi: 10.1016/j.stem.2010.12.008. PMID: 21295278.

Khan AA, Lip GYH. The prothrombotic state in atrial fibrillation: pathophysiological and management implications. Cardiovasc Res. 2019 Jan 1;115(1):31-45. doi: 10.1093/cvr/cvy272. PMID: 30388199.

Kim P, Chu N, Davis J, Kim DH. Mechanoregulation of Myofibroblast Fate and Cardiac Fibrosis. Adv Biosyst. 2018 Jan;2(1):1700172. doi: 10.1002/adbi.201700172. Epub 2017 Dec 4. PMID: 31406913; PMCID: PMC6690497.

Klabunde RE. Cardiovascular Physiology Concepts. 3rd ed., Lippincott Williams & Wilkins, 2021.

Klimanskaya I, Chung Y, Becker S, Lu SJ, Lanza R. Derivation of human embryonic stem cells from single blastomeres. Nat Protoc. 2007;2(8):1963-72. doi: 10.1038/nprot.2007.274. PMID: 17703208.

Koivumäki JT, Naumenko N, Tuomainen T, Takalo J, Oksanen M, Puttonen KA, Lehtonen Š, Kuusisto J, Laakso M, Koistinaho J, Tavi P. Structural Immaturity of Human iPSC-Derived Cardiomyocytes: In Silico Investigation of Effects on Function and Disease Modeling. Front Physiol. 2018 Feb 7;9:80. doi: 10.3389/fphys.2018.00080. PMID: 29467678; PMCID: PMC5808345.

Leemans J, Amálio N. Modelling a cardiac pacemaker visually and formally, 2012 IEEE Symposium on Visual Languages and Human-Centric Computing (VL/HCC), Innsbruck, Austria, 2012, pp. 257-258, doi: 10.1109/VLHCC.2012.6344542.

Lehman JJ, Kelly DP. Gene regulatory mechanisms governing energy metabolism during cardiac hypertrophic growth. Heart Fail Rev. 2002 Apr;7(2):175-85. doi: 10.1023/a:1015332726303. PMID: 11988641.

Leicht M, Briest W, Hölzl A, Zimmer HG. Serum depletion induces cell loss of rat cardiac fibroblasts and increased expression of extracellular matrix proteins in surviving cells. Cardiovasc Res. 2001 Dec;52(3):429-37. doi: 10.1016/s0008-6363(01)00391-1. PMID: 11738059.

Lesman A, Habib M, Caspi O, Gepstein A, Arbel G, Levenberg S, Gepstein L. Transplantation of a tissue-engineered human vascularized cardiac muscle. Tissue Eng Part A. 2010 Jan;16(1):115-25. doi: 10.1089/ten.TEA.2009.0130. PMID: 19642856.

Lewandowski J, Rozwadowska N, Kolanowski TJ, Malcher A, Zimna A, Rugowska A, Fiedorowicz K, Łabędź W, Kubaszewski Ł, Chojnacka K, Bednarek-Rajewska K, Majewski P, Kurpisz M. The impact of in vitro cell culture duration on the maturation of human cardiomyocytes derived from induced pluripotent stem cells of myogenic origin. Cell Transplant. 2018 Jul;27(7):1047-1067. doi: 10.1177/0963689718779346. Epub 2018 Jun 27. PMID: 29947252; PMCID: PMC6158549.

Li Y, Jian Z, Yang ZY, Chen L, Wang XF, Ma RY, Xiao YB. Increased expression of connective tissue growth factor and transforming growth factor-beta-1 in atrial myocardium of patients with chronic atrial fibrillation. Cardiology. 2013;124(4):233-40. doi: 10.1159/000347126. Epub 2013 Apr 6. PMID: 23571482.

Lip GY, Lowe GD, Rumley A, Dunn FG. Increased markers of thrombogenesis in chronic atrial fibrillation: effects of warfarin treatment. Br Heart J. 1995 Jun;73(6):527-33. doi: 10.1136/hrt.73.6.527. PMID: 7626351; PMCID: PMC483914.

Lyon RC, Zanella F, Omens JH, Sheikh F. Mechanotransduction in cardiac hypertrophy and failure. Circ Res. 2015 Apr 10;116(8):1462-1476. doi: 10.1161/CIRCRESAHA.116.304937. PMID: 25858069; PMCID: PMC4394185.

MacLennan DH, Kranias EG. Phospholamban: a crucial regulator of cardiac contractility. Nat Rev Mol Cell Biol. 2003 Jul;4(7):566-77. doi: 10.1038/nrm1151. PMID: 12838339.

Madden LR, Mortisen DJ, Sussman EM, Dupras SK, Fugate JA, Cuy JL, Hauch KD, Laflamme MA, Murry CE, Ratner BD. Proangiogenic scaffolds as functional templates for cardiac tissue engineering. Proc Natl Acad Sci U S A. 2010 Aug 24;107(34):15211-6. doi: 10.1073/pnas.1006442107. Epub 2010 Aug 9. PMID: 20696917; PMCID: PMC2930533.

Maillet M, van Berlo JH, Molkentin JD. Molecular basis of physiological heart growth: fundamental concepts and new players. Nat Rev Mol Cell Biol. 2013 Jan;14(1):38-48. doi: 10.1038/nrm3495. PMID: 23258295; PMCID: PMC4416212.

Man J, Barnett P, Christoffels VM. Structure and function of the NPPA-Nppb cluster locus during heart development and disease. Cell Mol Life Sci. 2018 Apr;75(8):1435-1444. doi: 10.1007/s00018-017-2737-0. Epub 2018 Jan 4. PMID: 29302701; PMCID: PMC5852170.

Mann DL. Inflammatory mediators and the failing heart: past, present, and the foreseeable future. Circ Res. 2002 Nov 29;91(11):988-98. doi: 10.1161/01.res.0000043825.01705.1b. PMID: 12456484.

Mann DL. Innate immunity and the failing heart: the cytokine hypothesis revisited. Circ Res. 2015 Mar 27;116(7):1254-68. doi: 10.1161/CIRCRESAHA.116.302317. PMID: 25814686; PMCID: PMC4380242.

Mann KG, Nesheim ME, Church WR, Haley P, Krishnaswamy S. Surface-dependent reactions of the vitamin K-dependent enzyme complexes. Blood. 1990 Jul 1;76(1):1-16. PMID: 2194585.

Marcus GM, Whooley MA, Glidden DV, Pawlikowska L, Zaroff JG, Olgin JE. Interleukin-6 and atrial fibrillation in patients with coronary artery disease: data from the Heart and Soul Study. Am Heart J. 2008 Feb;155(2):303-9. doi: 10.1016/j.ahj.2007.09.006. Epub 2007 Oct 25. PMID: 18215601; PMCID: PMC2247366.

Martens G, Cai Y, Hinke S, Stangé G, Van de Casteele M, Pipeleers D. Nutrient sensing in pancreatic beta cells suppresses mitochondrial superoxide generation and its contribution to apoptosis. Biochem Soc Trans. 2005 Feb;33(Pt 1):300-1. doi: 10.1042/BST0330300. PMID: 15667332.

Molè MA, Weberling A, Zernicka-Goetz M. Comparative analysis of human and mouse development: From zygote to pre-gastrulation. Curr Top Dev Biol. 2020;136:113-138. doi: 10.1016/bs.ctdb.2019.10.002. Epub 2019 Dec 26. PMID: 31959285.

Mononen MM, Leung CY, Xu J, Chien KR. Trajectory mapping of human embryonic stem cell cardiogenesis reveals lineage branch points and an ISL1 progenitor-derived cardiac fibroblast lineage. Stem Cells. 2020 Oct 1;38(10):1267-1278. doi: 10.1002/stem.3236. Epub 2020 Jun 19. PMID: 32497389.

Mostert D, Groenen B, Klouda L, Passier R, Goumans MJ, Kurniawan NA, Bouten CVC. Human pluripotent stem cell-derived cardiomyocytes align under cyclic strain when guided by cardiac fibroblasts. APL Bioeng. 2022 Dec 20;6(4):046108. doi: 10.1063/5.0108914. PMID: 36567768; PMCID: PMC9771596.

Moustakas A. Smad signalling network. J Cell Sci. 2002 Sep 1;115(Pt 17):3355-6. doi: 10.1242/jcs.115.17.3355. PMID: 12154066.

Nakao K, Minobe W, Roden R, Bristow MR, Leinwand LA. Myosin heavy chain gene expression in human heart failure. J Clin Invest. 1997 Nov 1;100(9):2362-70. doi: 10.1172/JCI119776. PMID: 9410916; PMCID: PMC508434.

Nigro P, Pompilio G, Capogrossi MC. Cyclophilin A: a key player for human disease. Cell Death Dis. 2013 Oct 31;4(10):e888. doi: 10.1038/cddis.2013.410. PMID: 24176846; PMCID: PMC3920964.

Nikolaev VO, Bünemann M, Hein L, Hannawacker A, Lohse MJ. Novel single chain cAMP sensors for receptor-induced signal propagation. J Biol Chem. 2004 Sep 3;279(36):37215-8. doi: 10.1074/jbc.C400302200. Epub 2004 Jul 1. PMID: 15231839.

Noom A, Sawitzki B, Knaus P, Duda GN. A two-way street - cellular metabolism and myofibroblast contraction. NPJ Regen Med. 2024 Apr 3;9(1):15. doi: 10.1038/s41536-024-00359-x. PMID: 38570493; PMCID: PMC10991391.

Nose N, Werner RA, Ueda Y, Günther K, Lapa C, Javadi MS, Fukushima K, Edenhofer F, Higuchi T. Metabolic substrate shift in human induced pluripotent stem cells during cardiac differentiation: Functional assessment using in vitro radionuclide uptake assay. Int J Cardiol. 2018 Oct 15;269:229-234. doi: 10.1016/j.ijcard.2018.06.089. Epub 2018 Jun 21. PMID: 30224033.

Noseda M, Peterkin T, Simões FC, Patient R, Schneider MD. Cardiopoietic factors: extracellular signals for cardiac lineage commitment. Circ Res. 2011 Jan 7;108(1):129-52. doi: 10.1161/CIRCRESAHA.110.223792. PMID: 21212394.

Nso N, Bookani KR, Metzl M, Radparvar F. Role of inflammation in atrial fibrillation: A comprehensive review of current knowledge. J Arrhythm. 2020 Dec 23;37(1):1-10. doi: 10.1002/joa3.12473. PMID: 33664879; PMCID: PMC7896450.

Ohara K, Inoue H, Nozawa T, Hirai T, Iwasa A, Okumura K, Lee JD, Shimizu A, Hayano M, Yano K. Accumulation of risk factors enhances the prothrombotic state in atrial fibrillation. Int J Cardiol. 2008 Jun 6;126(3):316-21. doi: 10.1016/j.ijcard.2007.06.020. Epub 2007 Aug 8. PMID: 17689760.

Ossovskaya VS, Bunnett NW. Protease-activated receptors: contribution to physiology and disease. Physiol Rev. 2004 Apr;84(2):579-621. doi: 10.1152/physrev.00028.2003. PMID: 15044683.

Pan X, Chen Z, Huang R, Yao Y, Ma G. Transforming growth factor β1 induces the expression of collagen type I by DNA methylation in cardiac fibroblasts. PLoS One. 2013;8(4):e60335. doi: 10.1371/journal.pone.0060335. Epub 2013 Apr 1. PMID: 23560091; PMCID: PMC3613378.

Petropoulos S, Edsgärd D, Reinius B, Deng Q, Panula SP, Codeluppi S, Plaza Reyes A, Linnarsson S, Sandberg R, Lanner F. Single-Cell RNA-Seq Reveals Lineage and X Chromosome Dynamics in Human Preimplantation Embryos. Cell. 2016 May 5;165(4):1012-26. doi: 10.1016/j.cell.2016.03.023. Epub 2016 Apr 7. Erratum in: Cell. 2016 Sep 22;167(1):285. doi: 10.1016/j.cell.2016.08.009. PMID: 27062923; PMCID: PMC4868821.

Pfeffer JM, Pfeffer MA, Braunwald E. Influence of chronic captopril therapy on the infarcted left ventricle of the rat. Circ Res. 1985 Jul;57(1):84-95. doi: 10.1161/01.res.57.1.84. PMID: 3891127.

Pinto AR, Ilinykh A, Ivey MJ, Kuwabara JT, D'Antoni ML, Debuque R, Chandran A, Wang L, Arora K, Rosenthal NA, Tallquist MD. Revisiting Cardiac Cellular Composition. Circ Res. 2016 Feb 5;118(3):400-9. doi: 10.1161/CIRCRESAHA.115.307778. Epub 2015 Dec 3. PMID: 26635390; PMCID: PMC4744092.

Pioner JM, Guan X, Klaiman JM, Racca AW, Pabon L, Muskheli V, Macadangdang J, Ferrantini C, Hoopmann MR, Moritz RL, Kim DH, Tesi C, Poggesi C, Murry CE, Childers MK, Mack DL, Regnier M. Absence of full-length dystrophin impairs normal maturation and contraction of cardiomyocytes derived from human-induced pluripotent stem cells. Cardiovasc Res. 2020 Feb 1;116(2):368-382. doi: 10.1093/cvr/cvz109. PMID: 31049579; PMCID: PMC8053310.

Pioner JM, Racca AW, Klaiman JM, Yang KC, Guan X, Pabon L, Muskheli V, Zaunbrecher R, Macadangdang J, Jeong MY, Mack DL, Childers MK, Kim DH, Tesi C, Poggesi C, Murry CE, Regnier M. Isolation and Mechanical Measurements of Myofibrils from Human Induced Pluripotent Stem Cell-Derived Cardiomyocytes. Stem Cell Reports. 2016 Jun 14;6(6):885-896. doi: 10.1016/j.stemcr.2016.04.006. Epub 2016 May 5. PMID: 27161364; PMCID: PMC4911495.

Ploeg MC, Munts C, Seddiqi T, Ten Brink TJL, Breemhaar J, Moroni L, Prinzen FW, van Nieuwenhoven FA. Culturing of Cardiac Fibroblasts in Engineered Heart Matrix Reduces Myofibroblast Differentiation but Maintains Their Response to Cyclic Stretch and Transforming Growth Factor β1. Bioengineering (Basel). 2022 Oct 14;9(10):551. doi: 10.3390/bioengineering9100551. PMID: 36290519; PMCID: PMC9598692.

Posma JJ, Posthuma JJ, Spronk HM. Coagulation and non-coagulation effects of Thrombin. J Thromb Haemost. 2016 Oct;14(10):1908-1916. doi: 10.1111/jth.13441. Epub 2016 Oct 5. PMID: 27513692.

Rajabi M, Kassiotis C, Razeghi P, Taegtmeyer H. Return to the fetal gene program protects the stressed heart: a strong hypothesis. Heart Fail Rev. 2007 Dec;12(3-4):331-43. doi: 10.1007/s10741-007-9034-1. PMID: 17516164.

Rebolledo DL, Lipson KE, Brandan E. Driving fibrosis in neuromuscular diseases: Role and regulation of Connective tissue growth factor (CCN2/CTGF). Matrix Biol Plus. 2021 Mar 6;11:100059. doi: 10.1016/j.mbplus.2021.100059. PMID: 34435178; PMCID: PMC8377001.

Reiser PJ, Portman MA, Ning XH, Schomisch Moravec C. Human cardiac myosin heavy chain isoforms in fetal and failing adult atria and ventricles. Am J Physiol Heart Circ Physiol. 2001 Apr;280(4):H1814-20. doi: 10.1152/ajpheart.2001.280.4.H1814. PMID: 11247796.

Ren Y, Lee MY, Schliffke S, Paavola J, Amos PJ, Ge X, Ye M, Zhu S, Senyei G, Lum L, Ehrlich BE, Qyang Y. Small molecule Wnt inhibitors enhance the efficiency of BMP-4-directed cardiac differentiation of human pluripotent stem cells. J Mol Cell Cardiol. 2011 Sep;51(3):280-7. doi: 10.1016/j.yjmcc.2011.04.012. Epub 2011 May 4. PMID: 21569778; PMCID: PMC3334336.

Ribeiro MC, Tertoolen LG, Guadix JA, Bellin M, Kosmidis G, D'Aniello C, Monshouwer-Kloots J, Goumans MJ, Wang YL, Feinberg AW, Mummery CL, Passier R. Functional maturation of human pluripotent stem cell derived cardiomyocytes in vitro--correlation between contraction force and electrophysiology. Biomaterials. 2015 May;51:138-150. doi: 10.1016/j.biomaterials.2015.01.067. Epub 2015 Feb 18. PMID: 25771005.

Rivera-Arbeláez JM, Cofiño-Fabres C, Schwach V, Boonen T, Ten Den SA, Vermeul K, van den Berg A, Segerink LI, Ribeiro MC, Passier R. Contractility analysis of human engineered 3D heart tissues by an automatic tracking technique using a standalone application. PLoS One. 2022 Apr 14;17(4):e0266834. doi: 10.1371/journal.pone.0266834. PMID: 35421132; PMCID: PMC9009597.

Ronaldson-Bouchard K, Ma SP, Yeager K, Chen T, Song L, Sirabella D, Morikawa K, Teles D, Yazawa M, Vunjak-Novakovic G. Advanced maturation of human cardiac tissue grown from pluripotent stem cells. Nature. 2018 Apr;556(7700):239-243. doi:

10.1038/s41586-018-0016-3. Epub 2018 Apr 4. Erratum in: Nature. 2019 Aug;572(7769):E16-E17. doi: 10.1038/s41586-019-1415-9. PMID: 29618819; PMCID: PMC5895513.

Ronaldson-Bouchard K, Yeager K, Teles D, Chen T, Ma S, Song L, Morikawa K, Wobma HM, Vasciaveo A, Ruiz EC, Yazawa M, Vunjak-Novakovic G. Engineering of human cardiac muscle electromechanically matured to an adult-like phenotype. Nat Protoc. 2019 Oct;14(10):2781-2817. doi: 10.1038/s41596-019-0189-8. Epub 2019 Sep 6. PMID: 31492957; PMCID: PMC7195192.

Rosenbaum DM, Rasmussen SG, Kobilka BK. The structure and function of G-protein-coupled receptors. Nature. 2009 May 21;459(7245):356-63. doi: 10.1038/nature08144. PMID: 19458711; PMCID: PMC3967846.

Rosenzweig A, Halazonetis TD, Seidman JG, Seidman CE. Proximal regulatory domains of rat atrial natriuretic factor gene. Circulation. 1991 Sep;84(3):1256-65. doi: 10.1161/01.cir.84.3.1256. PMID: 1832094.

Sack MN, Disch DL, Rockman HA, Kelly DP. A role for Sp and nuclear receptor transcription factors in a cardiac hypertrophic growth program. Proc Natl Acad Sci U S A. 1997 Jun 10;94(12):6438-43. doi: 10.1073/pnas.94.12.6438. PMID: 9177236; PMCID: PMC21068.

Sassoon DA, Garner I, Buckingham M. Transcripts of alpha-cardiac and alpha-skeletal actins are early markers for myogenesis in the mouse embryo. Development. 1988 Sep;104(1):155-64. doi: 10.1242/dev.104.1.155. PMID: 3075543.

Schaaf S, Eder A, Vollert I, Stöhr A, Hansen A, Eschenhagen T. Generation of strip-format fibrin-based engineered heart tissue (EHT). Methods Mol Biol. 2014;1181:121-9. doi: 10.1007/978-1-4939-1047-2_11. PMID: 25070332.Schiattarella GG, Hill JA. Inhibition of hypertrophy is a good therapeutic strategy in ventricular pressure overload. Circulation. 2015 Apr 21;131(16):1435-47. doi: 10.1161/CIRCULATIONAHA.115.013894. PMID: 25901069; PMCID: PMC4408778.

Schotten U, Duytschaever M, Ausma J, Eijsbouts S, Neuberger HR, Allessie M. Electrical and contractile remodeling during the first days of atrial fibrillation go hand in hand. Circulation. 2003 Mar 18;107(10):1433-9. doi: 10.1161/01.cir.0000055314.10801.4f. PMID: 12642366.

Sergeeva IA, Christoffels VM. Regulation of expression of atrial and brain natriuretic peptide, biomarkers for heart development and disease. Biochim Biophys Acta. 2013 Dec;1832(12):2403-13. doi: 10.1016/j.bbadis.2013.07.003. Epub 2013 Jul 12. PMID: 23851052.

Sergeeva IA, Hooijkaas IB, Van Der Made I, Jong WM, Creemers EE, Christoffels VM. A transgenic mouse model for the simultaneous monitoring of ANF and BNP gene activity during heart development and disease. Cardiovasc Res. 2014 Jan 1;101(1):78-86. doi: 10.1093/cvr/cvt228. Epub 2013 Oct 8. PMID: 24104878.

Shachar M, Tsur-Gang O, Dvir T, Leor J, Cohen S. The effect of immobilized RGD peptide in alginate scaffolds on cardiac tissue engineering. Acta Biomater. 2011 Jan;7(1):152-62. doi: 10.1016/j.actbio.2010.07.034. Epub 2010 Aug 3. PMID: 20688198.

Sheikh F, Ross RS, Chen J. Cell-cell connection to cardiac disease. Trends Cardiovasc Med. 2009 Aug;19(6):182-90. doi: 10.1016/j.tcm.2009.12.001. PMID: 20211433; PMCID: PMC3601820.

Shinde AV, Humeres C, Frangogiannis NG. The role of α-smooth muscle actin in fibroblast-mediated matrix contraction and remodeling. Biochim Biophys Acta Mol Basis Dis. 2017 Jan;1863(1):298-309. doi: 10.1016/j.bbadis.2016.11.006. Epub 2016 Nov 4. PMID: 27825850; PMCID: PMC5163362.

Spronk HM, De Jong AM, Verheule S, De Boer HC, Maass AH, Lau DH, Rienstra M, van Hunnik A, Kuiper M, Lumeij S, Zeemering S, Linz D, Kamphuisen PW, Ten Cate H, Crijns HJ, Van Gelder IC, van Zonneveld AJ, Schotten U. Hypercoagulability causes atrial fibrosis and promotes atrial fibrillation. Eur Heart J. 2017 Jan 1;38(1):38-50. doi: 10.1093/eurheartj/ehw119. Epub 2016 Apr 12. PMID: 27071821.

Staerk L, Sherer JA, Ko D, Benjamin EJ, Helm RH. Atrial Fibrillation: Epidemiology, Pathophysiology, and Clinical Outcomes. Circ Res. 2017 Apr 28;120(9):1501-1517. doi: 10.1161/CIRCRESAHA.117.309732. PMID: 28450367; PMCID: PMC5500874.

Strelchenko N, Verlinsky O, Kukharenko V, Verlinsky Y. Morula-derived human embryonic stem cells. Reprod Biomed Online. 2004 Dec;9(6):623-9. doi: 10.1016/s1472-6483(10)61772-5. PMID: 15670408.

Swynghedauw B. Developmental and functional adaptation of contractile proteins in cardiac and skeletal muscles. Physiol Rev. 1986 Jul;66(3):710-71. doi: 10.1152/physrev.1986.66.3.710. PMID: 2942954.

Swynghedauw B. Phenotypic plasticity of adult myocardium: molecular mechanisms. J Exp Biol. 2006 Jun;209(Pt 12):2320-7. doi: 10.1242/jeb.02084. PMID: 16731808.

Taegtmeyer H, Sen S, Vela D. Return to the fetal gene program: a suggested metabolic link to gene expression in the heart. Ann N Y Acad Sci. 2010 Feb;1188:191-8. doi: 10.1111/j.1749-6632.2009.05100.x. PMID: 20201903; PMCID: PMC3625436.

Takahashi K, Yamanaka S. A decade of transcription factor-mediated reprogramming to pluripotency. Nat Rev Mol Cell Biol. 2016 Mar;17(3):183-93. doi: 10.1038/nrm.2016.8. Epub 2016 Feb 17. PMID: 26883003.

Tanaka T, Narazaki M, Kishimoto T. IL-6 in inflammation, immunity, and disease. Cold Spring Harb Perspect Biol. 2014 Sep 4;6(10):a016295. doi: 10.1101/cshperspect.a016295. PMID: 25190079; PMCID: PMC4176007.

Tang Y, Nyengaard JR, Andersen JB, Baandrup U, Gundersen HJ. The application of stereological methods for estimating structural parameters in the human heart. Anat Rec (Hoboken). 2009 Oct;292(10):1630-47. doi: 10.1002/ar.20952. PMID: 19714657.

Tarone G, Brancaccio M. Keep your heart in shape: molecular chaperone networks for treating heart disease. Cardiovasc Res. 2014 Jun 1;102(3):346-61. doi: 10.1093/cvr/cvu049. Epub 2014 Feb 28. PMID: 24585203.

Teuwen CP, Korevaar TIM, Coolen RL, van der Wel T, Houck CA, Evertz R, Yaksh A, Roos-Hesselink JW, Bogers AJJC, de Groot NMS. Frequent atrial extrasystolic beats predict atrial fibrillation in patients with congenital heart defects. Europace. 2018 Jan 1;20(1):25-32. doi: 10.1093/europace/euw300. PMID: 27702860.

Thomson JA, Itskovitz-Eldor J, Shapiro SS, Waknitz MA, Swiergiel JJ, Marshall VS, Jones JM. Embryonic stem cell lines derived from human blastocysts. Science. 1998 Nov 6;282(5391):1145-7. doi: 10.1126/science.282.5391.1145. Erratum in: Science 1998 Dec 4;282(5395):1827. PMID: 9804556.

Tse HM, Gardner G, Dominguez-Bendala J, Fraker CA. The Importance of Proper Oxygenation in 3D Culture. Front Bioeng Biotechnol. 2021 Mar 30;9:634403. doi: 10.3389/fbioe.2021.634403. PMID: 33859979; PMCID: PMC8042214.

Uematsu M, Ohara Y, Navas JP, Nishida K, Murphy TJ, Alexander RW, Nerem RM, Harrison DG. Regulation of endothelial cell nitric oxide synthase mRNA expression by shear stress. Am J Physiol. 1995 Dec;269(6 Pt 1):C1371-8. doi: 10.1152/ajpcell.1995.269.6.C1371. PMID: 8572165.

Valon L, Levayer R. Dying under pressure: cellular characterisation and in vivo functions of cell death induced by compaction. Biol Cell. 2019 Mar;111(3):51-66. doi: 10.1111/boc.201800075. Epub 2019 Jan 17. PMID: 30609052.
van den Berg CW, Okawa S, Chuva de Sousa Lopes SM, van Iperen L, Passier R, Braam SR, Tertoolen LG, del Sol A, Davis RP, Mummery CL. Transcriptome of human foetal heart compared with cardiomyocytes from pluripotent stem cells. Development. 2015 Sep 15;142(18):3231-8. doi: 10.1242/dev.123810. Epub 2015 Jul 24. PMID: 26209647.

van Nieuwenhoven FA, Hemmings KE, Porter KE, Turner NA. Combined effects of interleukin-1α and transforming growth factor-β1 on modulation of human cardiac fibroblast function. Matrix Biol. 2013 Oct-Nov;32(7-8):399-406. doi: 10.1016/j.matbio.2013.03.008. Epub 2013 Apr 12. PMID: 23583823.

van Putten S, Shafieyan Y, Hinz B. Mechanical control of cardiac myofibroblasts. J Mol Cell Cardiol. 2016 Apr;93:133-42. doi: 10.1016/j.yjmcc.2015.11.025. Epub 2015 Nov 24. PMID: 26620422.

Voorhees AP, Han HC. Biomechanics of Cardiac Function. Compr Physiol. 2015 Sep 20;5(4):1623-44. doi: 10.1002/cphy.c140070. PMID: 26426462; PMCID: PMC4668273.

Walsh CT, Garneau-Tsodikova S, Gatto GJ Jr. Protein posttranslational modifications: the chemistry of proteome diversifications. Angew Chem Int Ed Engl. 2005 Dec 1;44(45):7342-72. doi: 10.1002/anie.200501023. PMID: 16267872.

Wakili R, Voigt N, Kääb S, Dobrev D, Nattel S. Recent advances in the molecular pathophysiology of atrial fibrillation. J Clin Invest. 2011 Aug;121(8):2955-68. doi: 10.1172/JCI46315. Epub 2011 Aug 1. PMID: 21804195; PMCID: PMC3148739.

Watson T, Shantsila E, Lip GY. Mechanisms of thrombogenesis in atrial fibrillation: Virchow's triad revisited. Lancet. 2009 Jan 10;373(9658):155-66. doi: 10.1016/S0140-6736(09)60040-4. PMID: 19135613.

White EZ, Pennant NM, Carter JR, Hawsawi O, Odero-Marah V, Hinton CV. Serum deprivation initiates adaptation and survival to oxidative stress in prostate cancer cells. Sci Rep. 2020 Jul 27;10(1):12505. doi: 10.1038/s41598-020-68668-x. PMID: 32719369; PMCID: PMC7385110.

Wilcken David EL. Physiology of the normal heart, Medicine, Volume 34, Issue 5, 2006. Pages 165-169, ISSN 1357-3039, https://doi.org/10.1383/medc.2006.34.5.165.(https://www.sciencedirect.com/science/article/pii/S1357303906001344)

Windt LM, Wiendels M, Dostanić M, Bellin M, Sarro PM, Mastrangeli M, Mummery CL, van Meer BJ. Miniaturized engineered heart tissues from hiPSC-derived triple cell type co-cultures to study human cardiac function. Biochem Biophys Res Commun. 2023 Nov 12;681:200-211. doi: 10.1016/j.bbrc.2023.09.034. Epub 2023 Sep 20. PMID: 37783118.

Workman AJ, Kane KA, Rankin AC. Cellular bases for human atrial fibrillation. Heart Rhythm. 2008 Jun;5(6 Suppl):S1-6. doi: 10.1016/j.hrthm.2008.01.016. Epub 2008 Jan 17. Erratum in: Heart Rhythm. 2008 Oct;5(10):1499. PMID: 18456193; PMCID: PMC2639647.

Workman AJ. Cardiac adrenergic control and atrial fibrillation. Naunyn Schmiedebergs Arch Pharmacol. 2010 Mar;381(3):235-49. doi: 10.1007/s00210-009-0474-0. Epub 2009 Dec 4. PMID: 19960186; PMCID: PMC2855383.

Xie X, Liu Y, Gao S, Wu B, Hu X, Chen J. Possible involvement of fibrocytes in atrial fibrosis in patients with chronic atrial fibrillation. Circ J. 2014;78(2):338-44. doi: 10.1253/circj.cj-13-0776. Epub 2013 Nov 7. PMID: 24200846.

Xu J, Cui G, Esmailian F, Plunkett M, Marelli D, Ardehali A, Odim J, Laks H, Sen L. Atrial extracellular matrix remodeling and the maintenance of atrial fibrillation. Circulation. 2004 Jan 27;109(3):363-8. doi: 10.1161/01.CIR.0000109495.02213.52. Epub 2004 Jan 19. PMID: 14732752.

Yamanaka S. Strategies and new developments in the generation of patient-specific pluripotent stem cells. Cell Stem Cell. 2007 Jun 7;1(1):39-49. doi: 10.1016/j.stem.2007.05.012. PMID: 18371333.

Yan J, Kong W, Zhang Q, Beyer EC, Walcott G, Fast VG, Ai X. c-Jun N-terminal kinase activation contributes to reduced connexin43 and development of atrial arrhythmias. Cardiovasc Res. 2013 Mar 1;97(3):589-97. doi: 10.1093/cvr/cvs366. Epub 2012 Dec 14. PMID: 23241357; PMCID: PMC3567788.

Yau JW, Teoh H, Verma S. Endothelial cell control of thrombosis. BMC Cardiovasc Disord. 2015 Oct 19;15:130. doi: 10.1186/s12872-015-0124-z. PMID: 26481314; PMCID: PMC4617895.

Yan J, Thomson JK, Zhao W, Wu X, Gao X, DeMarco D, Kong W, Tong M, Sun J, Bakhos M, Fast VG, Liang Q, Prabhu SD, Ai X. The stress kinase JNK regulates gap junction Cx43 gene expression and promotes atrial fibrillation in the aged heart. J Mol Cell Cardiol. 2018 Jan;114:105-115. doi: 10.1016/j.yjmcc.2017.11.006. Epub 2017 Nov 13. PMID: 29146153; PMCID: PMC5800987.

Yang X, Rodriguez ML, Leonard A, Sun L, Fischer KA, Wang Y, Ritterhoff J, Zhao L, Kolwicz SC Jr, Pabon L, Reinecke H, Sniadecki NJ, Tian R, Ruohola-Baker H, Xu H, Murry CE. Fatty Acids Enhance the Maturation of Cardiomyocytes Derived from Human Pluripotent Stem Cells. Stem Cell Reports. 2019 Oct 8;13(4):657-668. doi: 10.1016/j.stemcr.2019.08.013. Epub 2019 Sep 26. PMID: 31564645; PMCID: PMC6829750.

Yoshida Y, Yamanaka S. Induced Pluripotent Stem Cells 10 Years Later: For Cardiac Applications. Circ Res. 2017 Jun 9;120(12):1958-1968. doi: 10.1161/CIRCRESAHA.117.311080. PMID: 28596174.

Yu J, Vodyanik MA, Smuga-Otto K, Antosiewicz-Bourget J, Frane JL, Tian S, Nie J, Jonsdottir GA, Ruotti V, Stewart R, Slukvin II, Thomson JA. Induced pluripotent stem cell lines derived from human somatic cells. Science. 2007 Dec 21;318(5858):1917-20. doi: 10.1126/science.1151526. Epub 2007 Nov 20. PMID: 18029452.

Zaccolo M, Pozzan T. Discrete microdomains with high concentration of cAMP in stimulated rat neonatal cardiac myocytes. Science. 2002 Mar 1;295(5560):1711-5. doi: 10.1126/science.1069982. PMID: 11872839.

Zeng Z, Shen L, Li X, Luo T, Wei X, Zhang J, Cao S, Huang X, Fukushima Y, Bin J, Kitakaze M, Xu D, Liao Y. Disruption of histamine H2 receptor slows heart failure progression through reducing myocardial apoptosis and fibrosis. Clin Sci (Lond). 2014 Oct;127(7):435-48. doi: 10.1042/CS20130716. PMID: 24655024.

Zeuthen EL, Lassen JF, Husted SE. Is there a hypercoagulable phase during initiation of antithrombotic therapy with oral anticoagulants in patients with atrial fibrillation? Thromb Res. 2003 Mar 15;109(5-6):241-6. doi: 10.1016/s0049-3848(03)00240-8. PMID: 12818245.

Zhang J, Tao R, Campbell KF, Carvalho JL, Ruiz EC, Kim GC, Schmuck EG, Raval AN, da Rocha AM, Herron TJ, Jalife J, Thomson JA, Kamp TJ. Functional cardiac fibroblasts derived from human pluripotent stem cells via second heart field progenitors. Nat Commun. 2019 May 20;10(1):2238. doi: 10.1038/s41467-019-09831-5. PMID: 31110246; PMCID: PMC6527555.

Zhao G, Qiu Y, Zhang HM, Yang D. Intercalated discs: cellular adhesion and signaling in heart health and diseases. Heart Fail Rev. 2019 Jan;24(1):115-132. doi: 10.1007/s10741-018-9743-7. PMID: 30288656.

Zimmermann WH, Schneiderbanger K, Schubert P, Didié M, Münzel F, Heubach JF, Kostin S, Neuhuber WL, Eschenhagen T. Tissue engineering of a differentiated cardiac muscle construct. Circ Res. 2002 Feb 8;90(2):223-30. doi: 10.1161/hh0202.103644. PMID: 11834716.

Zornoff LA, Paiva SA, Duarte DR, Spadaro J. Ventricular remodeling after myocardial infarction: concepts and clinical implications. Arq Bras Cardiol. 2009 Feb;92(2):150-64. English, Portuguese, Spanish. doi: 10.1590/s0066-782x2009000200013. PMID: 19360249.

Appendix

Table of Contents

Introduction to the Appendix

As part of my PhD program, I undertook a training period at a private company, Breda Genetics, based in Brescia, where I received specialized training in whole exome and whole genome sequencing, with a focus on the interpretation of genetic variants involved in rare diseases. This training was part of a collaborative Project between the University of Florence and Breda Genetics, aimed at the genetic analysis of myectomy-derived tissue samples from patients affected by hypertrophic cardiomyopathy (HCM), using whole exome sequencing.

Although the Project presented in the appendix differs from the central topic of the dissertation, it shares important conceptual and methodological links. Both lines of research are concerned with the mechanisms of cardiac structural remodeling, a hallmark of several cardiac pathologies, including HCM. The appendix Project specifically investigates the genetic bases of this process, with the aim of identifying rare or novel variants that may contribute to disease onset or progression.

This genetic approach complements the main focus of the dissertation, which centers on the cellular and molecular pathways involved in cardiac remodeling. By integrating the data and insights obtained through exome sequencing, the project enriches our understanding of how genetic factors can influence structural and functional changes in the heart. Moreover, it highlights the importance of a multidisciplinary approach, combining molecular genetics with clinical and pathological *data*, to better characterize complex cardiac diseases.

Abstract

Hypertrophic Cardiomyopathy (HCM) is a genetically heterogeneous heart disease primarily caused by pathogenic variants in sarcomeric genes, with *MYBPC3* and *MYH7* being the most commonly implicated. Despite extensive research, the genetic basis of HCM remains incompletely understood, as approximately 40% of patients lack both a family history and an identifiable causative variant. This study aimed to investigate the prevalence and nature of genetic mutations in a cohort of 92 patients diagnosed with HCM who underwent myectomy and genetic testing. Of the 92 patients, 44 (48%) tested positive for a pathogenic or likely pathogenic variant, underscoring the genetic nature of the disease in this population. The cohort was balanced in terms of sex, with 22 males and 22 females, and the average age of onset was 53 years for women and 40 years for men.

Genetic testing revealed that the most frequent mutations were in the *MYBPC3* and *MYH7* genes, consistent with previous studies on HCM cohorts. The majority of identified mutations were *loss of function* (LoF) or missense mutations that impair sarcomeric protein function. Specifically, LoF mutations in *MYBPC3*, such as nonsense and frameshift mutations, lead to a reduction in cardiac myosin binding protein-C (cMyBP-C) production, which is crucial for heart muscle contraction and contributes to the pathogenesis of HCM. Missense mutations in *MYH7*, particularly in regions involved in myosin motor function, were also frequently detected. Interestingly, patients with a Complex Genotype, involving mutations in both *MYBPC3* and *MYH7*, demonstrated a more severe clinical phenotype.

Moreover, the study also highlighted sex-based differences in disease presentation, with women tending to present at an older age with more severe heart failure symptoms compared to men, which is consistent with previous reports on sex disparities in HCM.

This study emphasizes the critical role of genetic testing in diagnosing HCM and provides valuable insights into the distribution and clinical impact of specific genetic variants.

1 Introduction

1.1 Hypertrophic Cardiomyopathy: clinical features and genetic basis

Hypertrophic cardiomyopathy (HCM) is the most common inherited cardiomyopathy with a prevalence in the general population of 1:500 (Maron et al., 2004). It is characterized by hypertrophy of the left ventricle (LV) with a maximal end-diastolic wall thickness of ≥ 15 mm (Ommen et al., 2020). HCM has a broad spectrum of clinical manifestations, ranging from asymptomatic left ventricular hypertrophy to arrhythmias (atrial fibrillation and malignant ventricular arrhythmias) and refractory heart failure. Clinical variability has also been demonstrated within the same family (intrafamilial variability). A systematic clinical staging of the disease was proposed by Olivotto et al., in which four clinical stages were identified, emphasising the diagnosis, potential mechanisms, management challenges and objectives for future investigations. These are defined as *non-hypertrophic HCM*, *classic phenotype*, *adverse remodeling* and *overt dysfunction* (Figure 1). The *non-hypertrophic HCM* state is defined in individuals carrying pathogenic mutations causing HCM (as determined by systematic family screening) who do not exhibit LV hypertrophy (genotype-positive/phenotype-negative). The *classic phenotype* of HCM is characterized by fully expressed hypertrophy, in which the left ventricle is hyperdynamic (as defined by an ejection fraction [EF] >65%) in the absence of extensive fibrotic replacement (Olivotto et al., 2012). This condition is present in more than three-quarters of patients with HCM in cross-sectional studies (Olivotto et al., 2010). In this phase, the most common cause of symptoms is the obstruction of the left ventricular outflow tract (LVOTO) due to the systolic anterior motion (SAM) of the mitral valve. At the microscopic level, HCM is characterized by myocardial disorganization, microvascular remodeling, and interstitial fibrosis. *Adverse remodeling* occurs in approximately 15% of patients with HCM and is characterized by cardiac structural abnormalities superimposed on the classic phenotype, such as left ventricular (LV) fibrosis, along with worsening diastolic and systolic function within a low-normal Ejection Fraction (EF) range of 50% to 65% (Argirò et al., 2023). A smaller proportion of patients with adverse remodeling will ultimately progress to overt dysfunction, consisting in a severe dysfunction of the left ventricle (Ejection Fraction (LVEF) <50%), sustained fibrosis and remodeling (Yacoub et al., 2007).

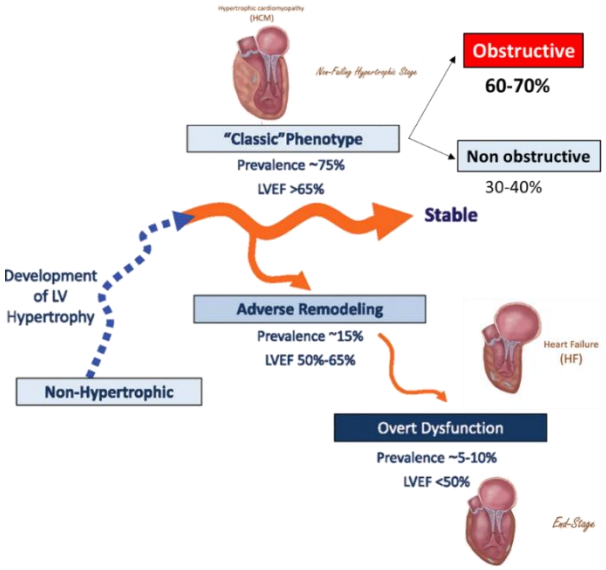

Figure 1. Stages of hypertrophic cardiomyopathy (HCM). Thick ness of the orange lines reflects prevalence of each stage in HCM cohorts. Prevalence of *non-hypertrophic* HCM is unknown. LVEF indicates Left Ventricular Ejection Fraction (Olivotto et al., 2012).

HCM is inherited in an autosomal dominant manner with variable expressivity and age-related penetrance. Mutations in genes that encode thick or thin myofilament proteins (Figure 2) within the cardiac sarcomere (or related structures) are common causes of HCM, with more than 1,500 mutations identified in these genes (Ingles et al., 2015). A study of 33 genes commonly tested for HCM found that only eight were definitively linked to the condition, three showed moderate evidence of being involved, and 22 of the 33 genes (67%) showed little or no evidence of a connection to HCM (Ingles et al., 2019). To date the pathophysiological mechanisms by which sarcomere gene mutations give HCM are not yet fully understood (Marian and Braunwald, 2017) and in about 40% of HCM patients, the causal genes remain unidentified. Most mutations responsible for HCM are missense mutations, where one normal amino acid is replaced with another, leading to changes in the protein's essential functional characteristics. Another common mutation type is frameshift mutations, which result in a shortened or truncated protein due to the insertion or deletion of one or more nucleotides.
Among most of the genes involved, the following genes have definitive evidence supporting their role as causative for the disease:

MYBPC3 gene (locus 11p11.2). This gene encodes cardiac myosin-binding protein C of the intermediate filament. Heterozygous mutations in the *MYBPC3* gene account for at least 50% of genetically determined hypertrophic cardiomyopathy cases (Cirino et al., 1993–2025) and at least 2% of dilated cardiomyopathy cases (Hershberger and Jordan, 2007). According to a 2023 review specific to this gene, *MYBPC3* mutations are the most represented, accounting for up to 61% of HCM cases. Most mutations are of the *loss-of-function* type (nonsense variants, frameshift mutations, splicing mutations, and insertions/deletions), while missense mutations account for approximately 15%. Although the pathogenic mechanism remains poorly understood, it is hypothesized that all types of genetic variants may involve haploinsufficiency or a dominant-negative effect (Tudurachi et al., 2023).

MYH7 gene (locus 14q11.2). The *MYH7* gene codes for the β-cardiac/slow skeletal myosin heavy chain (MyHC-slow), which is primarily expressed in the heart ventricles and slow-twitch (type 1) skeletal muscle fibers. Myosin functions as a molecular motor by interacting with actin in the thin filament, a crucial process for generating force in skeletal muscles (Beecroft et al., 2019). Heterozygous mutations in the *MYH7* gene account for 33% of genetically inherited cases of hypertrophic cardiomyopathy (HCM) (Cirino and Ho, 2008) and at least 4% of cases of dilated cardiomyopathy (DCM) (Hershberger and Jordan, 2007).

TNNT2 gene (locus 1q32.1). This encodes cardiac muscle troponin T of thin filament. Heterozygous mutations in the TNNT2 gene account for at least 4% of genetically inherited cases of hypertrophic cardiomyopathy (Cirino and Ho, 2008).

TNNI3 gene (locus 19q13.4). This encodes cardiac troponin I of thin filament and is present in 4-8% of cases. Mutations in the *TNNI3* gene account for up to 5% of cases of hypertrophic cardiomyopathy (Cirino and Ho, 2008). Less than 1% of heterozygous or biallelic mutations in the same gene may also cause dilated cardiomyopathy (Hershberger and Jordan, 2007). According to a 2023 publication, heterozygous missense mutations in the *TNNI3* gene appear to be more frequently associated with dilated, restrictive, hypertrophic, or intermediate cardiomyopathy, with significant phenotypic variability (both intrafamilial and interfamilial) and incomplete penetrance. Clinical evidence has suggested that biallelic *loss of function* mutations in the same gene cause a severe form of neonatal dilated cardiomyopathy (Sorrentino et al., 2023).

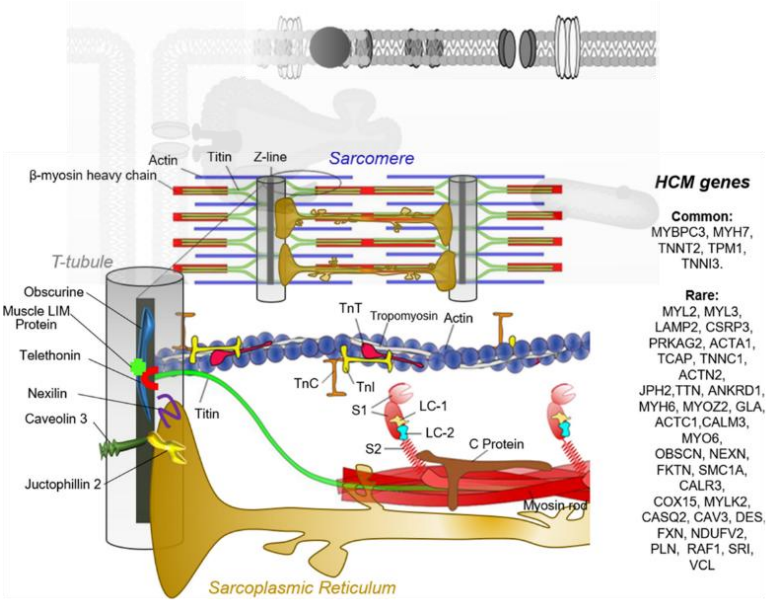

Figure 2. Gene mutations associated to HCM. Cartoon depicting the sarcomeres and the associated T-tubule sarcoplasmic reticulum structures. About 35–60% of patients with HCM are heterozygous for missense or truncating mutations in genes encoding sarcomeric proteins, with the most commonly involved being MYBPC3 (cardiac myosin-binding protein-C), MYH7 (β-myosin heavy-chain), and TNNT2 (Troponin T) or TPM1 (Tropomyosin). Rare forms of HCM (prevalence < 1%) are those associated to other genes that are listed on the right panel. Among them, additional sarcomere proteins and Z-line proteins, e.g. TnC, Troponin C; TnI, Troponin I, LC, light chain; TTN, Titin, OBSCN, Obscurine; or proteins involved in E–C coupling and muscle regulation/development (JPH2, Junctophillin 2; CAV3, Caveolin-3; CSRP3, Muscle LIM Protein; NEXN, Nexilin; TCAP, Telethonin) (Vitale et al., 2021).

1.2 Exome sequencing and Interpretation of variants (ACMG Guidelines)

The Sanger chain termination method, also known as the dideoxynucleotide method, first introduced in 1977 (Sanger et al., 1977), laid the foundation for the rapid development of DNA sequencing technologies now known as Next-Generation Sequencing (NGS). NGS is an advanced technology used in genomic research that analyzes millions of DNA fragments simultaneously, providing comprehensive insights into genome structure, genetic variations, gene activity, and changes in gene behavior. Sequencing reactions occur in parallel on millions of DNA fragments, generating vast amounts of sequence data in a single run, with storage capacities ranging from gigabytes (Gb) to terabytes (Tb) of information. NGS technologies have significantly reduced DNA sequencing costs, accelerated high-quality genome sequencing and offered benefits such as minimal DNA input, faster response times and the ability to drive genetic and genomic discoveries (Satam et al., 2023).

Currently, Illumina platforms dominate in high throughput sequencing market. The technology was originally developed by David Klenerman and other colleagues at the University of Cambridge, who designed a novel method for clonal amplification of DNA and founded the company Solexa. In 2006, the first platform for sequencing short DNA fragments was introduced, and later "Solexa Genome Analyzer" system was acquired by Illumina for the sequencing of clonally amplified DNA (Voelkerding et al. 2009). Illumina sequencing technology operates through the following steps (Figure 3):

Library Preparation: In this step, the DNA is fragmented into fragments of approximately 200-600 base pairs. Specific anchoring oligonucleotides called adapters are ligated to the DNA fragments. The adapter-ligated fragments are subsequently PCR amplified, and gel purified.

Cluster Generation: The library is loaded into a *flow cell* where fragments are captured on a lawn of surface-bound oligos complementary to the library adapters. The anchored sequences are then amplified by PCR using the bridge amplification technique. The double-stranded DNA is then broken down into single-stranded DNA using heat, leaving several million dense clusters of identical DNA sequences.

Sequencing: Primers and fluorescently labeled terminators (terminators are a version of nucleotide base that stop DNA synthesis) are added to the flow cell. Each of the terminator bases (A, C, G, and T) give off a different colour. The fluorescently labelled terminator group is then removed from the first base and the next fluorescently base can be beside added. And so, the process continues until millions of clusters have been sequenced.

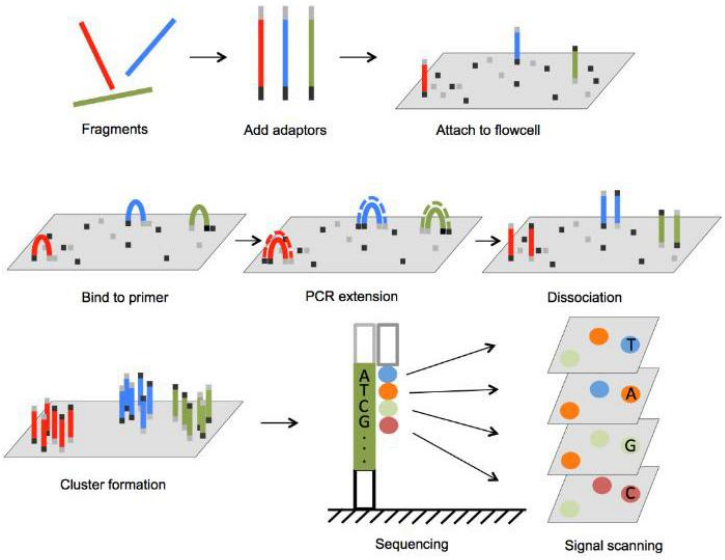

Figure 3. Illumina sequencing platform.

Data Analysis: The identified sequence reads are aligned to a reference genome (such as the human reference genome GRCh37) using software like BWA, Bowtie, or STAR. Once the reads are aligned, genetic variations (such as mutations, single nucleotide polymorphisms, or insertion/deletion variants) are analyzed. The identified variants are compared to reference databases to determine if they are known and potentially pathogenic.
Interpretation of Results: The final interpretation of the identified variants may require the integration of additional information, such as clinical, familial *data*, and access to disease-related databases. Based on the results, therapeutic, diagnostic, or clinical management decisions can be made.

An important branch of Next-Generation Sequencing (NGS) is exome sequencing, also known as Whole Exome Sequencing (WES). This technique focuses on analyzing the protein-coding regions of the genome, known as exons, which make up approximately 1% of the total DNA but contain most genetic variants associated with diseases (Ng et al., 2009). Due to its high efficiency and precision, exome sequencing is widely used in clinical and research settings to identify mutations responsible for genetic disorders, thereby contributing to diagnosis, therapy, and clinical management of patients (Ross et al., 2020).

The American College of Medical Genetics and Genomics (ACMG) outlines guidelines for the interpretation of genetic variants (Richards et al., 2015), establishing a system to classify variants based on their potential pathogenicity. Genetic variants are classified into five main categories: Pathogenic (P), where the variant is highly likely to cause disease (Table 1); Likely pathogenic (LP), where the variant is probably disease-causing, but the evidence is not as strong as for pathogenic variants; Variant of uncertain significance (VUS), where there is insufficient evidence to determine whether the variant is pathogenic or benign; Likely benign (LB), where the variant is probably not related to disease but may have some biological effect; and Benign (B), where the variant is not associated with disease and does not impact the phenotype or disease risk (Table 2). Variants are interpreted based on various criteria, including population *data* (frequency of the variant in control populations), functional evidence (whether the variant affects gene or protein function), family segregation (if the variant is present in family members with the disease), computational *data* (predictions on the variant's effect on protein function), and clinical studies linking the variant to disease. These guidelines emphasize a standardized approach to variant interpretation, aiming to improve the reliability of diagnoses and genetic counseling by using the most current available evidence.

Table 1. Criteria for classifying pathogenic variants

Criteria for Pathogenicity	Description
PVS1 *(Very Strong)*	Null variant (nonsense, frameshift, canonical ±1 or 2 splice sites, initiation codon, single or multiexon deletion) in a gene where *loss-of-function* is a known mechanism of disease
PS1 *(Strong)*	Same amino acid change as a previously established pathogenic variant regardless of nucleotide change
PS2 *(Strong)*	*De novo* (both maternity and paternity confirmed) in a patient with the disease and no family history
PS3 *(Strong)*	Well-established *in vitro* or *in vivo* functional studies supportive of a damaging effect on the gene or gene product Note: Functional studies that have been validated and shown to be reproducible and robust in a clinical diagnostic laboratory setting is considered the most well established

PS4 *(Strong)*	The prevalence of the variant in affected individuals is significantly increased compared with the prevalence in controls
PM1 *(Moderate)*	Located in a mutational hot spot and/or critical and well-established functional domain (e.g., active site of an enzyme) without benign variation
PM2 *(Moderate)*	Absent from controls (or at extremely low frequency if recessive) in Exome Sequencing Project,1000 Genomes Project, or Exome Aggregation Consortium
PM3 *(Moderate)*	For recessive disorders, detected in trans with a pathogenic variant
PM4 *(Moderate)*	Protein length changes as a result of in-frame deletions/insertions in a nonrepeat region or stop-loss variants
PM5 *(Moderate)*	Novel missense change at an amino acid residue where a different missense change determined to be pathogenic has been seen before
PM6 *(Moderate)*	Assumed *de novo*, but without confirmation of paternity and maternity
PP1 *(Supporting)*	Cosegregation with disease in multiple affected family members in a gene definitively known to cause the disease
PP2 *(Supporting)*	Missense variant in a gene that has a low rate of benign missense variation and in which missense variants are a common mechanism of disease
PP3 *(Supporting)*	Multiple lines of computational evidence support a deleterious effect on the gene or gene product (conservation, evolutionary, splicing impact, etc.)
PP4 *(Supporting)*	Patient's phenotype or family history is highly specific for a disease with a single genetic etiology
PP5 *(Supporting)*	Reputable source recently reports variant as pathogenic, but the evidence is not available to the laboratory to perform an independent evaluation

Table 2. Criteria for classifying benign variants

Criteria for Benign impact	Description
BA1 *(Stand-alone)*	Allele frequency is >5% in Exome Sequencing Project, 1000 Genomes Project, or Exome Aggregation Consortium
BS1 *(Strong)*	Allele frequency is greater than expected for disorder
BS2 *(Strong)*	Observed in a healthy adult individual for a recessive (homozygous), dominant (heterozygous), or X-linked (hemizygous) disorder, with full penetrance expected at an early age
BS3 *(Strong)*	Well-established *in vitro* or *in vivo* functional studies show no damaging effect on protein function or splicing
BS4 *(Strong)*	Lack of segregation in affected members of a family
BP1 *(Supporting)*	Missense variant in a gene for which primarily truncating variants are known to cause disease

BP2 *(Supporting)*	Observed *in trans* with a pathogenic variant for a fully penetrant dominant gene/disorder or observed *in cis* with a pathogenic variant in any inheritance pattern
BP3 *(Supporting)*	In-frame deletions/insertions in a repetitive region without a known function
BP4 *(Supporting)*	Multiple lines of computational evidence suggest no impact on gene or gene product (conservation, evolutionary, splicing impact, etc.)
BP5 *(Supporting)*	Variant found in a case with an alternate molecular basis for disease
BP6 *(Supporting)*	Reputable source recently reports variant as benign, but the evidence is not available to the laboratory to perform an independent evaluation
BP7 *(Supporting)*	A synonymous (silent) variant for which splicing prediction algorithms predict no impact to the splice consensus sequence nor the creation of a new splice site and the nucleotide is not highly conserved

The criteria for classification are organized into levels of evidence, which range from "very strong" (the highest level of evidence) to "supporting" (the lowest level). Each level of evidence reflects the quality and quantity of data available to support the variant's classification. The criteria are then combined according to the scoring rules in Table 3 to determine which classification a variant fall into.

Table 3. Rules for combining criteria to classify sequence variants

Pathogenic	1 Very strong (PVS1) AND • ≥1 Strong (PS1–PS4) OR • ≥2 Moderate (PM1–PM6) OR • 1 Moderate (PM1–PM6) and 1 supporting (PP1–PP5) OR • ≥2 Supporting (PP1–PP5) ≥2 Strong (PS1–PS4) OR 1 Strong (PS1–PS4) AND • ≥3 Moderate (PM1–PM6) OR • 2 Moderate (PM1–PM6) AND ≥2 Supporting (PP1–PP5) OR • 1 Moderate (PM1–PM6) AND ≥4 supporting (PP1–PP5)
Likely pathogenic	1 Very strong (PVS1) AND 1 moderate (PM1-PM6) OR 1 Strong (PS1–PS4) AND 1–2 moderate (PM1–PM6) OR 1 Strong (PS1–PS4) AND ≥2 supporting (PP1–PP5) OR ≥3 Moderate (PM1–PM6) OR 2 Moderate (PM1–PM6) AND ≥2 supporting (PP1–PP5) OR 1 Moderate (PM1–PM6) AND ≥4 supporting (PP1–PP5)
Benign	1 Stand-alone (BA1) OR ≥2 Strong (BS1–BS4)
Likely Benign	1 Strong (BS1–BS4) and 1 supporting (BP1-BP7) OR

Uncertain Significance	≥2 Supporting (BP1–BP7) Other criteria shown above are not met OR The criteria for benign and pathogenic are contradictory

These ACMG Standards and Guidelines were primarily developed as an educational resource for clinical laboratory geneticists to assist them in providing high-quality clinical laboratory services. The interpretation of genetic variants remains a highly debated and complex area, where each criterion must be applied through a comprehensive analysis tailored to the patient's phenotype. For example, a variant cannot be considered causative of a disease simply because it is *de novo* or rare. Even in healthy individuals, hundreds or even thousands of rare or *de novo* variants can be present. Therefore, multiple molecular evaluations are necessary, such as assessing whether the variant lies in a conserved region, within a known mutational hotspot for the disease, if the mutation affects the protein structure, or if it disrupts the splicing process.
Family history also plays a crucial role. Genetic testing should be extended to family members to determine whether the candidate variant co-segregates with the disease or, conversely, if it is found in healthy individuals, particularly in the case of dominant diseases. Additionally, many genetic variants can lead to a range of phenotypic expressions (variable expressivity), and the likelihood of disease development may not be 100% (reduced penetrance) (Richards et al, 2015).
By combining these molecular insights with the clinical context of the patient, healthcare providers can more effectively guide variant analysis.

1.3 Aim

In this study, over 92 heart muscle biopsy samples (myectomy samples) from patients with hypertrophic cardiomyopathy (HCM) were genotyped using exome sequencing. Exome analysis allows for the visualization of the patient's genetic profile and the identification of any pathogenic or likely pathogenic variants affecting sarcomeric genes.
Published *data* regarding the percentage of sarcomeric-positive and negative cases is sometimes inconsistent. Our study aims to (i) assess, in a sub-group of approximately 92 individuals with obstructive HCM who underwent myectomy, the percentage of individuals with mutations compared to those without mutations; (ii) clarifying the impact of mutations in sarcomeric genes on the patient’s phenotype. Additionally, the study provides clinical and demographic *data* on the patients, evaluating the prevalence of sex among myofilament-positive individuals and the age at which they underwent myectomy. Once the genetic profiles and demographic *data* were defined, clinical parameters were also evaluated, including the thickness of the septum and the Left Ventricular Ejection Fraction. Each mutation was also associated with an electrophysiological parameter: the duration of the Action Potential at 1 Hz.
These data will help determine whether there are phenotypic differences among the identified mutations, such as whether certain variants contribute to a more severe phenotype or earlier disease onset, or if they affect clinical parameters and *in vitro* findings differently.

2 Material and Methods

2.1 Patients Cohorts

We enrolled 92 HCM genotyped patients from the Referral Center for Cardiomyopathies in Florence, Italy, consecutively referred to surgical myectomy for relief of drug-refractory symptoms related to left ventricular outflow tract obstruction. All of them agreed to undergo mutational screening in sarcomeric genes. The study conforms with the principles of World Medical Association's Declaration of Helsinki for medical research involving human subjects. The experimental protocols were approved by the ethics committee of Careggi University Hospital (2006/0024713; renewed May 2009). Each patient gave written informed consent.

2.2 Tissue Processing

Septal specimens from HCM were washed and rapidly processed. Briefly, a small portion of the tissue was frozen in liquid nitrogen and used for DNA isolation. Cardiac tissue was minced and subjected to enzymatic dissociation to obtain viable single myocytes.

2.3 DNA Extraction

Genomic DNA was extracted from mammalian tissue using the PureLink™ Genomic DNA Mini Kit (Invitrogen, Cat. No. K1820-00), following the manufacturer's protocol. Briefly, up to 25 mg of fresh or frozen tissue was finely chopped and transferred to a 1.5 mL microcentrifuge tube. Lysis was performed by adding 180 µL of PureLink™ Genomic Digestion Buffer and 20 µL of Proteinase K, followed by incubation at 55°C for 1 to 4 hours until complete tissue digestion was achieved. To remove any particulate materials, centrifuge the lysate at maximum speed for 3 minutes at room temperature. Then, the supernatant was transferred to a new sterile tube. To remove RNA contamination, 20 µL of RNase A was added to the lysate, and the sample was incubated at room temperature for 2 minutes. For DNA binding, 200 µL of PureLink™ Genomic Lysis/Binding Buffer and 200 µL of 96-100% ethanol were added to the lysate, and the mixture was transferred to a PureLink™ Spin Column placed in a collection tube. The column was centrifuged at 10,000 x g for 1 minute at room temperature, and the flow-through was discarded. DNA purification was carried out by sequential washes with 500 µL of Wash Buffer 1 and 500 µL of Wash Buffer 2, each followed by centrifugation at 10,000 x g. After the final wash, the column was centrifuged for an additional 3 minutes to ensure complete removal of wash buffer. For elution, the column was transferred to a clean 1.5 mL microcentrifuge tube, and 25–200 µL of PureLink™ Genomic Elution Buffer was applied directly onto the membrane. After incubating at room temperature for 1 minute, the column was centrifuged at 10,000 x g for 1 minute to recover the purified genomic DNA.

2.4 Exome sequencing

After extracting DNA, performing quantification and assessing quality, a sequencing library was prepared using the Illumina cBot platform. Paired-end sequencing was conducted to capture all human genes (approximately 20,000 genes) and their untranslated regions (5'-UTR and 3'-UTR), covering roughly 90 megabases of human exonic content. Alignment was performed using the GCRh37/hg19 assembly. Mitochondrial DNA sequences were derived by aligning off-target reads. The samples have been sequenced at an Illumina certified facility. Obtained data have been analysed through primary, secondary and tertiary bioinformatic analysis, annotating variants against major mutational databases and making in silico predictions with a validated set of algorithms.

3 Results

3.1 Prevalence of myofilament-positive patients who underwent myectomy

Within this cohort of 92 genotyped HCM patients who underwent myectomy, 44 (48%) were found to carry at least one pathogenic or likely pathogenic variant in sarcomeric genes (Figure 4, A). Among these genetically positive patients, 22 were male (aged 20-73 years) and 22 were female (aged 17-81 years) (see Table 5 for demographic details).

The distribution of pathogenic and likely pathogenic variants was as follows: 25 patients (57%) carried mutations in the *MYBPC3* gene, while *MYH7* variants were identified in 15 patients (34%). Less common mutations were also observed, with one patient (2%) harboring a *TNNT2* mutation and three patients (7%) carrying multiple pathogenic or likely pathogenic mutations across different sarcomeric genes. These cases were classified as Complex Genotypes (Figure 4, B).

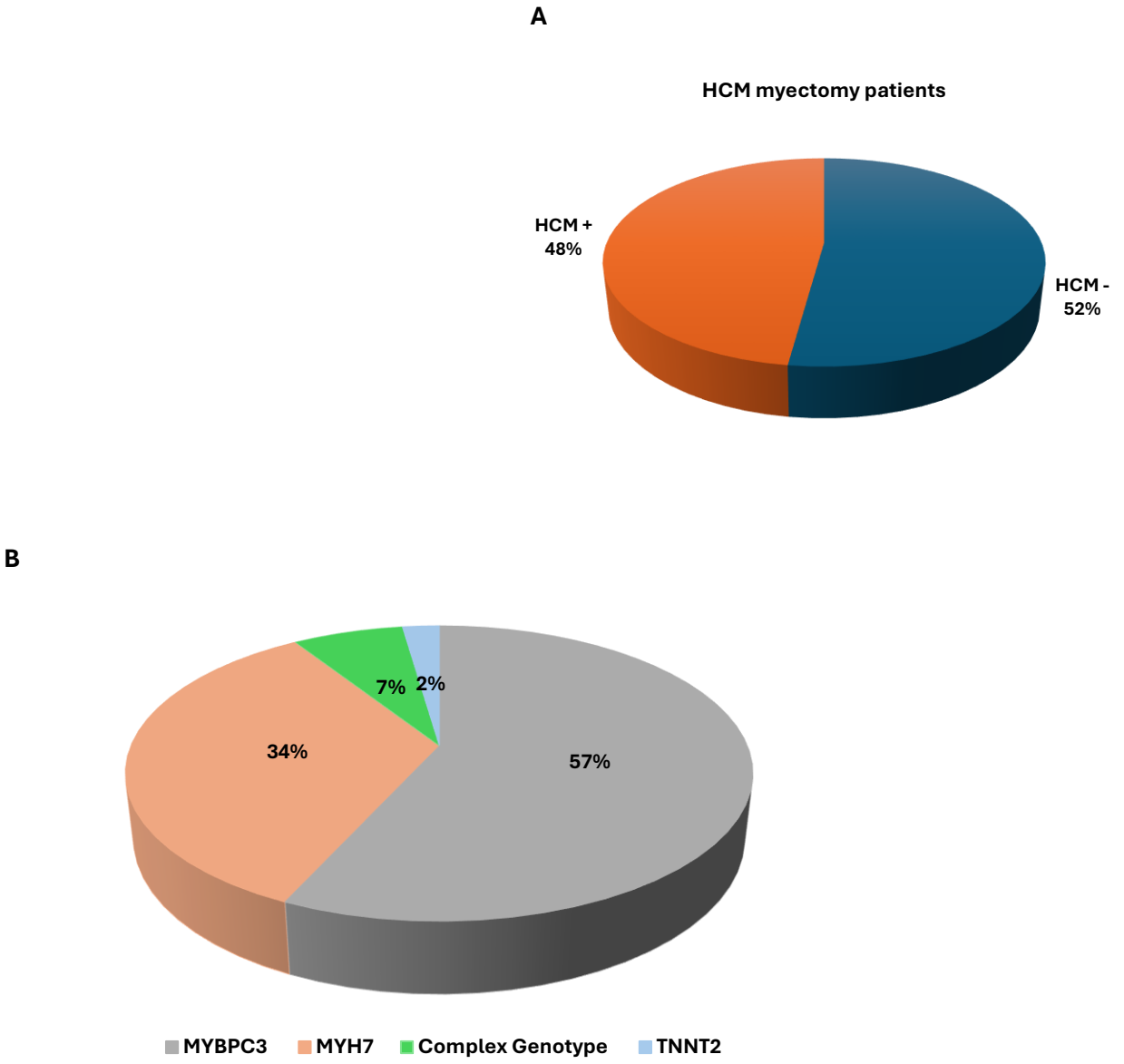

Figure 4. Pie charts representing hypertrophic cardiomyopathy (HCM) data. **(A)** Distribution of HCM myectomy patients, with 52% HCM-negative and 48% HCM-positive. **(B)** Genetic distribution of HCM patients, showing the prevalence of *MYBPC3* (57%), *MYH7* (34%), Complex Genotype (7%) and *TNNT2* (2%).

3.2 Classification of variants

Table 4 presents genetic variants identified in HCM patients who tested positive in genetic screening. These variants are classified as pathogenic or likely pathogenic based on the criteria established by the American College of Medical Genetics and Genomics (ACMG) (Richards et al., 2015), which include evaluation of molecular, clinical and familial *data*. Additionally, the allele frequencies of these variants in GnomAD population databases are provided to assist in understanding their rarity and potential pathogenic significance. The main ACMG criteria include PVS1 (*loss of function,* LoF), PS4 (high prevalence in affected individuals), PM2 (absence or low frequency in control populations), PP1 (familial segregation) and PS3 (functional studies).

In addition, specific *in silico* prediction tools such as AlphaMissense and SpliceAI were consulted. AlphaMissense is a machine-learning model designed to predict the pathogenicity of missense variants by assessing how amino acid substitutions affect protein structure and function (Minton, 2023). It generates scores between 0 and 1, with higher scores indicating greater pathogenicity (Strong: >0.984, Moderate: >0.869, Supporting: >0.761) and lower scores suggesting benign variants (Supporting: <0.331, Moderate: <0.147, Strong: <0.073) (Cheng et al., 2023).

SpliceAI is an open-source network developed by Illumina to predict the effects of genetic variants on RNA splicing. This algorithm is designed to identify potential splicing alterations caused by DNA variations, such as the activation of nearby cryptic splice sites or the disruption of canonical splice sites. These changes can lead to the generation of abnormal transcript isoforms, which may affect gene function and contribute to disease (Caminsky et al., 2014). SpliceAI score can range from 0 to 1, when scores can be interpreted as the probability of the variant being splice-altering.

Values that were not available are indicated as N/A in the Table.

In this study, many *loss of function* variants (genetic mutation in which a gene or protein loses its normal function or activity) in *MYBPC3* (25 variants) have been identified and some of them are recurrent. For example, the c.772G>A (p.Glu258Lys) variant is observed in 7 out of the total *MYBPC3* mutations, representing 28% of the total *MYBPC3* cases, while c.3192dup (p.Lys1065Glnfs*12) appears 5 times (20%). Notably, in one patient, the c.3192dup (p.Lys1065Glnfs*12) variant was identified together with the VUS (variant of uncertain significance) c.1112C>G (p.Pro371Arg) in the same gene. The c.3192dup (p.Lys1065Glnfs*12) and c.1112C>G (p.Pro371Arg) variants seem to form a haplotype, having been identified *in cis* in several related individuals with a family history of sudden premature death and hypertrophic cardiomyopathy (Girolami et al., 2010). Additionally, c.2309-2A>G appears twice, while the c.506-2A>C variant is found both as a single variant in *MYBPC3* and as part of a Complex Genotype with the *MYH7* c.2167C>T (p.Arg723Cys) variant.

Regarding the *MYH7* gene, this study revealed that out of a total of 15 identified variants, some are recurrent. For example, c.2606G>A (p.Arg869His) was identified 5 times, representing 33% of the total *MYH7* variants, while c.1816G>A (p.Val606Met) was identified twice.

Additionally, a pathogenic variant was identified in the *TNNT2* gene, c.832C>T (p.Arg288Cys), in one patient, along with three Complex Genotypes. The first two Complex Genotypes (*MYH7* c.2594A>G + *MYBPC3* c.772G>A and *MYBPC3* c.506-2A>C + *MYH7* c.2167C>T) involve well-known pathogenic variants in two genes primarily associated with HCM while the third one (*MYH7* c.5342G>A + *MYH7* c.4166C>T + *FHL2* c.734A>G) involves multiple variants, with two mutations in *MYH7* and an additional *FHL2* variant that may have a *modifier* role.

Table 4. Genetic profile of myofilament-positive myectomy patients

	Mutation	Pathogenic	Likely Pathogenic	ACMG Criteria	GnomAD	AlphaMissense	SpliceAI
***MYBPC3* (25)**							
1	c.3331-1G>A	✓		(PS4, PVS1, PM2)	N/A	N/A	Strong (1)
2	c.1174del (p.Ala392Leufs*14)	✓		(PS4, PVS1, PM2)	N/A	N/A	Uncertain (0.15)
3	c.772G>A (p.Glu258Lys)		✓	(PS4, PP1, PS3, PM2, PP3)	0.0022%	Benign (Supporting) (0.164)	N/A
4	c.3192dup (p.Lys1065Glnfs*12)	✓		(PS4, PP1, PVS1, PM2)	N/A	N/A	N/A
5	c.1790G>A (p.Arg597Gln)	✓		(PS4, PP1, PS3, PM2, PM5, PP3)	0.003%	Benign (Supporting) (0.199)	N/A
6	c.3192dup (p.Lys1065Glnfs*12)	✓		(PS4, PP1, PVS1, PM2)	N/A	N/A	N/A
7	c.2309-2A>G	✓		(PS4, PP1, PVS1, PM2)	N/A	N/A	Strong (1)
8	c.1828G>C (p.Asp610His)	✓		(PS4, PM2, PM1, PM5, PP3)	0.0032%	Deleterious (Moderate) (0.977)	N/A
9	c.2309-2A>G	✓		(PS4, PP1, PVS1, PM2)	N/A	N/A	Strong (1)
10	c.3034C>T (p.Gln1012*)	✓		(PS4, PVS1, PM2)	N/A	N/A	N/A
11	c.1999_2000del (p.Leu667Thrfs*25)		✓	(PVS1, PM2)	N/A	N/A	N/A
12	c.2113dup (p.Thr705Asnfs*3)	✓		(PS4, PVS1, PM2)	0.0004%	N/A	N/A
13	c.772G>A (p.Glu258Lys)		✓	(PS4, PP1, PS3, PM2, PP3)	0.0022%	Benign (Supporting) (0.164)	N/A
14	c.772G>A (p.Glu258Lys)		✓	(PS4, PP1, PS3, PM2, PP3)	0.0022%	Benign (Supporting) (0.164)	N/A
15	c.2454G>A (p.Trp818*)	✓		(PS4, PP1, PVS1, PM2)	N/A	N/A	N/A
16	c.506-2A>C	✓		(PS4, PP1, PS3, PVS1, PM2)	N/A	N/A	Strong (0.99)
17	c.3192dup (p.Lys1065Glnfs*12)	✓		(PS4, PP1, PVS1, PM2)	N/A	N/A	N/A

18	c.3192dup (p.Lys1065Glnfs*12) + c.1112C>G (p.Pro371Arg)	✓		(PS4, PP1, PVS1, PM2) + (PM2, PP3)	N/A	N/A + Uncertain (0.515)	N/A
19	c.772G>A (p.Glu258Lys)		✓	(PS4, PP1, PS3, PM2, PP3)	0.0022%	Benign (Supporting) (0.164)	N/A
20	c.2258dup (p.Lys754Glufs*79)	✓		(PS4, PVS1, PM2)	0.0008%		
21	c.772G>A (p.Glu258Lys)		✓	(PS4, PP1, PS3, PM2, PP3)	0.0022%	Benign (Supporting) (0.164)	N/A
22	c.3192dup (p.Lys1065Glnfs*12)	✓		(PS4, PP1, PVS1, PM2)	N/A	N/A	N/A
23	c.772G>A (p.Glu258Lys)		✓	(PS4, PP1, PS3, PM2, PP3)	0.0022%	Benign (Supporting) (0.164)	N/A
24	c.2864_2865del (p.Pro955Argfs*95)	✓		(PS4, PVS1, PM2)	0%	N/A	N/A
25	c.772G>A (p.Glu258Lys)		✓	(PS4, PP1, PS3, PM2, PP3)	0.0022%	Benign (Supporting) (0.164)	N/A
***MYH7* (15)**							
1	c.2606G>A (p.Arg869His)	✓		(PS4, PP1, PM1, PP2, PM2, PM5, PP3)	0.0024%	Benign (Supporting) (0.199)	N/A
2	c.920C>A (p.Pro307His)		✓	(PM1, PP2, PM2, PP3)	N/A	Deleterious (Moderate) (0.95)	N/A
3	c.2606G>A (p.Arg869His)	✓		(PS4, PP1, PM1, PP2, PM2, PM5, PP3)	0.0024%	Benign (Supporting) (0.199)	N/A
4	c.2631G>T (p.Met877Ile)	✓		(PS4, PP1, PS1, PM5, PM1, PP2, PM2, PP3)	N/A	Uncertain (0.645)	N/A
5	c.2779G>A (p.Glu927Lys)	✓		(PS4, PP1, PM1, PP2, PM2, PP3)	N/A	Uncertain (0.749)	N/A
6	c.2080C>T (p.Arg694Cys)		✓	(PS4, PP1, PM1, PP2, PM2, PM5, PP3)	0.002%	Deleterious (Moderate) (0.901)	N/A
7	c.1816G>A (p.Val606Met)	✓		(PS4, PP1, PS3, PM1, PP2, PM2, PP3)	0.0007%	Uncertain (0.744)	N/A
8	c.2606G>A (p.Arg869His)	✓		(PS4, PP1, PM1, PP2, PM2, PM5, PP3)	0.0024%	Benign (Supporting) (0.199)	N/A
9	c.2389G>A (p.Ala797Thr)	✓		(PM3, PP1, PM2, PM1, PP2, PM5, PP3)	0.0024%	Benign (Supporting) (0.178)	N/A

10	c.976G>C (p.Ala326Pro)		✓	(PM1, PP2, PM2, PP3)	0.0088%	Uncertain (0.646)	N/A
11	c.2606G>A (p.Arg869His)	✓		(PS4, PP1, PM1, PP2, PM2, PM5, PP3)	0.0024%	Benign (Supporting) (0.199)	N/A
12	c.2348G>A (p.Arg783His)	✓		(PS4, PM1, PP2, PM2, PM5, PP3)	0.0021%	Benign (Moderate) (0.126)	N/A
13	c.1816G>A (p.Val606Met)	✓		(PS4, PP1, PS3, PM1, PP2, PM2, PP3)	0.0007%	Uncertain (0.744)	N/A
14	c.2606G>A (p.Arg869His)	✓		(PS4, PP1, PM1, PP2, PM2, PM5, PP3)	0.0024%	Benign (Supporting) (0.199)	N/A
15	c.1987C>T (p.Arg663Cys)	✓		(PS4, PM1, PP2, PM2, PM5, PP3)	N/A	Uncertain (0.528)	N/A
***TNNT2* (1)**							
1	c.832C>T (p.Arg288Cys)	✓		(PS4, PP1, PS3, PM2, PM5, PP2)	0.0356%	N/A	N/A
Complex Genotype (3)							
1	*MYH7* c.2594A>G (p.Lys865Arg) + *MYBPC3* c.772G>A (p.Glu258Lys)	✓	✓	(PS4, PM1, PP2, PM2, PM5, PP3) + (PS4, PP1, PS3, PM2, PP3)	0.0004% + 0.0022%	Benign (Moderate) (0.117) + Benign (Supporting) (0.164)	N/A
2	*MYBPC3* c.506-2A>C[1] + *MYH7* c.2167C>T (p.Arg723Cys)[2]	✓		(PS4, PP1, PS3, PVS1, PM2) + (PP1, PS4, PM1, PP2, PM2, PM5, PM6, PP3)	N/A + 0.0012%	[2]Uncertain (0.62)	[1]Strong (0.99)
3	*MYH7* c.5342G>A (p.Arg1781His) + *MYH7* c.4166C>T (p.Ala1389Val) + *FHL2* c.734A>G (p.His245Arg)		✓	(PS4, PM1, PP2, PM2, PM5, PP3) + (PM1, PP2, PM2, PP3) + (PP3, PM2)	0.0018% + N/A + N/A	Deleterious (Moderate) (0.877) + Uncertain (0.647) + Deleterious (Strong) (0.997)	N/A

3.3 Genotype-Phenotype Correlation

Table 5 presents demographic and clinical information for HCM patients who tested positive for pathogenic mutations in sarcomeric genes, along with an electrophysiological parameter, Action Potential Duration (AP duration) at 1 Hz, measured in cells derived from cardiac tissue after myectomy. Values that were not available are indicated as N/A in the Table.

The first column of the Table presents the specific sarcomeric gene mutations identified in HCM patients, while the second column provides demographic information, including the patient's sex and the age at which they underwent myectomy. Among patients with *MYBPC3* mutations, 60% are male and 40% are female. Males underwent myectomy at an average age of 40 years, whereas females had the procedure at a later average age of 57 years. The age at myectomy for *MYBPC3* positive patients ranges from 23 to 59 years for males and from 35 to 80 years for females.

For *MYH7* positive patients, the age at myectomy ranges from 20 to 73 years for males and from 29 to 81 years for females. *MYH7* mutations are more prevalent in females (60%) than in males (40%). The average age at myectomy for males with *MYH7* mutations is 39 years, while for females, it is significantly later at 51 years. In this study, only three patients were identified with a Complex Genotype, all of them are female, with ages ranging from 17 to 67 years. Additionally, a 49-year-old male patient was identified at the time of the intervention, seeking a pathogenic mutation in *TNNT2*.

The following two columns present clinical *data* on the patients at the time of the intervention, including septal thickness and Left Ventricular Ejection Fraction (LVEF). Specifically, patients positive for HCM due to *MYBPC3* show an average septal thickness of approximately 23 mm, with a minimum of 16 mm and a maximum of 38 mm. The average LVEF in these patients is 67%, with a minimum of 53% and a maximum of 85%. Patients positive for *MYH7* presented, at the time of the intervention, an average septal thickness of 24 mm, with a minimum of 15 mm and a maximum of 39 mm. Their average LVEF is 68%, with a minimum of 58% and a maximum of 80%. The three Complex Genotype patients had septal thicknesses of 15 mm, 32 mm and 19 mm, while a LVEF of 61%, 65%, and 55%, respectively. The *TNNT2* positive patient had a septal thickness of 28 mm and an LVEF of 73%.

Regarding the electrophysiological parameter of Action Potential Duration stimulated at 1 Hz, it was observed that patients positive for *MYBPC3* had an average duration of 528 ms, with a minimum of 355 ms and a maximum of 734 ms. Meanwhile, patients positive for *MYH7* had an average duration of 542 ms, with a minimum of 321 ms and a maximum of 713 ms. The three Complex Genotypes had durations of 582 ms, 530 ms and 471 ms, while the TNNT2-positive patient had a duration of 402 ms.

Table 5. Genotype-phenotype correlation

Genetic Data	Demographic Data	Clinical Data		Electrophysiological Data
Mutation	**Sex [M/F] (Age of operation)**	**Max Thickness (mm)**	**Left Ventricular Ejection Fraction (LVEF)**	**AP Duration 1Hz (ms)**
MYBPC3				
c.3331-1G>A	M (35)	25	64%	449
c.1174del (p.Ala392Leufs*14)	F (38)	18	55%	399
c.772G>A (p.Glu258Lys)	M (46)	19	76%	594
c.3192dup (p.Lys1065Glnfs*12)	M (36)	34	85%	585
c.1790G>A (p.Arg597Gln)	M (44)	32	76%	612
c.3192dup (p.Lys1065Glnfs*12)	F (35)	30	62%	521
c.2309-2A>G	F (57)	23	68%	512
c.1828G>C (p.Asp610His)	M (40)	24	70%	734
c.2309-2A>G	M (37)	24	60%	N/A
c.3034C>T (p.Gln1012*)	M (33)	N/A	N/A	N/A
c.1999_2000del (p.Leu667Thrfs*25)	F (61)	20	76%	455
c.2113dup (p.Thr705Asnfs*3)	M (31)	N/A	N/A	N/A
c.772G>A (p.Glu258Lys)	F (46)	17	72%	566
c.772G>A (p.Glu258Lys)	M (33)	23	73%	N/A
c.2454G>A (p.Trp818*)	M (36)	28	70%	666

c.506-2A>C	M (23)	38	71%	675
c.3192dup (p.Lys1065Glnfs*12)	M (56)	22	60%	550
c.3192dup (p.Lys1065Glnfs*12) + c.1112C>G (p.Pro371Arg)	F (60)	20	53%	355
c.772G>A (p.Glu258Lys)	M (45)	16	71%	N/A
c.2258dup (p.Lys754Glufs*79)	F (67)	22	60%	585
c.772G>A (p.Glu258Lys)	M (59)	17	69%	390
c.3192dup (p.Lys1065Glnfs*12)	M (38)	30	65%	493
c.772G>A (p.Glu258Lys)	F (80)	18	65%	N/A
c.2864_2865del (p.Pro955Argfs*95)	F (62)	19	62%	372
c.772G>A (p.Glu258Lys)	F (66)	23	68%	N/A
MYH7				
c.2606G>A (p.Arg869His)	M (58)	N/A	N/A	N/A
c.920C>A (p.Pro307His)	F (50)	19	74%	502
c.2606G>A (p.Arg869His)	F (37)	33	58%	449
c.2631G>T (p.Met877Ile)	F (44)	22	74%	707
c.2779G>A (p.Glu927Lys)	M (23)	39	71%	467
c.2080C>T (p.Arg694Cys)	F (81)	19	72%	421
c.1816G>A (p.Val606Met)	M (21)	22	61%	N/A

c.2606G>A (p.Arg869His)	M (20)	23	73%	609
c.2389G>A (p.Ala797Thr)	F (29)	29	69%	631
c.976G>C (p.Ala326Pro)	F (70)	21	68%	544
c.2606G>A (p.Arg869His)	M (73)	15	60%	N/A
c.2348G>A (p.Arg783His)	F (56)	21	60%	713
c.1816G>A (p.Val606Met)	F (58)	27	75%	594
c.2606G>A (p.Arg869His)	F (32)	24	80%	321
c.1987C>T (p.Arg663Cys)	M (44)	19	63%	N/A
TNNT2				
c.832C>T (p.Arg288Cys)	M (49)	28	73%	402
Complex Genotype				
MYH7 c.2594A>G (p.Lys865Arg) + MYBPC3 c.772G>A (p.Glu258Lys)	F (61)	15	61%	582
MYBPC3 c.506-2A>C + MYH7 c.2167C>T (p.Arg723Cys)	F (17)	32	65%	530
MYH7 c.5342G>A (p.Arg1781His) + MYH7 c.4166C>T (p.Ala1389Val) + FHL2 c.734A>G (p.His245Arg)	F (67)	19	55%	471

4 Discussion

Myofilament-positive Prevalence

Hypertrophic cardiomyopathy (HCM) has traditionally been considered a monogenic disease caused by pathogenic variants in cardiac sarcomere genes, with *MYBPC3* and *MYH7* being among the most frequently involved (Ingles et al., 2019). However, the genetic basis of HCM remains only partially understood and approximately 40% of patients lack both a family history and an identified causative variant (Ingles et al., 2017).

Several genetic studies on HCM cohorts have provided valuable insights into the distribution of pathogenic variants. Current genetic testing identifies a pathogenic or likely pathogenic variant in approximately 30% of individuals, while this percentage rises to 60% in those with a family history of the disease (Alfares et al., 2015; Ireland & Ho, 2024). A study by Maurizi et al. reported a higher percentage of genetically positive patients: among 1,107 patients with clinically diagnosed obstructive HCM who underwent genetic testing, 46% (507 patients) carried a pathogenic or likely pathogenic variant. Of these, 311 (58%) had a variant in *MYBPC3*, 156 (29%) in *MYH7*, 110 (25%) in *TNNT2*, and, to a lesser extent, variants in *TNNI3*, *TPM1*, *ACTC*, *MYL2*, and *MYL3* (Maurizi et al., 2024).

In our study, the prevalence of sarcomeric gene mutations was consistent with the findings of Maurizi et al. Among 92 HCM patients who underwent myectomy and genetic testing, 48% (44 patients) had at least one pathogenic or likely pathogenic variant in *MYBPC3*, *MYH7*, *TNNT2*, or within a Complex Genotype. Among these genetically positive patients, 22 were male and 22 were female (50% male vs. 50% female). The average age of onset was 53 years vs. 40 years (range: 17-81 years vs. 20-73 years) for women and men, respectively.

Sex differences in HCM have been highlighted in multiple studies. Women tend to receive a diagnosis at an older age, present more frequently with an obstructive phenotype, exhibit worse diastolic function, and experience more severe heart failure symptoms at the time of diagnosis (Kim et al., 2021). Additionally, women are more likely to be sarcomere positive. In contrast, men tend to be sarcomere-negative, with no family history of HCM and no identifiable genetic variant (Ingles et al., 2017). However, this disparity may also be influenced by factors such as diagnostic biases and the underdiagnosis of HCM in women, which could contribute to differences in observed prevalence and disease presentation.

Analysis of variants

Loss of function (LoF) mutations in the MYBPC3 gene are among the primary genetic causes of HCM (Helms et al., 2020). The *MYBPC3* gene encodes for cardiac myosin binding protein-C (cMyBP-C), a crucial component of the cardiac sarcomere responsible for regulating the contractile function of the heart. LoF mutations in *MYBPC3* are predominantly heterozygous and include frameshift, nonsense, missense and splicing site mutations. Among them, nonsense mutations result in the emergence of premature termination codons (PTCs) in one of the two alleles, leading to nonsense-mediated decay (NMD), a cellular mechanism that degrades transcripts containing PTCs. This reduction in cMyBP-C synthesis causes a decrease in the amount of cMyBP-C in the sarcomere, contributing to functional deficits and promoting the progression of HCM (Helms et al., 2020). NMD serves as a protective mechanism against the production of potentially harmful truncated proteins; however, this same process also amplifies the haploinsufficiency of cMyBP-C, where a single functional copy of the gene is insufficient to maintain adequate levels of cMyBP-C production. This mechanism further aggravates the clinical phenotype of HCM. In advanced stages of the disease, a 40% decrease in MyBP-C protein activity has been observed in cardiac tissue obtained from surgical myectomy (O'Leary et al., 2019).

In addition to mutations that induce NMD, missense mutations or splicing alterations can lead to the production of structurally unstable or non-functional cMyBP-C proteins. Missense mutations are frequently concentrated in the central domains of the cMyBP-C molecule, which appear to play a critical role in the overall function of the protein (Harris et al., 2011). These mutations disrupt the interaction between thin filaments and myosin, while others impair myofibril structure or protein stability (Pearce et al., 2023). Errors in RNA splicing, commonly involving donor and acceptor splicing sites, are another frequent cause of mutations in *MYBPC3* (Walsh et al., 2017). These errors are typically due to mutations in the conserved *GT* and *AG* dinucleotides found at the ends of introns (Shapiro et al., 1987).
In our study, we identified 25 mutations in the *MYBPC3* gene, with the majority being nonsense mutations, frameshift, missense mutations and splicing variants. This distribution underscores the prevalence of mutations that lead to the loss of protein function in the pathology of HCM. An example is the c.772G>A (p.Glu258Lys) variant, which was observed in 7 cases (28%) of the *MYBPC3* mutations in our study. This variant has been extensively studied and classified as pathogenic due to its frequent occurrence in patients with HCM and its co-segregation with the disease has been reported within families (Girolami et al., 2006; Olivotto et al., 2008). Furthermore, c.772G>A has been identified as a founder mutation in Tuscany (Pioner et al., 2023). In our study, the prevalence of c.772G>A in Tuscan patients further corroborates the role of this variant as a founder mutation in the population.
The c.3192dup (p.Lys1065Glnfs*12) variant in the *MYBPC3* gene is another example of LoF mutation. This heterozygous mutation results in the formation of a premature stop codon and was observed in approximately 20% of the cases tested in our study. Literature indicates that the c.3192dup variant is often found *in cis* with another variant, c.1112C>G (p.Pro371Arg), which is classified as a VUS (variant of uncertain significance) in the ClinVar database (Variation ID: 42505). The co-occurrence of these two variants has been reported in multiple family members with a history of sudden premature death and hypertrophic cardiomyopathy (Girolami et al., 2010; Olivotto et al., 2011). However, it is important to emphasize that the c.3192dup (p.Lys1065Glnfs*12) variant has also been identified in isolation in some patients with HCM (Kaski et al., 2009). In our study, the c.3192dup (p.Lys1065Glnfs*12) variant was identified in 5 cases, and in only one patient it was found alongside the c.1112C>G (p.Pro371Arg) variant in the same gene. However, the demographic, clinical and functional *data* for this patient did not show significant differences compared to the other patients who carried only the c.3192dup (p.Lys1065Glnfs*12) mutation. Further investigations are necessary to evaluate the potential pathogenic role of the c.1112C>G (p.Pro371Arg) variant in the context of HCM and to determine whether its co-occurrence with c.3192dup may contribute to disease severity.

Of the 44 patients who tested positive for the genetic test, 15 carried a mutation in the *MYH7* gene, responsible for approximately 33% of HCM cases caused by pathogenic variants in the gene (Cirino et al., 1993-2025). In this case, some variants were recurrent, such as c.2606G>A (p.Arg869His), which was identified 5 times, representing 33% of the total *MYH7* variants, while c.1816G>A (p.Val606Met) was identified twice. The missense variant c.2606G>A (p.Arg869His) substitutes arginine with histidine at codon 869, within a highly conserved region of the myosin head domain. Missense variants in this region have been shown to be significantly overrepresented in HCM individuals (Walsh et al., 2017; Van Driest et al., 2004). Furthermore, this variant has been reported to segregate with the disease in an affected family member (Song et al., 2005; Olivotto et al., 2008; Girolami et al., 2010). In some cases, it has been observed that the variant cosegregates with other pathogenic variants in *MYBPC3* and double heterozygous patients exhibited an earlier onset of HCM, more rapid disease progression and severe phenotype compared indicating a possible additive effect of the co-occurring variants (Girolami et al., 2010; Olivotto et al., 2011). However, in our case, this variant was not found to be isolated alongside other pathogenic variants.
Another variant found at least twice in our cohort of patients is c.1816G>A (p.Val606Met), a missense substitution located in the myosin motor domain and functional studies suggest that the variant protein

shows altered kinetics compared to the wild-type protein (Roopnarine, 1998). This variant has been reported in several HCM patients and the co-segregation of the variant with the disease has been demonstrated in multiple unrelated families (Watkins et al., 1992; Fananapazir et al., 1994). However, the disease manifestation associated with this variant shows significant variability, both between individuals and among unrelated families showing variable penetrance and expressivity (Watkins et al., 1992).

Genotype-Phenotype correlation

From a Genotype-Phenotype correlation perspective, the clinical and electrophysiological *data* collected to date remain preliminary. However, some emerging differences between the genetic groups are observed. Specifically, patients with a Complex Genotype tend to exhibit a lower average Left Ventricular Ejection Fraction (LVEF) of approximately 60%, compared to those with *MYBPC3* (67%) and *MYH7* (68%) mutations, despite having a similar degree of hypertrophy (around 23 mm). The septal thickness in *MYBPC3* patients aligns with the expected hypertrophic phenotype typically associated with this mutation (Aurensanz et al., 2017).

Interestingly, no significant differences in systolic mechanical function have been observed between the groups. Expanding the analysis to include a wider array of clinical parameters will be crucial in identifying further genotype-phenotype correlations and offering a more comprehensive understanding of the underlying mechanisms.

5 Conclusion

This study emphasizes the intricate genetic landscape of Hypertrophic Cardiomyopathy (HCM), highlighting the critical role of genetic testing in enhancing diagnosis and management. Our findings confirm the high prevalence of *MYBPC3* and *MYH7* mutations in HCM patients, consistent with prior studies, and suggest that Complex Genotypes may be associated with a more severe clinical phenotype, as evidenced by a lower Left Ventricular Ejection Fraction (LVEF) compared to patients with *MYBPC3* and *MYH7* mutations. These insights underscore the importance of personalized approaches to treatment and the potential for genetic information to guide more effective management strategies in HCM patients.

References

Alfares AA, Kelly MA, McDermott G, Funke BH, Lebo MS, Baxter SB, Shen J, McLaughlin HM, Clark EH, Babb LJ, Cox SW, DePalma SR, Ho CY, Seidman JG, Seidman CE, Rehm HL. Results of clinical genetic testing of 2,912 probands with hypertrophic cardiomyopathy: expanded panels offer limited additional sensitivity. Genet Med. 2015 Nov;17(11):880-8. doi: 10.1038/gim.2014.205. Epub 2015 Jan 22. Erratum in: Genet Med. 2015 Apr;17(4):319. doi: 10.1038/gim.2015.16. PMID: 25611685.

Argirò A, Zampieri M, Marchi A, Cappelli F, Del Franco A, Mazzoni C, Cecchi F, Olivotto I. Stage-specific therapy for hypertrophic cardiomyopathy. Eur Heart J Suppl. 2023 Apr 26;25(Suppl C):C155-C161. doi: 10.1093/eurheartjsupp/suad042. PMID: 37125313; PMCID: PMC10132571.

Aurensanz Clemente E, Ayerza Casas A, García Lasheras C, Ramos Fuentes F, Bueno Martínez I, Pelegrín Díaz J, Ruiz Frontera P, Montserrat Iglesias L. Familial hypertrophic cardiomyopathy associated with a new mutation in gene MYBPC3. Clin Case Rep. 2017 Jan 27;5(3):232-237. doi: 10.1002/ccr3.832. PMID: 28265379; PMCID: PMC5331257.

Beecroft SJ, van de Locht M, de Winter JM, Ottenheijm CA, Sewry CA, Mohammed S, Ryan MM, Woodcock IR, Sanders L, Gooding R, Davis MR, Oates EC, Laing NG, Ravenscroft G, McLean CA, Jungbluth H. Recessive MYH7-related myopathy in two families. Neuromuscul Disord. 2019 Jun;29(6):456-467. doi: 10.1016/j.nmd.2019.04.002. Epub 2019 Apr 12. PMID: 31130376.

Bongiorno R, Colombo MP, Lecis D. Deciphering the nonsense-mediated mRNA decay pathway to identify cancer cell vulnerabilities for effective cancer therapy. J Exp Clin Cancer Res. 2021 Dec 1;40(1):376. doi: 10.1186/s13046-021-02192-2. PMID: 34852841; PMCID: PMC8638473.

Caminsky N, Mucaki EJ, Rogan PK. Interpretation of mRNA splicing mutations in genetic disease: review of the literature and guidelines for information-theoretical analysis. F1000Res. 2014 Nov 18;3:282. doi: 10.12688/f1000research.5654.1. PMID: 25717368; PMCID: PMC4329672.

Cheng J, Novati G, Pan J, Bycroft C, Žemgulytė A, Applebaum T, Pritzel A, Wong LH, Zielinski M, Sargeant T, Schneider RG, Senior AW, Jumper J, Hassabis D, Kohli P, Avsec Ž. Accurate proteome-wide missense variant effect prediction with AlphaMissense. Science. 2023 Sep 22;381(6664):eadg7492. doi: 10.1126/science.adg7492. Epub 2023 Sep 22. PMID: 37733863.

Cirino AL, Channaoui N, Ho C. Nonsyndromic Hypertrophic Cardiomyopathy Overview. 2008 Aug 5 [updated 2025 Mar 6]. In: Adam MP, Feldman J, Mirzaa GM, Pagon RA, Wallace SE, Amemiya A, editors. GeneReviews® [Internet]. Seattle (WA): University of Washington, Seattle; 1993–2025. PMID: 20301725.

Cirino AL, Ho C. Hypertrophic Cardiomyopathy Overview. 2008 Aug 5 [updated 2021 Jul 8]. In: Adam MP, Feldman J, Mirzaa GM, Pagon RA, Wallace SE, Amemiya A, editors. GeneReviews® [Internet]. Seattle (WA): University of Washington, Seattle; 1993–2025. PMID: 20301725.

Fananapazir L, Epstein ND. Genotype-phenotype correlations in hypertrophic cardiomyopathy. Insights provided by comparisons of kindreds with distinct and identical beta-myosin heavy chain gene mutations. Circulation. 1994 Jan;89(1):22-32. doi: 10.1161/01.cir.89.1.22. PMID: 8281650.

Girolami F, Ho CY, Semsarian C, Baldi M, Will ML, Baldini K, Torricelli F, Yeates L, Cecchi F, Ackerman MJ, Olivotto I. Clinical features and outcome of hypertrophic cardiomyopathy associated with triple sarcomere protein gene mutations. J Am Coll Cardiol. 2010 Apr 6;55(14):1444-53. doi: 10.1016/j.jacc.2009.11.062. PMID: 20359594.

Girolami F, Olivotto I, Passerini I, Zachara E, Nistri S, Re F, Fantini S, Baldini K, Torricelli F, Cecchi F. A molecular screening strategy based on beta-myosin heavy chain, cardiac myosin binding protein C and troponin T genes in Italian patients with hypertrophic cardiomyopathy. J Cardiovasc Med (Hagerstown). 2006 Aug;7(8):601-7. doi: 10.2459/01.JCM.0000237908.26377.d6. PMID: 16858239.

Harris SP, Lyons RG, Bezold KL. In the thick of it: HCM-causing mutations in myosin binding proteins of the thick filament. Circ Res. 2011 Mar 18;108(6):751-64. doi: 10.1161/CIRCRESAHA.110.231670. PMID: 21415409; PMCID: PMC3076008.

Helms AS, Davis FM, Coleman D, Bartolone SN, Glazier AA, Pagani F, Yob JM, Sadayappan S, Pedersen E, Lyons R, Westfall MV, Jones R, Russell MW, Day SM. Sarcomere mutation-specific expression patterns in human hypertrophic cardiomyopathy. Circ Cardiovasc Genet. 2014 Aug;7(4):434-43. doi: 10.1161/CIRCGENETICS.113.000448. Epub 2014 Jul 16. PMID: 25031304; PMCID: PMC4254656.

Helms AS, Tang VT, O'Leary TS, Friedline S, Wauchope M, Arora A, Wasserman AH, Smith ED, Lee LM, Wen XW, Shavit JA, Liu AP, Previs MJ, Day SM. Effects of MYBPC3 loss-of-function mutations preceding hypertrophic cardiomyopathy. JCI Insight. 2020 Jan 30;5(2):e133782. doi: 10.1172/jci.insight.133782. PMID: 31877118; PMCID: PMC7098724.

Hershberger RE, Jordan E. Dilated Cardiomyopathy Overview. 2007 Jul 27 [updated 2024 Dec 12]. In: Adam MP, Feldman J, Mirzaa GM, Pagon RA, Wallace SE, Amemiya A, editors. GeneReviews® [Internet]. Seattle (WA): University of Washington, Seattle; 1993–2025. PMID: 20301486.

Ho CY, Day SM, Ashley EA, Michels M, Pereira AC, Jacoby D, Cirino AL, Fox JC, Lakdawala NK, Ware JS, Caleshu CA, Helms AS, Colan SD, Girolami F, Cecchi F, Seidman CE, Sajeev G, Signorovitch J, Green EM, Olivotto I. Genotype and Lifetime Burden of Disease in Hypertrophic Cardiomyopathy: Insights from the Sarcomeric Human Cardiomyopathy Registry (SHaRe). Circulation. 2018 Oct 2;138(14):1387-1398. doi: 10.1161/CIRCULATIONAHA.117.033200. Epub 2018 Aug 23. PMID: 30297972; PMCID: PMC6170149.

Ingles J, Burns C, Bagnall RD, Lam L, Yeates L, Sarina T, Puranik R, Briffa T, Atherton JJ, Driscoll T, Semsarian C. Nonfamilial Hypertrophic Cardiomyopathy: Prevalence, Natural History, and Clinical Implications. Circ Cardiovasc Genet. 2017 Apr;10(2):e001620. doi: 10.1161/CIRCGENETICS.116.001620. PMID: 28408708.

Ingles J, Burns C, Barratt A, Semsarian C. Application of Genetic Testing in Hypertrophic Cardiomyopathy for Preclinical Disease Detection. Circ Cardiovasc Genet. 2015 Dec;8(6):852-9. doi: 10.1161/CIRCGENETICS.115.001093. PMID: 26671970.

Ingles J, Goldstein J, Thaxton C, Caleshu C, Corty EW, Crowley SB, Dougherty K, Harrison SM, McGlaughon J, Milko LV, Morales A, Seifert BA, Strande N, Thomson K, Peter van Tintelen J, Wallace K, Walsh R, Wells Q, Whiffin N, Witkowski L, Semsarian C, Ware JS, Hershberger RE, Funke B. Evaluating the Clinical Validity of Hypertrophic Cardiomyopathy Genes. Circ Genom Precis Med. 2019 Feb;12(2):e002460. doi: 10.1161/CIRCGEN.119.002460. PMID: 30681346; PMCID: PMC6410971.

Ireland CG, Ho CY. Genetic Testing in Hypertrophic Cardiomyopathy. Am J Cardiol. 2024 Feb 1;212S:S4-S13. doi: 10.1016/j.amjcard.2023.10.032. Epub 2024 Jan 29. PMID: 38368035.

Kaski JP, Syrris P, Esteban MT, Jenkins S, Pantazis A, Deanfield JE, McKenna WJ, Elliott PM. Prevalence of sarcomere protein gene mutations in preadolescent children with hypertrophic cardiomyopathy. Circ Cardiovasc Genet. 2009 Oct;2(5):436-41. doi: 10.1161/CIRCGENETICS.108.821314. Epub 2009 Jul 16. PMID: 20031618.

Kim M, Kim B, Choi YJ, Lee HJ, Lee H, Park JB, Lee SP, Han KD, Kim YJ, Kim HK. Sex differences in the prognosis of patients with hypertrophic cardiomyopathy. Sci Rep. 2021 Mar 1;11(1):4854. doi: 10.1038/s41598-021-84335-1. PMID: 33649405; PMCID: PMC7921653.

Marian AJ, Braunwald E. Hypertrophic Cardiomyopathy: Genetics, Pathogenesis, Clinical Manifestations, Diagnosis, and Therapy. Circ Res. 2017 Sep 15;121(7):749-770. doi: 10.1161/CIRCRESAHA.117.311059. PMID: 28912181; PMCID: PMC5654557.

Maron BJ, Spirito P, Roman MJ, Paranicas M, Okin PM, Best LG, Lee ET, Devereux RB. Prevalence of hypertrophic cardiomyopathy in a population-based sample of American Indians aged 51 to 77 years (the Strong Heart Study). Am J Cardiol. 2004 Jun 15;93(12):1510-4. doi: 10.1016/j.amjcard.2004.03.007. PMID: 15194022.

Maurizi N, Antiochos P, Owens A, Lakdwala N, Saberi S, Russell MW, Fumagalli C, Skalidis I, Lin KY, Nathan AS, De Feria Alsina A, Reza N, Stendahl JC, Abrams D, Semsarian C, Clagget B, Lampert R, Wheeler M, Parikh VN, Ashley E, Michels M, Rossano J, Ryan TD, Ingles J, Ware J, Ho CY, Helms AS, Day SM, Olivotto I. Long-Term Outcomes After Septal Reduction Therapies in Obstructive Hypertrophic Cardiomyopathy: Insights From the SHARE Registry. Circulation. 2024 Oct 22;150(17):1377-1390. doi: 10.1161/CIRCULATIONAHA.124.069378. Epub 2024 Oct 2. PMID: 39355918; PMCID: PMC11493522.

Minton K. Predicting variant pathogenicity with AlphaMissense. Nat Rev Genet. 2023 Dec;24(12):804. doi: 10.1038/s41576-023-00668-9. PMID: 37821682.

Ng SB, Turner EH, Robertson PD, Flygare SD, Bigham AW, Lee C, Shaffer T, Wong M, Bhattacharjee A, Eichler EE, Bamshad M, Nickerson DA, Shendure J. Targeted capture and massively parallel sequencing of 12 human exomes. Nature. 2009 Sep 10;461(7261):272-6. doi: 10.1038/nature08250. Epub 2009 Aug 16. PMID: 19684571; PMCID: PMC2844771.

O'Leary TS, Snyder J, Sadayappan S, Day SM, Previs MJ. MYBPC3 truncation mutations enhance actomyosin contractile mechanics in human hypertrophic cardiomyopathy. J Mol Cell Cardiol. 2019 Feb;127:165-173. doi: 10.1016/j.yjmcc.2018.12.003. Epub 2018 Dec 11. PMID: 30550750; PMCID: PMC6592272.

Olivotto I, Cecchi F, Poggesi C, Yacoub MH. Patterns of disease progression in hypertrophic cardiomyopathy: an individualized approach to clinical staging. Circ Heart Fail. 2012 Jul 1;5(4):535-46. doi: 10.1161/CIRCHEARTFAILURE.112.967026. PMID: 22811549.

Olivotto I, Girolami F, Ackerman MJ, Nistri S, Bos JM, Zachara E, Ommen SR, Theis JL, Vaubel RA, Re F, Armentano C, Poggesi C, Torricelli F, Cecchi F. Myofilament protein gene mutation screening and outcome of patients with hypertrophic cardiomyopathy. Mayo Clin Proc. 2008 Jun;83(6):630-8. doi: 10.4065/83.6.630. PMID: 18533079.

Olivotto I, Girolami F, Sciagrà R, Ackerman MJ, Sotgia B, Bos JM, Nistri S, Sgalambro A, Grifoni C, Torricelli F, Camici PG, Cecchi F. Microvascular function is selectively impaired in patients with hypertrophic cardiomyopathy and sarcomere myofilament gene mutations. J Am Coll Cardiol. 2011 Aug 16;58(8):839-48. doi: 10.1016/j.jacc.2011.05.018. PMID: 21835320.

Olivotto I, Maron BJ, Appelbaum E, Harrigan CJ, Salton C, Gibson CM, Udelson JE, O'Donnell C, Lesser JR, Manning WJ, Maron MS. Spectrum and clinical significance of systolic function and myocardial fibrosis assessed by cardiovascular magnetic resonance in hypertrophic cardiomyopathy. Am J Cardiol. 2010 Jul 15;106(2):261-7. doi: 10.1016/j.amjcard.2010.03.020. PMID: 20599013.

Ommen SR, Mital S, Burke MA, Day SM, Deswal A, Elliott P, Evanovich LL, Hung J, Joglar JA, Kantor P, Kimmelstiel C, Kittleson M, Link MS, Maron MS, Martinez MW, Miyake CY, Schaff HV, Semsarian C, Sorajja P. 2020 AHA/ACC Guideline for the Diagnosis and Treatment of Patients With Hypertrophic Cardiomyopathy: Executive Summary: A Report of the American College of Cardiology/American Heart Association Joint Committee on Clinical Practice Guidelines. Circulation. 2020 Dec 22;142(25):e533-e557. doi: 10.1161/CIR.0000000000000938. Epub 2020 Nov 20. PMID: 33215938.

Pearce A, Ponnam S, Holt MR, Randall T, Beckingham R, Kho AL, Kampourakis T, Ehler E. Missense mutations in the central domains of cardiac myosin binding protein-C and their potential contribution to hypertrophic cardiomyopathy. J Biol Chem. 2024 Jan;300(1):105511. doi: 10.1016/j.jbc.2023.105511. Epub 2023 Nov 30. PMID: 38042491; PMCID: PMC10772716.

Pioner JM, Vitale G, Steczina S, Langione M, Margara F, Santini L, Giardini F, Lazzeri E, Piroddi N, Scellini B, Palandri C, Schuldt M, Spinelli V, Girolami F, Mazzarotto F, van der Velden J, Cerbai E, Tesi C, Olivotto I, Bueno-Orovio A, Sacconi L, Coppini R, Ferrantini C, Regnier M, Poggesi C. Slower Calcium Handling Balances Faster Cross-Bridge Cycling in Human MYBPC3 HCM. Circ Res. 2023 Mar 3;132(5):628-644. doi: 10.1161/CIRCRESAHA.122.321956. Epub 2023 Feb 6. PMID: 36744470; PMCID: PMC9977265.

Richards S, Aziz N, Bale S, Bick D, Das S, Gastier-Foster J, Grody WW, Hegde M, Lyon E, Spector E, Voelkerding K, Rehm HL; ACMG Laboratory Quality Assurance Committee. Standards and guidelines for the interpretation of sequence variants: a joint consensus recommendation of the American College of Medical Genetics and Genomics and the Association for Molecular Pathology. Genet Med. 2015 May;17(5):405-24. doi: 10.1038/gim.2015.30. Epub 2015 Mar 5. PMID: 25741868; PMCID: PMC4544753.

Roopnarine O, Leinwand LA. Functional analysis of myosin mutations that cause familial hypertrophic cardiomyopathy. Biophys J. 1998 Dec;75(6):3023-30. doi: 10.1016/S0006-3495(98)77743-4. PMID: 9826622; PMCID: PMC1299973.

Ross JP, Dion PA, Rouleau GA. Exome sequencing in genetic disease: recent advances and considerations. F1000Res. 2020 May 6;9:F1000 Faculty Rev-336. doi: 10.12688/f1000research.19444.1. PMID: 32431803; PMCID: PMC7205110.

Sanger F, Nicklen S, Coulson AR. DNA sequencing with chain-terminating inhibitors. Proc Natl Acad Sci U S A. 1977 Dec;74(12):5463-7. doi: 10.1073/pnas.74.12.5463. PMID: 271968; PMCID: PMC431765.

Satam H, Joshi K, Mangrolia U, Waghoo S, Zaidi G, Rawool S, Thakare RP, Banday S, Mishra AK, Das G, Malonia SK. Next-Generation Sequencing Technology: Current Trends and Advancements. Biology (Basel). 2023 Jul 13;12(7):997. doi: 10.3390/biology12070997. Erratum in: Biology (Basel). 2024 Apr 24;13(5):286. doi: 10.3390/biology13050286. PMID: 37508427; PMCID: PMC10376292.

Shapiro MB, Senapathy P. RNA splice junctions of different classes of eukaryotes: sequence statistics and functional implications in gene expression. Nucleic Acids Res. 1987 Sep 11;15(17):7155-74. doi: 10.1093/nar/15.17.7155. PMID: 3658675; PMCID: PMC306199.

Song L, Zou Y, Wang J, Wang Z, Zhen Y, Lou K, Zhang Q, Wang X, Wang H, Li J, Hui R. Mutations profile in Chinese patients with hypertrophic cardiomyopathy. Clin Chim Acta. 2005 Jan;351(1-2):209-16. doi: 10.1016/j.cccn.2004.09.016. PMID: 15563892.

Sorrentino U, Gabbiato I, Canciani C, Calosci D, Rigon C, Zuccarello D, Cassina M. Homozygous *TNNI3* Mutations and Severe Early Onset Dilated Cardiomyopathy: Patient Report and Review of the Literature. Genes (Basel). 2023 Mar 19;14(3):748. doi: 10.3390/genes14030748. PMID: 36981019; PMCID: PMC10048074.

Tudurachi BS, Zăvoi A, Leonte A, Țăpoi L, Ureche C, Bîrgoan SG, Chiuariu T, Anghel L, Radu R, Sascău RA, Stătescu C. An Update on MYBPC3 Gene Mutation in Hypertrophic Cardiomyopathy. Int J Mol Sci. 2023 Jun 22;24(13):10510. doi: 10.3390/ijms241310510. PMID: 37445689; PMCID: PMC10341819.

Van Driest SL, Jaeger MA, Ommen SR, Will ML, Gersh BJ, Tajik AJ, Ackerman MJ. Comprehensive analysis of the beta-myosin heavy chain gene in 389 unrelated patients with hypertrophic cardiomyopathy. J Am Coll Cardiol. 2004 Aug 4;44(3):602-10. doi: 10.1016/j.jacc.2004.04.039. PMID: 15358028.

Vitale G, Coppini R, Tesi C, Poggesi C, Sacconi L, Ferrantini C. T-tubule remodeling in human hypertrophic cardiomyopathy. J Muscle Res Cell Motil. 2021 Jun;42(2):305-322. doi: 10.1007/s10974-020-09591-6. Epub 2020 Nov 22. PMID: 33222034; PMCID: PMC8332592.

Voelkerding KV, Dames SA, Durtschi JD. Next-generation sequencing: from basic research to diagnostics. Clin Chem. 2009 Apr;55(4):641-58. doi: 10.1373/clinchem.2008.112789. Epub 2009 Feb 26. PMID: 19246620.

Voigt N, Li N, Wang Q, Wang W, Trafford AW, Abu-Taha I, Sun Q, Wieland T, Ravens U, Nattel S, Wehrens XH, Dobrev D. Enhanced sarcoplasmic reticulum Ca2+ leak and increased Na+-Ca2+ exchanger function underlie delayed afterdepolarizations in patients with chronic atrial fibrillation. Circulation. 2012 May 1;125(17):2059-70. doi: 10.1161/CIRCULATIONAHA.111.067306. Epub 2012 Mar 28. PMID: 22456474; PMCID: PMC4663993.

Walsh R, Thomson KL, Ware JS, Funke BH, Woodley J, McGuire KJ, Mazzarotto F, Blair E, Seller A, Taylor JC, Minikel EV, Exome Aggregation Consortium, MacArthur DG, Farrall M, Cook SA, Watkins H. Reassessment of Mendelian gene pathogenicity using 7,855 cardiomyopathy cases and 60,706 reference samples. Genet Med. 2017 Feb;19(2):192-203. doi: 10.1038/gim.2016.90. Epub 2016 Aug 17. PMID: 27532257; PMCID: PMC5116235.

Watkins H, Rosenzweig A, Hwang DS, Levi T, McKenna W, Seidman CE, Seidman JG. Characteristics and prognostic implications of myosin missense mutations in familial hypertrophic cardiomyopathy. N Engl J Med. 1992 Apr 23;326(17):1108-14. doi: 10.1056/NEJM199204233261703. PMID: 1552912.

Yacoub MH, Olivotto I, Cecchi F. 'End-stage' hypertrophic cardiomyopathy: from mystery to model. Nat Clin Pract Cardiovasc Med. 2007 May;4(5):232-3. doi: 10.1038/ncpcardio0859. PMID: 17457348.

UNIONE EUROPEA
Fondo Sociale Europeo
Ministero dell'Università e della Ricerca
PON RICERCA E INNOVAZIONE 2014 - 2020
REACT EU

La borsa di dottorato è stata cofinanziata con risorse del
Programma Operativo Nazionale Ricerca e Innovazione 2014-2020, risorse FSE REACT-EU
Azione IV.4 “Dottorati e contratti di ricerca su tematiche dell’innovazione”
e Azione IV.5 “Dottorati su tematiche Green”